UNIVERSITY OF CALIFORNIA, SAN DIEGO

# The Design, Synthesis, and Evaluation of Compounds that Bind to Alzheimer's-related and HIV-1-related Amyloids

A dissertation submitted in partial satisfaction of the requirements for the degree Doctor of Philosophy

in

Chemistry

by

Christina Cecilia Capule

Committee in charge:

Professor Jerry Yang, Chair
Professor Patricia Jennings
Professor Eliezer Masliah
Professor Tadeusz Molinski
Professor Yitzhak Tor

2012

This Dissertation of Christina Cecilia Capule is approved, and it is acceptable in quality and form for publication on microfilm and electronically:

_____

_____

_____

_____

_____

Chair

University of California, San Diego

2012

# DEDICATION

I dedicate this thesis to my two lolas,  Lola Maring and Lola Chit.

TABLE OF CONTENTS

LIST OF FIGURES

LIST OF TABLES

# LIST OF ABBREVIATIONS

| | |
|---|---|
| Aβ | β-amyloid |
| AIDS | Acquired Immune Deficiency Syndrome |
| AD | Alzheimer's Disease |
| BBB | Blood-brain barrier |
| BTA | Benzothiazole aniline |
| BTA-$EG_4$ | Benzothiazole aniline tetra(ethylene glycol) |
| BTA-$EG_6$ | Benzothiazole aniline hexa(ethylene glycol) |
| CCR5 | Chemokine receptor type 5 |
| CXCR4 | Chemokine receptor type 4 |
| CD4 | Cluster of differentiation 4, cell surface receptor |
| DCC | Dicyclohexylcarbodiimide |
| DCM | Dichloromethane |
| DMAP | 4-Dimethylamino pyridine |
| DMF | Dimethylformamide |
| DMSO | Dimethyl sulfoxide |
| EDC-HCl | 1-Ethyl-3-[3-dimethylaminopropyl]carbodiimide hydrochloride |
| ELISA | Enzyme-linked Immunosorbent Assay |
| EtOAc | Ethyl Acetate |
| FTIR | Fourier-transform Infrared |
| HeLa | Immortalized human cell line derived from Henrietta Lacks |
| HEPES | 4-(2-hydroxyethyl)-1-piperazineethanesulfonic acid |

| | |
|---|---|
| Hex. | Hexane |
| HIV-1 | Human Immunodeficiency Virus, Type 1 |
| HPLC | High performance liquid chromatography |
| LTR | Long terminal repeats |
| MeOH | Methanol |
| MNBA | 2-methyl-6-nitrobenzoic anhydride |
| MS | Mass spectrometry |
| NMR | Nuclear Magnetic Resonance |
| PAP | Prostatic acid phophatase |
| PBS | Phosphate-buffered saline |
| PS | Polystyrene |
| PMPS | Plasma-modified polystyrene |
| RF | Radiofrequency |
| SEVI | Semen-derived enhancer of virus infection |
| ThT | Thioflavin T |

# ACKNOWLEDGEMENTS

First and foremost, I would like to thank my family for all their love and support. I would not have made it without my mom's voice of reason and my dad's sense of humor. I would like to thank my sister Connie and my brother Daniel, my two best friends, for going above and beyond. I would like to thank my husband Miguel for his endless support. Although the distance between us was hard on our relationship, he encouraged me to follow through and continue on with the graduate program. I am so lucky to have him in my life.

I would like to thank Dr. Green, my high school chemistry teacher for introducing me to the world of chemistry and sparking my love for science.

I would like to thank all of the members of the Yang lab, past and present, for being a great support system. They've been there for me through all the ups and downs. Mark, you were a great source of dark humor. Mike, I will remember the stories we shared together very fondly. Lila, whenever I needed to steal away or take a break, you were always ready to take a break with me. Lani, you are a great friend and a great listener and I am grateful for your guidance in the early years of my graduate career. Alice, what would I have done without you? You calmed me down in my times of stress and you've become one of my closest friends. Yuchen, it was great having you sit right by me and your optimism is infectious. Xiaobei, I will miss our hot pot days. Leibniz and Kevin, you two were always so thoughtful; I thought it was especially nice that you would escort me to my car at night. To the rest of the Yang lab members, hang in there, you'll make it through!

I would like to acknowledge my roommate Mela Mulvihill. We were two strangers who took a gamble and decided to move in together. After five years, I still say that you are the best roommate ever.

I would like to thank my collaborators, Dr. Theodorakis, Dr. Sigurdson, Dr. Dewhurst, as well as their research groups.

I would like to thank my Committee: Dr. Jennings, Dr. Masliah, Dr. Molinski, and Dr. Tor for the time and effort that they've invested in me.

Finally, I would like to thank Dr. Yang for his guidance, his support, and for believing in me. The skills I've acquired while working in his lab will no doubt aid me in my future endeavors.

**Notes about the Chapters**

Chapter 4 is based on material that appears in "Rational Design of Amyloid-binding Agents based on the Molecular Rotor Motif." Sutharsan, J.; Dakanali, M.; Capule, C. C.; Haidekker, M. A.; Yang, J.; Theodorakis, E. A. *Chemmedchem* **2010**, *5*, 56-60. I am a co-author on this publication.

Chapter 5 is based on material that appears in "ANCA: A Family of Fluorescent Probes that Bind and Stain Amyloid Plaques in Human Tissue." Chang, W. M.; Dakanali, M.; Capule, C. C.; Sigurdson, C. J.; Yang, J.; Theodorakis, E. A. *ACS Chem. Neurosci.* **2011**, *2*, 249-255. I am a co-author on this publication.

Chapter 6 is based on material that appears in "Amyloid-binding Small Molecules Efficiently Block SEVI (Semen-derived Enhancer of Virus Infection)-

and Semen-mediated Enhancement of HIV-1 Infection." Olsen, J. S.; Brown, C.; Capule, C. C.; Rubinshtein, M.; Doran, T. M.; Srivastava, R. K.; Feng, C. Y.; Nilsson, B. L.; Yang, J.; Dewhurst, S. *J. Biol. Chem.* **2010**, *285*, 35488-35496. I am a co-author on this publication.

Chapter 7 is based on material currently being prepared for submission for publication: "Oligovalent Amyloid-Binding Agents Reduce SEVI-Mediated Enhancement of HIV-1 Infection." Capule, C.C.; Brown, C.; Olsen, J.S.; Dewhurst, S.; Yang, J. I am the primary author of this pending manuscript.

# VITA

| | |
|---|---|
| 2004 | Bachelor of Science in Chemistry, San Francisco State University |
| 2008 | Master of Science in Chemistry, University of California, San Diego |
| 2012 | Doctor of Philosophy in Chemistry, University of California, San Diego |

## PUBLICATIONS

1. **Capule, C.C.**; Brown, C.; Olsen, J.S.; Dewhurst, S.; Yang, J. "Oligovalent Amyloid-Binding Agents Reduce SEVI-Mediated Enhancement of HIV-1 Infection." **Submitted.*

2. **Capule, C.C.**; Yang, J. "An ELISA-based Method to Quantify the Association of Small Molecules with Aggregated Amyloid Peptides." **Submitted.*

3. Song, J.M.; Spitzer, M.H.; Megill, A.; Rubinshtein, M.; Habib, L.K.; **Capule, C.C.**; Xie, Y.; Keenoy, K.E.; Mayer, M.; Turner, R.S.; Yang, J.; Pak, D.T.S.; Lee, H.; Hoe, H.S. "Pharmacological targeting of beta amyloid enhances dendritic spine density and memory." **In preparation.*

4. Chang, W.M.; Dakanali, M.; **Capule, C.C.**; Yang, J.; Theodorakis, E.A. "ANCA: A Family of Fluorescent Probes that Bind and Stain Amyloid Plaques in Human Tissue." *ACS Chemical Neuroscience*, **2011**, *2*, 249-255.

5. Olsen, J.S.; Brown, C.; **Capule, C.C.**; Rubinshtein, M.; Doran, T.M.; Srivastava, R.K.; Feng, C.; Nilsson, B.L.; Yang, J.; Dewhurst, S. "Amyloid Binding Small Molecules Efficiently Block SEVI and Semen Mediated Enhancement of HIV-1 Infection." *Journal of Biological Chemistry*, **2010**, *285*, 35488-35496.

6. Sutharsan, J.; Dakanali, M.; **Capule, C.C.**; Haidekker, M.A.; Yang, J.; Theodorakis, E.A."Rational Design of Amyloid Binding Agents Based on the Molecular Rotor Motif." *ChemMedChem*, **2010**, *5*, 56-60.

7. Wong, F.M.; **Capule, C.C.**; Chen, D.X.; Gronert, S.; Wu, W."Surprisingly Low Aqueous Acidity at the α-Positions of Pyridiniums and Pyrimidinium: The Role of Solvation." *Organic Letters*, **2008**, *10 (13)*, 2757-2760.

8. Yeoh, F.Y.; Cuasito, R.R.; **Capule, C.C.**; Wong, F.M.; Wu, W. "Carbanions from Decarboxylation of Orotate analogs: Stability and Mechanistic Implications." *Bioorganic Chemistry*, **2008**, *35(4)*, 338-343.

9. Wong, F.M.; **Capule, C.C.**; Wu, W. "Stability of the 6-Carbanion of Uracil Analogues: Mechanistic Implications for Model Reactions of Orotidine-5'-monophosphate Decarboxylase." *Organic Letters*, **2006**, *8(26)*, 6019–6022.

10. Patris, N.; **Capule, C.**; Leifer, R.; Raccah, F.; Geyh, A.; Williams, D.; Chillrud, S.; Thiemens, M.H. "Complete Isotope Study of the New York City Aerosol Before and During the WTC Disaster." *American Geophysical Union, Fall Meeting*, **2002**, abstract #B71A-0728.

## FELLOWSHIPS

2001-2003 MARC-NIH Scholarship

2004-2005 MBRS-RISE-NIH Scholarship

2006-2007 GAANN Fellowship

ABSTRACT OF THE DISSERTATION

The Design, Synthesis, and Evaluation of Compounds that Bind to Alzheimer's-related and HIV-1-related Amyloids

by

Christina Cecilia Capule

Doctor of Philosophy in Chemistry

University of California, San Diego, 2012

Professor Jerry Yang, Chair

Amyloids—misfolded, aggregated peptides—have been implicated in over thirty human diseases. This thesis focused on the study of two different amyloids—Aβ(1-42) and SEVI (semen-derived enhancer of virus infection)—associated with two distinct conditions—Alzheimer's Disease (AD) and Acquired Immune Deficiency Syndrome (AIDS), respectively.

Aβ aggregates are a hallmark of AD and may play a central, causative role in the pathogenesis of this disease. Aβ-amyloid-targeting small molecules have, therefore, attracted wide interest as potential agents for the treatment or diagnosis of AD. This thesis describes the development of a general method to evaluate small molecule-β-amyloid binding interactions via a modified quantitative ELISA protocol. The implementation of an *in vitro* model to evaluate the blood-brain barrier permeability of β-amyloid-targeting compounds is also discussed in this thesis.

The design and evaluation of a new class of fluorescent probes that bind to Aβ aggregates is described in this thesis. The advantage of these compounds is that their spectroscopic properties can be altered and fine-tuned via simple synthetic methods.

The second portion of this thesis discusses the study of small molecules that bind to SEVI, a naturally abundant amyloid found in semen. SEVI can potentially increase the infectivity of HIV-1 in cells by up to 400,000-fold. Although the mechanism of SEVI-mediated transmission of HIV-1 remains poorly understood, evidence suggests that SEVI binds to both HIV-1 virions and cell membranes, thereby facilitating viral infection. We hypothesized that BTA-$EG_6$, a derivative of the well-known amyloid-binding compound Thioflavin T, could coat SEVI fibrils, thereby inhibit HIV-1 interactions with SEVI fibrils, and thus, reduce SEVI-mediated enhancement of HIV-1 infectivity. The results of these investigations are presented in this thesis.

The final project described in this thesis is the design, synthesis, and evaluation of multivalent analogs of BTA-$EG_6$. The goals of this project were 2-fold: 1) Create compounds that bind with high affinity to both Aβ fibrils and SEVI fibrils based on the multivalent design strategy and 2) evaluate whether oligomers of the BTA moiety exhibit improved ability over the BTA monomer to inhibit SEVI-mediated enhancement of HIV-1 infectivity. The results of this project are presented in this thesis.

# Chapter 1

# Introduction: Amyloids and Disease

## 1.1 Amyloids

"Amyloid" is an encompassing term for insoluble, abnormally-folded proteins that possess the following structural features: 1) fibrillar morphology, 2) β-sheet secondary structure, and 3) upon staining with Congo Red, apple-green birefringence under polarized light.[1] Although their peptide sequences, origin, and native structures can widely vary, all amyloids possess the aforementioned characteristics. The intrinsic structural feature of amyloids is the cross-β sheet configuration. In a cross-β sheet configuration, β-sheet extended chains and sheet–sheet stacking interactions are oriented perpendicular to the long axis of the fibril, while β-sheet hydrogen bonds are parallel to the length of the fibril. Because of their limited solubility, the structural elucidation of amyloids via crystallization has been

difficult to near impossible. However, there are a number of techniques available that can assess fibrillar morphology.[2] X-ray diffraction is routinely used to confirm the cross-β sheet structure inherent in amyloid fibrils (Figure 1.1a). The typical x-ray diffraction pattern for amyloids consist of two signals at 4.7 Å and at ~10-11 Å, indicative of the interstrand and the stacking distances in β-sheet, respectively (Figure 1.1b). Microscopy techniques, such as atomic force microscopy and transmission electron microscopy have also proved useful in confirming the presence of fibrils. Additionally, histologic dyes such as Congo Red (CR) and Thioflavin T (ThT), which both possess intrinsic spectroscopic properties upon binding to fibrils, are routinely used to determine the presence or formation of fibrils.[1] Circular Dichroism (CD) and Fourier Transform Infrared Spectroscopy (FTIR) are additional analytical tools that can monitor the conformation of proteins and confirm the presence of β-sheet secondary structure in amyloids.

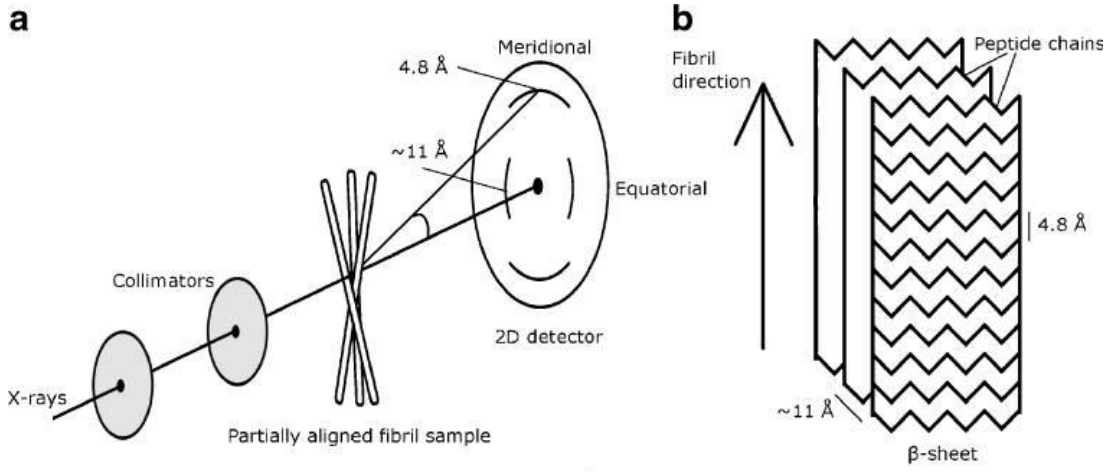


*Figure 1.1. a) A typical x-ray diffraction pattern for amyloids b) The interstrand & stacking distances in a cross β-sheet pattern.[3] Adapted with kind permission from Springer Science+Business Media: Journal of Chemical Biology, Binding mode of Thioflavin T and other molecular probes in the context of amyloid fibrils- current status, 3(1), 2010, page 2, Minna Groenning, Figure 1, copyright 2009.*

Amyloids are implicated in over 30 human diseases, which are collectively known as "amyloidosis."[4] Each disease is characterized by a distinct protein that aggregates to form insoluble amyloid deposits. While AIDS is not categorically defined as an amyloidosis, recent findings have revealed that amyloids may play a pivotal role in the infectivity of HIV-1 via sexual transmission.[5] This thesis focused on the study of two different amyloids—Aβ(1-42) and SEVI (semen-derived enhancer of virus infection)—associated with two different conditions—Alzheimer's Disease (AD) and Acquired Immune Deficiency Syndrome (AIDS), respectively.

## 1.2 Alzheimer's Disease

### 1.2.1 History and Current Statistics

Alzheimer's Disease (AD) is a progressive, irreversible neurodegenerative disorder and is the most common form of dementia. The earliest known case of AD was documented in 1901 by Alois Alzheimer, when he observed a female patient named Auguste Deter at the Frankfurt Asylum in Germany.[6,7] He continued to monitor Auguste, and her symptoms, until her death in 1906. Autopsy and subsequent histologic staining of her brain tissue revealed the presence of abnormal protein deposits(Figure 1.2)[8]—now referred to as amyloid plaques (APs) and neurofibrillary tangles (NFTs) [9]

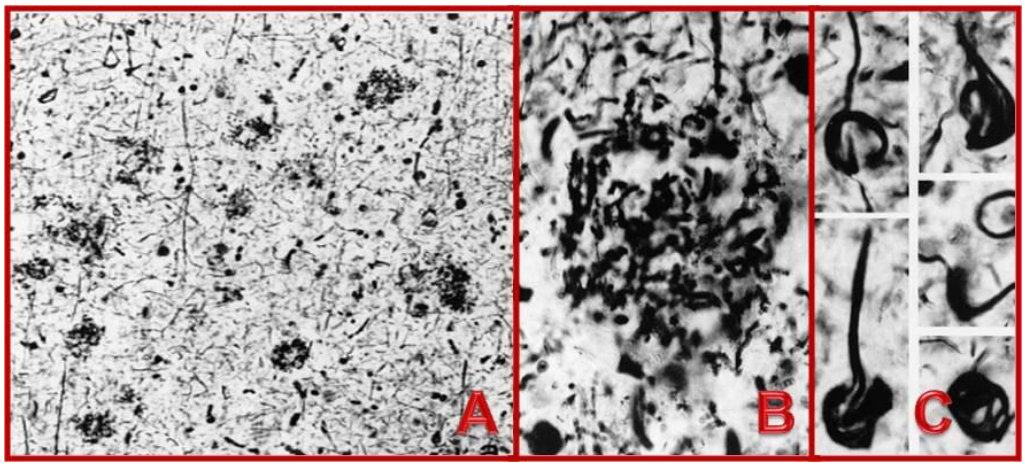


*Figure 1.2. A) β-amyloid plaques and neurofibrillary tangles in the cerebral cortex of Auguste Deter[8] B) Zoom in of an amyloid plaque C) Zoom in of the neurofibrillary tangles. Adapted with kind permission from Springer Science+Business Media: Neurogenetics, Histopathology and APOE genotype of the first Alzheimer disease patient, Auguste D. 1(3). 1998, page 225, Minna Graeber, Figure 2, copyright 1998.*

Symptoms of Alzheimer's Disease can range in severity, depending on the stage of the disease. Early stages of AD are marked by mild cognitive decline, such as short-term memory loss, associated irritability, and the inability to correctly solve elementary puzzles or problems. In the more advanced stages of AD, patients suffer significant memory failure and are unable to perform routine daily functions without the aid of a caretaker. Moreover, as the disease progresses, there is considerable atrophy of the brain due to a significant loss in brain cells. Figure 1.3 shows a side-by-side comparison of a normal, healthy brain (upper left) and a brain ravaged by AD (upper right). Cross-sections of the healthy brain and the AD brain (lower left and right) show that there is considerable shrinkage in the cortical and hippocampal areas of the AD brain, the areas that are associated with memory and learning.

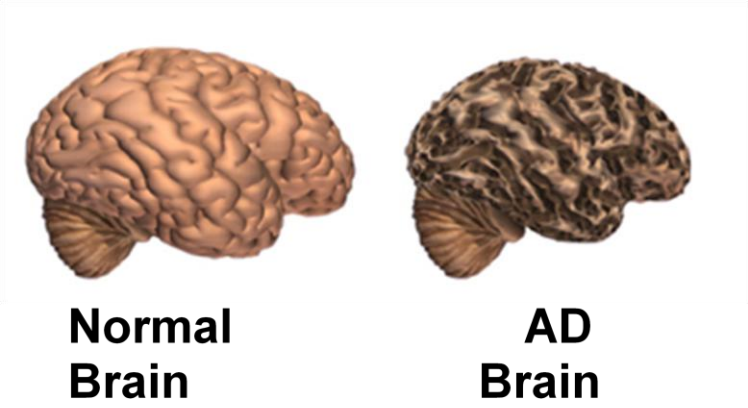


*Figure 1.3. Side-by-side comparison of a normal brain (left) and an AD brain (right). Adapted with permission. © 2011 Alzheimer's Association. www.alz.org. All rights reserved. Illustrations by Stacy Janis.*

According to the Alzheimer's Association, Alzheimer's Disease currently afflicts an estimated 5.2 million Americans.[10] Approximately 96% of these cases are of persons aged 65 or older. Because the majority of individuals diagnosed with AD are in this upper age bracket, AD is a disease that is associated with old age. Although it is not a normal process of aging, the greatest risk factor for developing AD seems to be advancing age. Since the baby boomer generation (approximately 76 million individuals born between the years 1945-1964) is now entering retirement age, and because average life expectancies continue to lengthen, the number of AD cases is expected to rise dramatically in the coming years. Projected numbers estimate that by the year 2050, the number of AD cases may triple from 5.2 million to as many as 16 million cases (Figure 1.4).

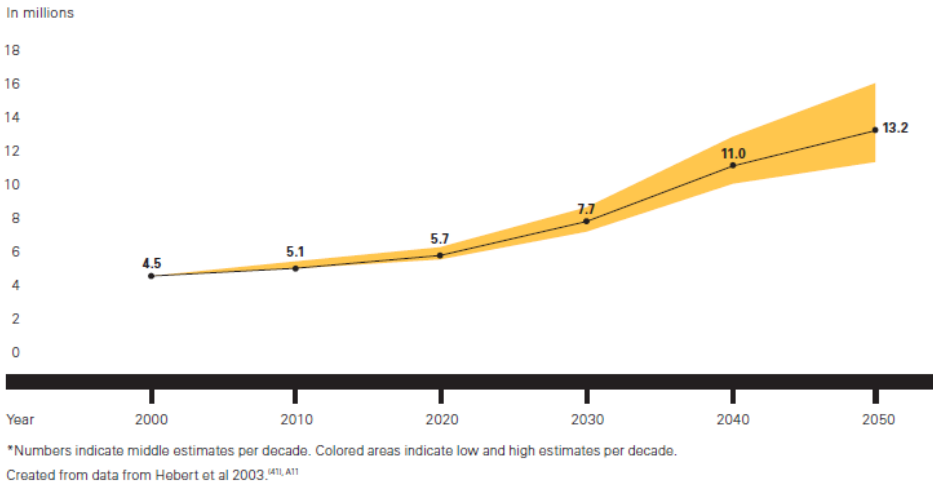


*Figure 1.4. Projected numbers of people aged 65 and over in the US population with Alzheimer's Disease (in millions).*[10] *Reprinted from Alzheimer's & Dementia, 2011 Alzheimer's Disease Facts and Figures, 208-244, copyright 2011, with permission from Elsevier.*

There is currently no FDA-approved disease-modifying treatment or preventative measure for Alzheimer's Disease.[11] This and other factors have contributed to the fact that, while other major causes of deaths have observed a continued decline over the years due to available medications and known prevention methods, the number of deaths due to AD continue to rise (Figure 1.5). Between 2000 and 2008, the number of deaths attributed to the number one cause of death, heart disease, decreased by 13%. In stark contrast, the number of deaths due to Alzheimer's Disease has risen by 66%.

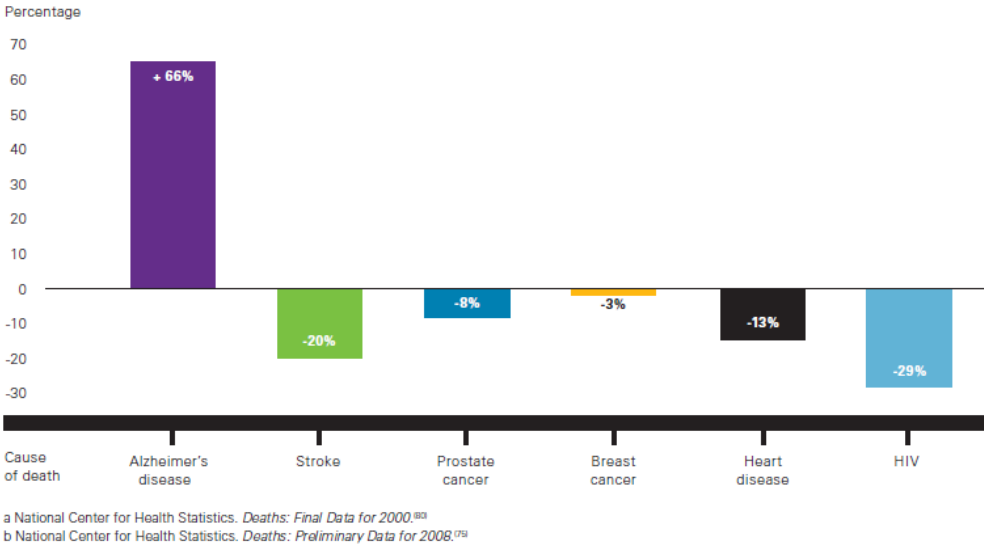


*Figure 1.5. Percentage changes in selected causes of death (all ages) between 2000-2008.*[10] *Reprinted from Alzheimer's & Dementia, 2011 Alzheimer's Disease Facts and Figures, 208-244, copyright 2011, with permission from Elsevier.*

## 1.2.2 Available Treatments

At this time, there is no FDA-approved disease-modifying treatment to reverse or prevent Alzheimer's Disease.[11] There are two types of medication that are currently approved by the United States Food and Drug Administration (U.S. FDA) to treat symptoms of memory loss: acetylcholinesterase (AChE) inhibitors and one drug that acts as an antagonist on the N-methyl d-Aspartate (NMDA) receptor (Figure 1.6).

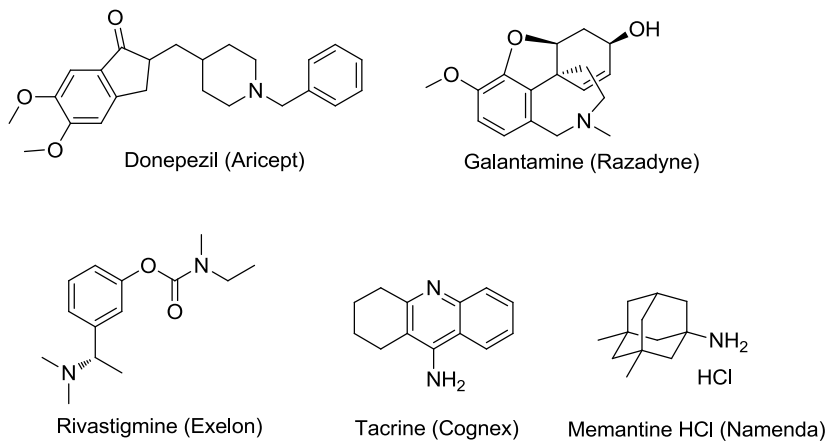


*Figure 1.6. Commercially available treatments to alleviate symptoms of Alzheimer's Disease.*

Acetylcholine (ACh) is an important neurotransmitter for learning and for the formation and retention of memory. A number of AChE inhibitors were developed because of the observed dwindling production of acetylcholine in the hippocampal and cortical areas of AD brains.[12] Inhibiting the enzymatic activity of AChE delays the degradation of acetylcholine, resulting in the accumulation of acetylcholine and the retention of its function. Tacrine (Cognex®) was the first cholinesterase inhibitor approved by the FDA, but because of its poor oral availability and severe adverse side effects,[13] it has been largely supplanted by the other FDA-approved AChE inhibitors. The most commonly prescribed AChE inhibitors for treating mild to moderate symptoms of Alzheimer's Disease are Donepezil (Aricept®), Rivastigmine (Exelon®), and Galantamine (Razadyne®).

Memantine hydrochloride, a derivative of adamantine, is the first FDA-approved drug for AD that targets the NMDA receptor. Glutamate, like acetylcholine, is a neurotransmitter that plays a central role in learning and memory. At normal levels, glutamate binds to NMDA receptors to trigger the controlled influx

of $Ca^{2+}$ into cells, which is important for synaptic plasticity. However, excessive glutamate concentrations cause abnormally high levels of $Ca^{2+}$ to enter cells, which ultimately leads to excitotoxicity, the damage and death of cells. The dysregulation of $Ca^{2+}$ has previously been suggested to be one of the factors that lead to the pathogenesis of AD.[14] Memantine HCl helps to restore cellular $Ca^{2+}$ homeostasis by binding to NMDA receptors, consequently blocking glutamate from the NMDA receptor and hindering its activity.[15] Memantine HCl is approved by the FDA for the treatment of moderate to severe AD.[16] In later stages of the disease, memantine HCl is sometimes taken in combination with the AChE inhibitor donepezil, because of the superior combined benefits observed in some individuals.

Unfortunately, these available medications only delay the inevitable loss of cognitive function. Studies have shown that while these medicines do improve cognition, these effects are only temporary and last an average of 6-12 months at best. As AD progresses and as symptoms worsen, these medications eventually become ineffective.

## 1.2.3. Aβ Deposits: A Hallmark of Alzheimer's Disease

The accumulation of amyloid plaques and neurofibrillary tangles (NFTs) observed by Alois Alzheimer in the brain tissue of his first AD patient are now the hallmarks of Alzheimer's Disease. The major component of amyloid plaques has been identified as a 40 to 42 amino acid peptide called Aβ (or β-amyloid) peptide that aggregate into insoluble fibrils. While the deposition of Aβ plaques are definitive of and unique to AD, NFTs have been associated with other dementias,

such as frontotemporal dementia,[17] Pick's disease,[18] and other tauopathies.[19] Thus, I've focused my research efforts on the study of Aβ aggregates.

Aβ is a by-product of the sequential proteolytic cleavage of a transmembrane protein called amyloid precursor protein (APP). Initially, APP is cut extracellularly by β-secretase to produce the N-terminal side of Aβ. Subsequent cleavage of the transmembrane region of APP by γ-secretase produces the C-terminal end of Aβ peptide, which can generate isoforms of Aβ ranging from 39-43 amino acid lengths (Figure 1.7).[20]


*Figure 1.7.The amino acid sequence of Aβ peptide*

The most common isoforms of Aβ *in vivo* are Aβ(1-40) and Aβ(1-42). I've focused my research on the study of Aβ(1-42) in particular because studies indicate that it is the initially deposited and predominant form[21] in amyloid plaques. Moreover, Aβ(1-42) has a higher propensity for aggregation than Aβ(1-40)[22] and has been shown to be the most toxic form.[23,24]

Aβ production, degradation, and clearance from the brain is believed to be a natural process.[25] However, the accumulation of Aβ, due to either overproduction or inefficient clearance of Aβ, leads to the misfolding, aggregation, and deposition of Aβ in the AD brain.[26] According to the amyloid cascade hypothesis, which was first

articulated by Hardy *et al.*,[27] Aβ plays a central, causative role in the pathogenesis of Alzheimer's Disease. In the amyloid cascade hypothesis, the pathology of AD is initiated by the accumulation and deposition of Aβ peptide, which then triggers an inflammatory response, oxidative injury, synaptic dysfunction, neuronal loss, and then, ultimately, dementia. This hypothesis has been modified over the years as increasing evidence show that soluble oligomers, not insoluble fibrils, are the most toxic forms.[28-30]

## 1.2.4 Available Diagnostic Tools

The development of effective treatments for AD has been hindered, in large part, by the lack of methods available to definitively diagnose AD in living patients. Although AD is routinely diagnosed clinically after a series of mental status tests and physical examination, it can only be irrefutably confirmed by demonstrating that the pathologic hallmarks of AD—protein deposits of amyloid plaques and neurofibrillary tangles—are present in the brain. The presence of these deposits is typically confirmed post mortem through autopsy of the brain. Autopsied brain tissue are treated with histologic dyes, such as Thioflavin T (ThT)[31,32] or Congo Red (CR),[33] that have an affinity for and stain amyloid plaques (Figure 1.8). These dyes are limited to post mortem use because their inherent charges prevent them from crossing the blood-brain barrier *in vivo*.

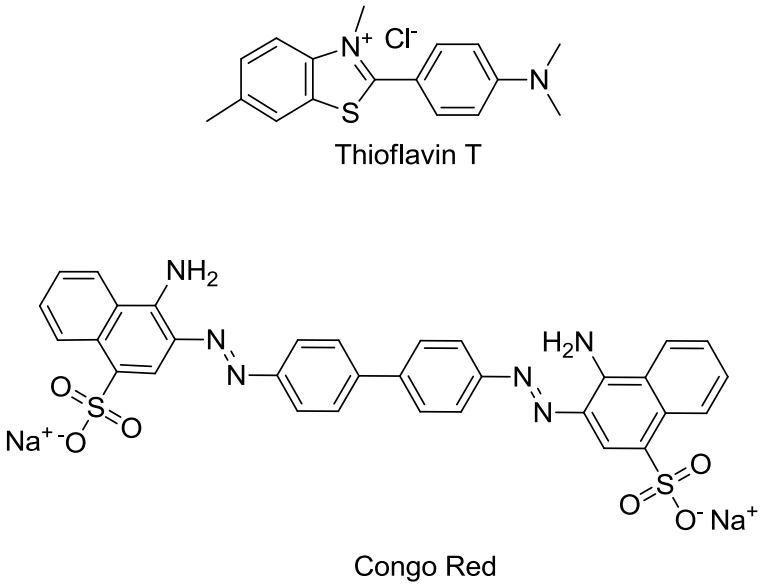


*Figure 1.8. Common histological dyes used for staining amyloid plaques*

In recent years, tremendous efforts have focused on the development of imaging agents that target the biomarkers of AD in living patients, particularly β-amyloid plaques in the brain. Agents that can image amyloid plaques in live patients would make it possible to 1) monitor the progression of AD and thus enhance our understanding of the pathology of this disease and to 2) properly diagnose AD ante mortem, ideally before clinical symptoms or significant memory failure present themselves. Figure 1.9 shows a partial list of β-amyloid imaging agents that are currently in clinical trials. These radiolabeled compounds have been developed for use in positron emission tomography (PET). The first PET agent to show success in clinical trials is the compound Pittsburgh Compound B ($^{11}$C-PiB),[34] a compound derived from the structure of the histologic dye Thioflavin T. Human clinical trials demonstrated a good correlation of PET imaging of Aβ plaques *in vivo* with the post mortem analysis of brain tissue. The widespread use of Pittsburgh Compound B has

been limited because of the short half-life (20.4 min) of the $^{11}C$ radioisotope. This short half-life necessitates the on-site synthesis and immediate use of $^{11}C$-PiB for PET scanning.[35] On the other hand, the $^{18}F$ radioisotope has a longer half-life (109.7 min), which would perhaps extend the clinical access of Aβ-targeting PET tracers. Accordingly, a number of research groups have focused their attention on developing β-amyloid-binding compounds that are labeled with $^{18}F$. The original inventors of $^{11}C$-PiB modified their compound to include a $^{18}F$ radioisotope, and completely removed the $^{11}C$ radiolabel ($^{18}F$-flutemetamol).[35] Bayer® developed a stilbene-based $^{18}F$ compound ($^{18}F$-florbetaben),[36] while Eli Lilly® developed a strikingly structurally similar compound, an $^{18}F$-labelled styrylpyridine derivative ($^{18}F$-florbetapir).[37] While these compounds have shown great promise in clinical trials as potential diagnostic tools for Alzheimer's Disease, no imaging agent has yet been approved by the FDA for extensive clinical use.

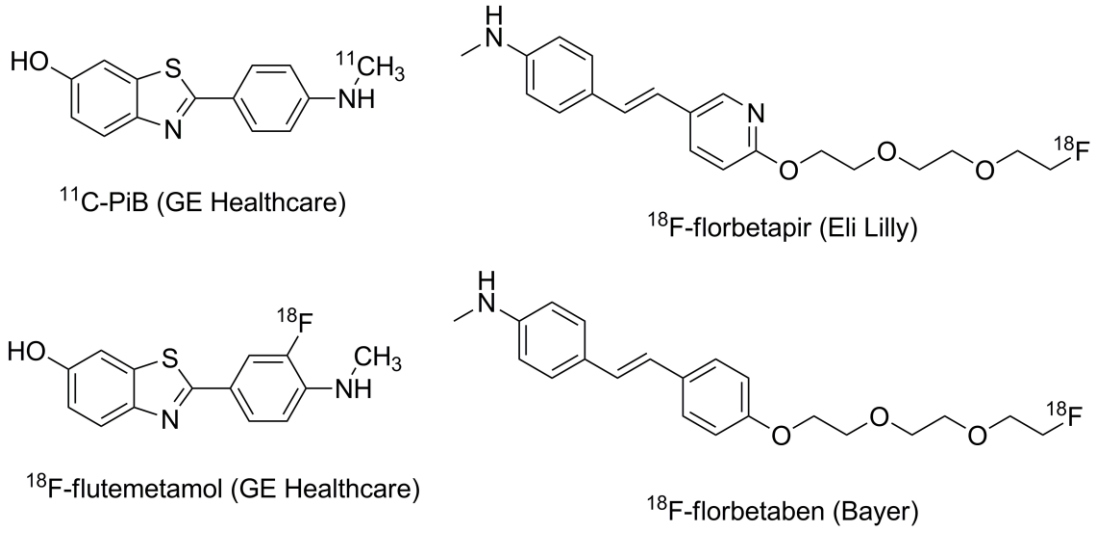


*Figure 1.9. Imaging agents that are currently in clinical trials to probe the accumulation of amyloid deposits in living patients.*

While there have been great gains in the field of Alzheimer's research in the past few years, the pursuit of new, improved therapeutics and diagnostics remains. One criteria for therapeutics and diagnostics that target Aβ is that they have a high binding affinity for aggregated Aβ. One goal of my thesis was to develop an assay that can quantitatively measure the interactions of small molecules with aggregated Aβ. Molecules identified by this assay to bind tightly with aggregated Aβ may be further developed into potential imaging agents or potential therapeutics. Chapter 3 of this thesis details the results of these efforts.

My second research goal aimed at investigating a rational design strategy to develop compounds that bind with high affinity to Aβ aggregates. Chapter 7 discusses the results of these efforts.

## 1.3 HIV and AIDS

### 1.3.1 History and Current Statistics

Acquired immune deficiency syndrome (AIDS, also called acquired immunodeficiency syndrome) is a disease of the immune system that is caused by the human immunodeficiency virus (HIV).[38,39] Infection with HIV gradually weakens the immune system, leaving infected individuals vulnerable to opportunistic infections and tumors that a healthy immune system can fight off under normal circumstances. The first clinical cases of AIDS were documented in the early 1980s. In 1980-81, homosexual men and intravenous drug users exhibited symptoms of a rare form of pneumonia, called pneumocystis carinii pneumonia (PCP), known to

manifest in individuals with compromised immune systems.[40,41] In addition, other homosexual men developed a rare skin cancer called Kaposi's sarcoma (KS).[42] Soon thereafter, many more cases of PCP and KS were documented, prompting the U.S. Centers for Disease Control (CDC) to put together a research team focused on monitoring the emerging outbreak. At a meeting in 1982, after determining that the outbreak was not unique to gay men, the CDC coined the acronym AIDS to refer to this disease.[43]

The CDC estimates that in the U.S. alone, there are more than one million people infected with HIV.[44] The World Health Organization has estimated that 33.4 million people worldwide are infected with HIV/AIDS.[45] Because of these staggering statistics, AIDS has recently been declared a pandemic.

## 1.3.2 Transmission, Diagnosis, and Available Treatments

HIV is transmitted via three main routes: 1) through sexual intercourse, 2) through blood, and 3) from mother-to-child (in the ante-, intra-, and postpartum periods). The most prevalent route of transmission is via sexual intercourse, as over 80% of infections are acquired this way.[46] Preventative measures can be taken to decrease the likelihood of contracting the virus. For example, safe sexual practices, such as using condoms during intercourse, and avoiding exposure to tainted needles or blood, greatly reduces the risk of HIV infection. However, at this time, there is no disease-modifying treatment for AIDS.

An individual infected with HIV is officially diagnosed with AIDS when the number of $CD4^+$ T cells per µL of blood falls below a 200 cell count.[47] In the early

stage of AIDS, the HIV-infected individual does not exhibit any associated symptoms since the immune system is still robust and attempts to fight off the infection. In the latter stage of AIDS, symptoms of HIV infection appear, as the virus has succeeded in weakening and compromising the immune system, rendering the individual vulnerable to opportunistic infections. In addition, people in the latter stage of AIDS have an increased risk of developing cancers such as Kaposi's sarcoma and lymphoma.[38]

There are currently 25 FDA-approved medications to treat AIDS symptoms. These medications belong to a class of compounds called antiretroviral drugs.[48] These drugs interfere with various stages of the HIV life cycle (section 1.3.3) and are often used in combination to suppress viral reproduction as much as possible. Figure 1.10 lists the compounds frequently used in combination drug therapies in the U.S. Among these compounds, tenofovir and emtricitabine are the two drugs that are regular components in combination therapies.

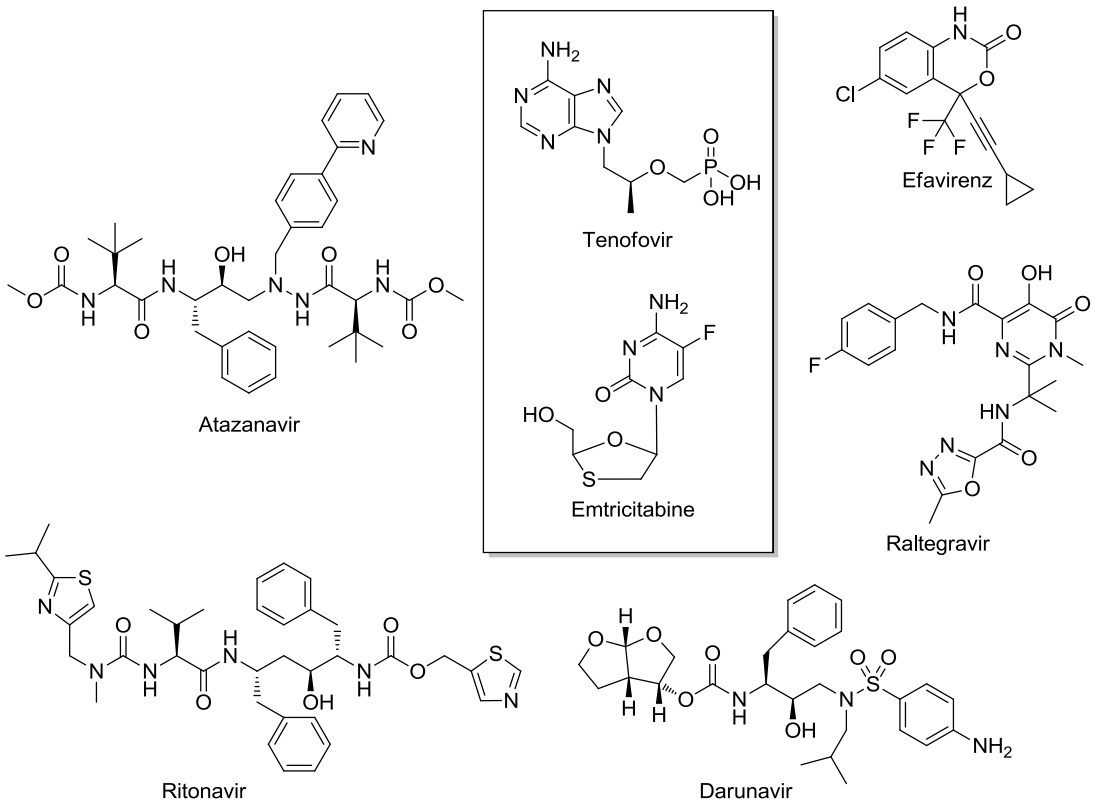


*Figure 1.10. FDA-approved drugs to treat AIDS symptoms*

## 1.3.3 The Life Cycle of HIV

The human immunodeficiency virus targets cells of the immune system, such as $CD4^+$ T lymphocytes, macrophages, and dendritic cells.[49-51] Like all viruses, HIV replicates by using the machinery of the cell it infects. Figure 1.11 shows the six steps—1) fusion, 2) reverse transcription, 3) integration, 4) transcription, 5) assembly, and 6) budding—in the life cycle of HIV.[52,53] In the first step, HIV fuses to and penetrates the target cell. The fusion of HIV onto cells requires the presence of specific receptors on the cell's surface. HIV anchors onto a target cell via the binding of its extracellular glycoprotein, gp120, to a CD4 receptor and to a

coreceptor, such as CXCR4 or CCR5. Conformational changes in gp120 and another glycoprotein of HIV, the transmembrane gp41, facilitates the fusion of HIV with the host cell. Once inside the host cell, the virus releases its RNA along with three enzymes that are key for viral replication: reverse transcriptase, integrase, and protease. Reverse transcriptase converts viral RNA into viral DNA. At this point, several variants of HIV arise since reverse transcriptase is prone to errors during the conversion of viral RNA to viral DNA.[52] Viral DNA then enters the nucleus of the cell and becomes integrated into the cell's DNA by the retroviral integrase enzyme. The host cell genome now contains the genetic code of HIV. Activation of the host cell induces transcription of the proviral DNA which then produces RNA and proteins that are essential building blocks for the production of new viruses. The viral protease enzyme cleaves the long chains of HIV proteins into smaller individual proteins. These smaller HIV proteins, along with RNA of HIV and key replication enzymes, come together to assemble a new, immature virus particle. After this immature virus is formed, it pushes through the membrane of the cell, forms a protective coating around itself using a small portion of the cell membrane, and pinches off from the infected cell. This immature virus can infect new cells only after the HIV protease enzyme cleaves structural proteins in the virus, which leads to the formation of a mature virus.

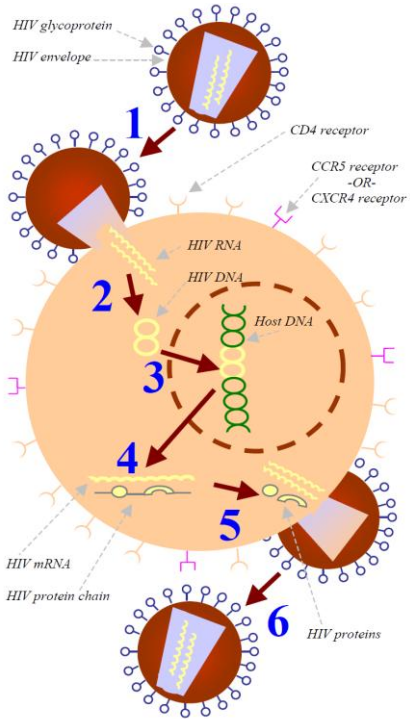


*Figure 1.11. The life cycle of HIV*[54]

Drugs that were developed to treat HIV infection are based on the concept that inhibiting one or all of the steps of the life cycle of HIV (i.e. replication, cell fusion, etc.) would limit the production of new viruses and thus reduce the number of infected cells.

## 1.3.4 The Critical Role of SEVI in HIV-1 infectivity

It was only 4 years ago that researchers published seminal findings that a proteolytic fragment of prostatic acid phophatase (PAP), a naturally abundant protein found in semen, greatly enhances the infectivity of HIV-1, by as much as 400,000-fold.[5]

In search of potential factors that modulate HIV-1 infection, researchers analyzed 294 fractions of peptides and proteins that are found naturally in seminal fluid. They discovered that one fraction, which contained fragments of PAP, enhanced the HIV-1 infection of $CD4^+$ T cells *in vitro*. Further analysis revealed that these active PAP fragments corresponded to residues 248-286 of PAP (Figure 1.12). Another key finding was that PAP248-286 was only active when it was in fibrillar form. Neither fresh solutions of PAP248-286 nor full-length PAP promoted HIV-1 infection. Fibrils of PAP248-286 were aptly dubbed 'SEVI', an acronym for 'semen-derived enhancer of virus infection'.


*Figure 1.12. Amino acid sequence of PAP248-286*

*In vitro* experiments, including timelapse microscopy, demonstrated that SEVI boosts HIV-1 infectivity by promoting HIV virion binding and fusion to target cells. SEVI is believed to improve virion fusion to target cells via two mechanisms. First, SEVI is intrinsically cationic, so it decreases the electrostatic repulsion between the negatively charged surface of the virion and the negatively charged surface of the target cell. Second, SEVI captures the HIV-1 virion and increases its rate of deposition onto the surface of the target cell, thereby promoting the likelihood of receptor-mediated viral entry.[55]

In light of these recent findings, inhibiting the enhancing effects of SEVI seems to be a promising objective in the prevention of HIV transmission. Our group has demonstrated that compounds that bind to SEVI can inhibit its ability to enhance HIV-1 infectivity.[56] We've shown that our proprietary compound BTA-$EG_6$ (Figure 1.13) inhibits both SEVI-mediated and semen-mediated enhancement of HIV-1 infectivity in a dose-dependent manner, while remaining nontoxic to cervical cells (Chapter 6). Based on these results, BTA-$EG_6$ may be a potential candidate as an additional ingredient in formulations of microbicides. Moreover, I've synthesized additional derivatives similar in structure to BTA-$EG_6$ that possess higher binding affinities toward SEVI fibrils. Chapter 7 goes into further detail about our experimental results.

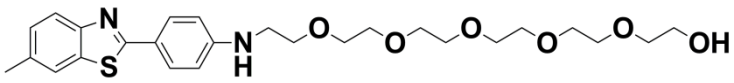


*Figure 1.13. Structure of BTA-$EG_6$*

## 1.4 Thesis Research Goals

When I began my graduate career in the Yang Research Group 5 years ago, I expressed to Dr. Yang that I wanted to expand my laboratory skill set. I came to UCSD with some synthetic knowledge; since joining the Yang lab, my breadth in scientific knowledge and laboratory skill set has indeed expanded. I believe this will be readily apparent to anybody that reads through the following chapters. A summary of my thesis research goals are listed below.

In the beginning of my graduate career, the Yang lab had developed two promising compounds, BTA-$EG_4$ (benzothiazole aniline tetra(ethylene glycol)) and BTA-$EG_6$ (benzothiazole aniline hexa(ethylene glycol)), derivatives of the well-known amyloid-binding compound, Thioflavin T. They demonstrated that BTA-$EG_4$ and BTA-$EG_6$ densely coat Aβ(1-42) aggregates[57] and, in doing so, block harmful protein-amyloid interactions in cellular assays.[58] However, to be useful for *in vivo* brain-related therapeutic applications, these compounds, *fundamentally*, must be able to permeate the brain to reach their intended target (Aβ aggregates). I, thus, implemented a practical and cost effective *in vitro* blood-brain barrier (BBB) model to assess the feasibility of taking these compounds forward to pre-clinical studies (*in vivo* mouse studies). I discuss in Chapter 2 the evaluation of the blood-brain barrier permeability of BTA-$EG_4$ and BTA-$EG_6$ by a previously described *in vitro* blood-brain barrier assay.[59] This BBB assay has since been used by other lab members in their Alzheimer's-related research and is a staple analytical tool in our lab.

In Chapter 3 I discuss the development of another analytical tool, an ELISA-based method that quantifies the association of small molecules to aggregated Aβ. Currently, the association of small molecules with Aβ is quantified by either fluorescence-based assays or by radioligand assays. This limits the type of compounds that can be analyzed to those that possess inherent fluorescence or to those that are radiolabelled. I developed an ELISA method that can estimate binding constants of small molecules from the low nanomolar to the low micromolar range, regardless of the inherent physical properties (i.e., spectroscopic properties) of the

molecules. This ELISA assay addresses the major limitation of previously reported binding assays by making it possible to evaluate small molecule-amyloid binding interactions without any obvious restrictions on the molecules that can be analyzed. This assay should, therefore, serve as a valuable tool in both industry and academic laboratories for developing novel diagnostics[36,37,60-62] (and possibly therapeutics[58]) for amyloid-associated neurodegenerative diseases.

Chapters 4 and 5 discuss our collaborative effort with the Theodorakis Research Group and I discuss the design and evaluation of a new class of compounds that bind to Aβ aggregates. These compounds have the advantage that their spectroscopic properties can be modified and fine-tuned via simple synthetic methods.

Halfway through the course of my graduate career, my thesis research evolved to include the study of small molecules that bind to an amyloid found in semen, called SEVI. Münch *et al.* revealed that SEVI fibrils significantly enhance the infectivity of HIV-1.[5] *In vitro* experiments, including timelapse microscopy, demonstrated that SEVI boosts HIV-1 infectivity by promoting HIV virion binding and fusion to target cells. SEVI is believed to improve virion fusion to target cells via two mechanisms. First, SEVI is intrinsically cationic, so it decreases the electrostatic repulsion between the negatively charged surface of the virion and the negatively charged surface of the target cell. Second, SEVI captures the HIV-1 virion and increases its rate of deposition onto the surface of the target cell, thereby promoting the likelihood of receptor-mediated viral entry.[55] Thioflavin T and its

derivatives are believed to bind to Aβ based on the β-sheet motif that is common to all amyloid fibrils.[63] We hypothesized that BTA-$EG_6$, a derivative of Thioflavin T and a compound that we previously demonstrated densely coats Aβ aggregates,[57] might also coat SEVI fibrils based on its β-sheet secondary structure, and thus inhibit HIV-1 interactions with SEVI fibrils and reduce SEVI-mediated enhancement of HIV-1 infectivity. We collaborated with the Dewhurst Research Group at Rochester University to explore our hypothesis. Chapter 6 details the results of these investigations.

As an extension to the work in Chapter 6, Chapter 7 details the design, synthesis, and evaluation of multivalent analogs of BTA-$EG_6$. The goals of this project, outlined in Chapter 7, were 2-fold: 1) Create compounds that would bind with high affinity to both Aβ fibrils and SEVI fibrils based on the multivalent design strategy and 2) evaluate whether oligomers of the BTA moiety exhibit improved ability over the BTA monomer to inhibit SEVI-mediated enhancement of HIV infectivity. For this particular project we again collaborated with the Dewhurst Research Group at Rochester University. Chapter 7 discusses the results of these investigations.

# Chapter 2

# The evaluation of the blood-brain barrier permeability of Aβ-targeting compounds by an *in vitro* model

## 2.1 Introduction

The blood-brain barrier (BBB) presents a major obstacle in the delivery of therapeutic and diagnostic agents that target brain-related conditions since the discriminatory BBB prohibits over 98% of drugs from entering into the brain. The impermeability of the BBB relative to other lipophilic membranes arises from the unique characteristics of the endothelial cells that comprise the BBB.[64] These endothelial cells interact with perivascular elements, such as pericytes and astrocyte end-feet to form a cooperative unit. These interactions, especially with astrocytes,

have been strongly implicated in inducing the distinctive properties of the BBB.[65-67] In addition to forming cell-cell adherens junctions, these endothelial cells effectively constrict the paracellular pathway by forming complex tight junctions via the interactions of several tight junction associated proteins—primarily occludin, the claudins, and the junctional adhesion molecules (JAMS). Moreover, the BBB possesses an active transport system that is arranged by a number of cytoplasmic accessory proteins, including the zonula occludens (ZO-1 and ZO-2) and cingulin.

We previously demonstrated that amyloid-targeting compounds developed in our lab—BTA-$EG_4$ and BTA-$EG_6$ (Figure 2.1)—densely coat Aβ(1-42) aggregates[57] and block harmful protein-amyloid interactions in cellular assays.[58] However, to be useful for brain-related therapeutic applications, these compounds, fundamentally, must be able to permeate the brain. Lipinski's rules for drugability are often applied in predicting the ability of potential drug candidates to passively diffuse through the blood-brain barrier.[68] BBB-permeable drugs are typically lipophilic, uncharged, and weigh less than 500 Daltons (Da). The molecular weight of both BTA-$EG_4$ and BTA-$EG_6$ fall within the required weight restrictions, at 417 Da and 505 Da, respectively. Moreover, both BTA-$EG_4$ and BTA-$EG_6$ are uncharged molecules and both possess a log*P* value of ~1 (determined by octanol:water partitioning experiments), which fall within the desired log*P* range of 1-3 for BBB-permeable compounds.[57] Thus, according to Lipinski's rules, both BTA-$EG_4$ and BTA-$EG_6$ are predicted to cross the BBB with relative ease. Though they offer useful pieces of

information, these rudimentary calculations are mere predictions and must be supplemented and confirmed with experimental evidence.

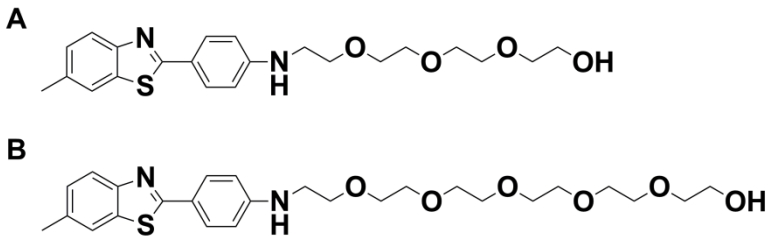


*Figure 2.1. The structures of amyloid-targeting compounds developed in the Yang lab (A) BTA-EG$_4$ and (B) BTA-EG$_6$*

Modeling the BBB *in vitro* provides a relatively rapid, inexpensive, and convenient method to evaluate the practicality of taking compounds designed and developed in our lab forward to pre-clinical trials (i.e. *in vivo* animal studies). To evaluate whether BTA-EG$_4$ and BTA-EG$_6$ crosses the blood-brain barrier in sufficient amounts, I implemented a previously reported *in vitro* BBB assay that has been demonstrated to reliably predict brain uptake of neuropharmaceuticals *in vivo*.[69] The correlation diagram of the *in vitro* BBB model vs. *in vivo* uptake in the brain of various compounds (Figure 2.2) demonstrates that this *in vitro* BBB model accurately predicts whether *in vivo* uptake will be low (i.e. sucrose) or high (i.e. nicotine).

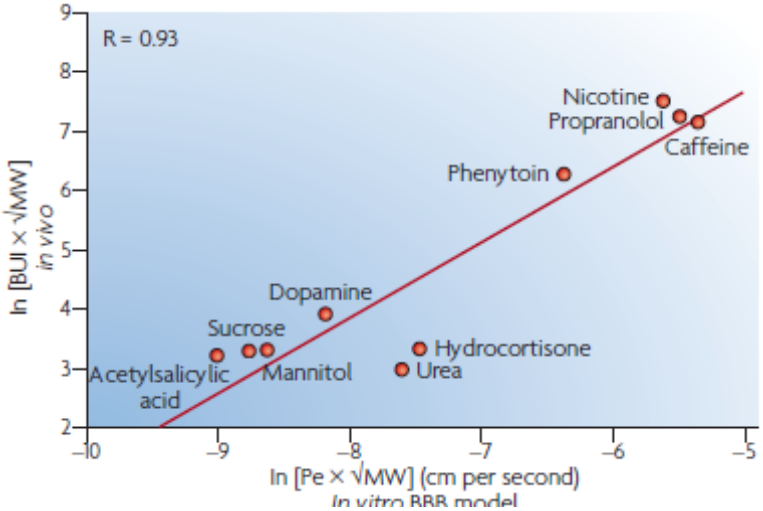


*Figure 2.2. Correlation diagram of the in vitro BBB model vs in vivo brain uptake.*[70] *Adapted with permission from Macmillan Publishers Ltd: NATURE REVIEWS DRUG DISCOVERY. Cecchelli, R.; Berezowski, V.; Lundquist, S.; Culot, M.; Renftel, M.; Dehouck, M. P.; Fenart, L. Nature Reviews Drug Discovery 2007, 6, 650-661, copyright 2007.*

In this *in vitro* BBB model, bovine brain microvascular endothelial cells (BBMVEC) are co-cultured with rat astrocytes (RA) (Figure 2.3) since there is strong evidence to suggest that astrocytes induce the intrinsic characteristics of the BBB. [65-67] BBMVEC co-cultured with RA exhibit a much higher transendothelial electrical resistance (TEER) value across the confluent monolayer (661 ± 48 Ω $cm^2$) than BBMVEC cultured without astrocytic input (416 ± 57 Ω $cm^2$),[71] which is attributed to the complex tight junctions that are formed in co-cultured BBMVEC. In addition, BBMVEC grown in the co-culture system express high levels of cell receptors, such as low-density lipoprotein and transferrin (which is important for *in vitro* studies geared towards receptor-mediated BBB entry),[72-74] as well as the active

efflux transporter P-glycoprotein (P-gp).[59] This *in vitro* model, therefore, presents a comprehensive and functional system that closely simulates the *in vivo* system.

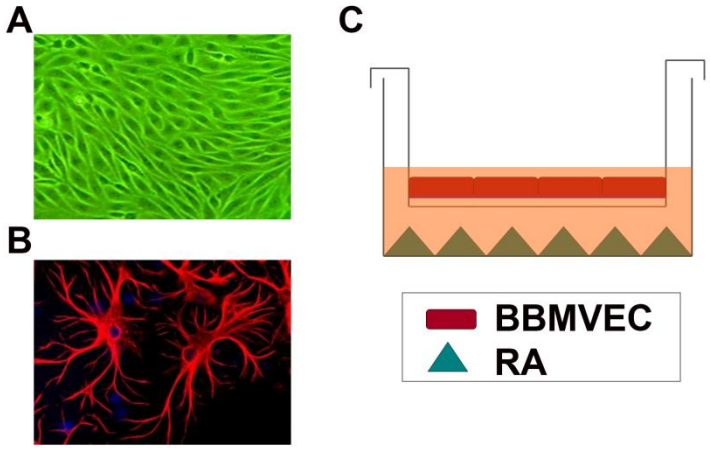


*Figure 2.3. An in vitro BBB model for examining the uptake of neuropharmaceuticals into the brain. A) A confluent layer of bovine brain microvascular endothelial cells B) Rat astrocytes C) Schematic diagram of the co-culture system, where RA are cultured on the bottom of a 6-well plate and BBMVEC are cultured on a microporous filter insert suspended in shared medium.*

## 2.2 Results and Discussion

I evaluated the BBB permeability of BTA-$EG_4$ and BTA-$EG_6$ using the *in vitro* system described above. In this assay format, solutions of the compound are added to microporous filters containing confluent monolayers of BBMVEC (Figure 2.4A). The filters are placed inside the wells of a 6-well plate and switched to new wells at 15 minute intervals to assess the amount of compound that crossed the BBMVEC monolayer at each time point and to minimize back diffusion of the compound from the lower chamber into the upper compartment. Filters containing no cells were also assayed to subtract any restrictive contributions from the filters (Figure 2.4B).

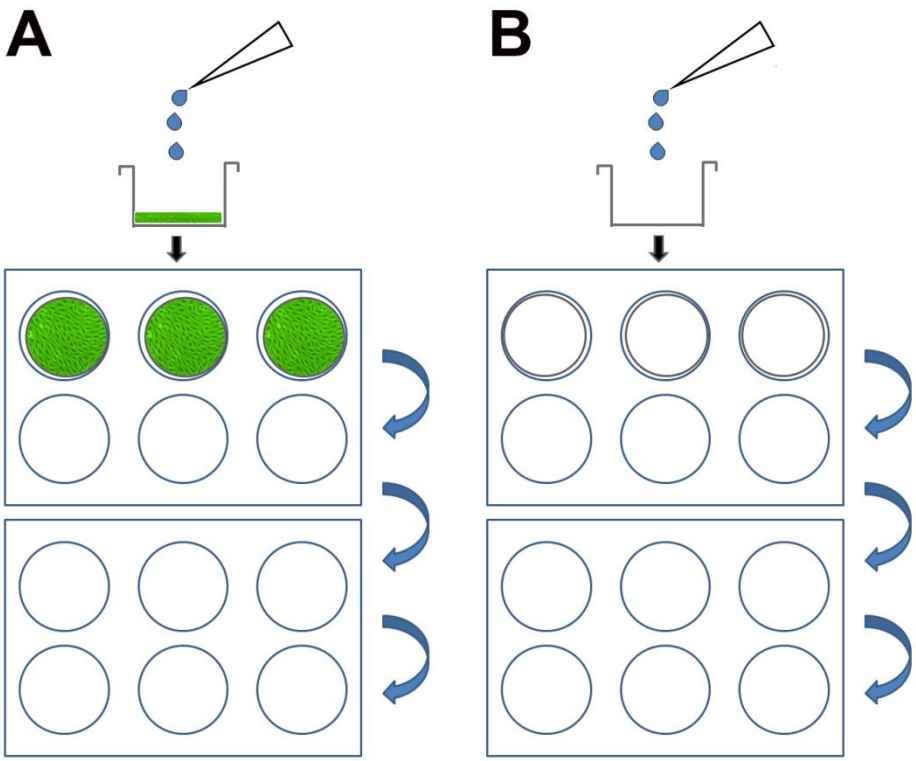


*Figure 2.4. Schematic Diagram of the in vitro BBB assay. Test compound is added to microporous filters containing confluent monolayers of BBMVEC (A) and to microporous filters alone (B). The filters are placed inside the wells of a 6-well plate and switched to new wells at 15 minute intervals to assess the amount of compound that crossed the BBMVEC at each time point.*

To assess the reproducibility of the BBB model with respect to reported literature values, I also evaluated Lucifer Yellow (LY), a charged compound with known low BBB permeability[75] and (-)-Nicotine, a compound known to be highly BBB permeable (Figure 2.5),[76] in this assay.

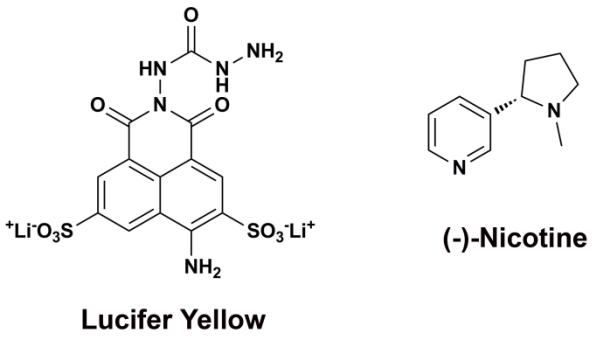


*Figure 2.5. Compounds with known low (Lucifer Yellow) and high ((-)-Nicotine) BBB permeability*

As expected, only small amounts of Lucifer Yellow were able to cross the BBB (Figure 2.6). Indeed, this highly charged compound is often used as a BBB integrity marker.[75] Since LY crossed only to a small extent, this provides evidence that, in our hands, we were able to replicate a functional, restrictive *in vitro* BBB system. I also evaluated the BBB permeability of (-)-Nicotine, and found that it crossed the BBB with relative ease. After 60 minutes, approximately 55% of (-)-Nicotine crossed the blood brain barrier. In contrast, only 12% of Lucifer Yellow crossed the BBB after 60 minutes (Figure 2.6).

Although they are structurally similar, BTA-$EG_4$ crossed the BBB to a greater extent than BTA-$EG_6$, which may be attributed to the slightly more lipophilic nature of BTA-$EG_4$ due to its shorter hydrophilic ethylene glycol chain. While only 21 % of BTA-$EG_6$ crossed the BBB, 41 % of BTA-$EG_4$ was able to cross the BBB after 60 minutes (Figure 2.6).

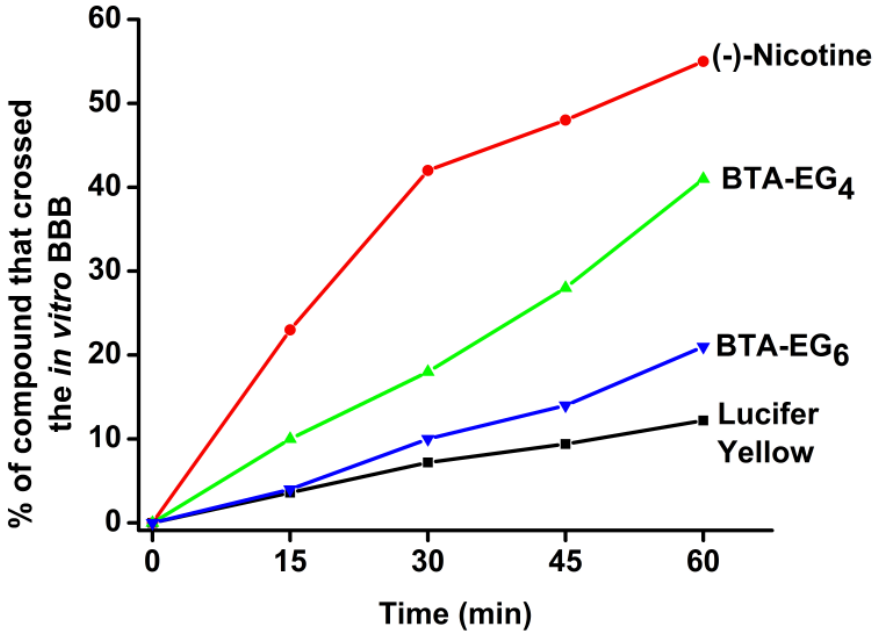


*Figure 2.6. Percentage of test compound that crossed the in vitro BBB over time.*

Next, in order to quantify the *in vitro* BBB permeability of these compounds, I calculated their permeability coefficients ($P_e$) and compared them to reported literature values (Table 2.1).[75,76] The $P_e$ values for Lucifer Yellow and (-)-Nicotine that I obtained in these experiments—$1.7 \times 10^{-3}$ cm/min and $22 \times 10^{-3}$ cm/min, respectively—are slightly higher than the reported values of $0.4 \times 10^{-3}$ cm/min for Lucifer Yellow and $17 \times 10^{-3}$ cm/min for (-)-Nicotine. These differences in experimental and literature $P_e$ values may arise from the slight modifications in my experimental methods compared to published methods. In published methods, bovine brain endothelial cells are cultured from seeded capillaries that are freshly harvested from the cortex of bovine brain.[75] In contrast, the bovine endothelial cells that I use are purchased as cryopreserved primary cells at low passage, from a commercial source. Nevertheless, the $P_e$ values that we obtained for LY and (-)-

Nicotine are consistent from experiment to experiment, and, as such, they provide a relative scale for $P_e$ comparison. BTA-$EG_4$ has a $P_e$ value of $16 \times 10^{-3}$ cm/min, while BTA-$EG_6$ has a $P_e$ value of $11 \times 10^{-3}$ cm/min. Because BTA-$EG_4$ possesses a higher $P_e$ value, it is predicted to cross the BBB to a higher extent in the *in vivo* situation than BTA-$EG_6$.

*Table 2.1. The permeability coefficients ($P_e$) of the compounds evaluated by this BBB assay*

| Compound | Results $P_e$ (* $10^{-3}$ cm/min) | Literature Value $P_e$ (* $10^{-3}$ cm/min) |
|---|---|---|
| Lucifer Yellow | 1.7 | 0.4 |
| (-) Nicotine | 22 | 17 |
| BTA-$EG_4$ | 16 | - |
| BTA-$EG_6$ | 11 | - |

## 2.3 Conclusions

Since I demonstrated that BTA-$EG_4$ crosses the BBB more efficiently than BTA-$EG_6$ in this BBB model, we've taken BTA-$EG_4$ (rather than BTA-$EG_6$) forward to *in vivo* animal testing. In these studies, BTA-$EG_4$ (10 mg/kg) was administered intraperitoneally in wild-type mice and rapidly distributed to the brain. The logarithmic ratio of the concentration of BTA-$EG_4$ partitioned in the brain and in the blood (log BB), at equilibrium, was calculated to be 0.43. These results are encouraging since mepyramine, a first generation antihistamine, has a similar log BB value of 0.46, and is known to readily distribute to the brain.[77] In addition, a survey of a library of compounds revealed that compounds with a log BB value >0.3 readily

permeate the brain.[78] In conclusion, the preliminary results I obtained using this *in vitro* BBB model established the basis for current and ongoing brain-related investigations with BTA-$EG_4$. The effects of BTA-$EG_4$ on the cognitive performance of wild-type mice are currently being investigated.[79]

## 2.4 Materials and Methods

### 2.4.1 Materials

Rat Astrocytes (Catalog #R1800) and Astrocyte Medium (Catalog #1801) were purchased from Sciencell. Bovine Brain Microvascular Endothelial Cells (#B840-05) and Bovine Brain Microvascular Endothelial Cells Growth Medium (#B819-500) were purchased from Cell Applications.

Collagen Type 1 (rat tail, Catalog # 354236), 100 mm Poly-D-Lysine culture dishes (Catalog # 356469), Poly-D-Lysine 6-well culture plates (Catalog # 356413), 100 mm Collagen I culture dishes (Catalog # 356450) were from BD Biosciences.

Polyethylene Terephthalate (PET) 1.0 μm inserts (Catalog #PIRP30R48) and uncoated 6-well cell culture plates (Catalog # PIMW50650) were purchased from Millipore. UV-transparent flat-bottomed 96-well plates were purchased from Corning (Catalog #3635).

Water (18.2 μΩ/cm) was filtered through a NANOPure Diamond™ (Barnstead) water purification system before use. HEPES (free acid) was purchased from EMD Biosciences, Inc. Sodium Phosphate Monobasic, $NaHCO_3$, NaCl were purchased from Fisher Scientific. KCl was purchased from JT Baker Chemicals. $CaCl_2$, $MgCl_2$, (+)-Glucose were from Sigma-Aldrich. (-)-Nicotine was from Sigma-

Aldrich (Catalog N3876). Lucifer Yellow was purchased from Invitrogen (Catalog # L-453). BTA-$EG_4$ and BTA-$EG_6$ were synthesized as previously described.[57]

## 2.4.2 Experimental Methods

**Culture of Bovine Brain Microvascular Endothelial Cells (BBMVEC)**: Cryopreserved BBMVEC (2nd passage, >5 x $10^5$ cells/ampoule) were seeded onto a collagen-coated 100 mm culture dish containing 15 mL BBMVEC medium and incubated overnight (in a humidified atmosphere of 95% air, 5% $CO_2$, at 37 °C) to promote cell attachment. After several days, confluent BBMVEC were subcultured at a split ratio of 1:20. Subcultured cells (up to passage 8) were cryopreserved in liquid nitrogen until further use.

**Culture of Rat Astrocytes (RA):** Cryopreserved RA (2nd passage, >1 x $10^6$ cells/ampoule) were seeded onto a poly-D-lysine-coated 100 mm culture dish containing 15 mL RA medium and incubated overnight (in a humidified atmosphere of 95% air, 5% $CO_2$, at 37 °C) to promote cell attachment. After several days, confluent RA were subcultured at a split ratio of 1:10. Subcultured cells were cryopreserved in liquid nitrogen until further use.

**Preparation of filters:** Rat tail collagen type I was dissolved in 70% ethanol (in $H_2O$) at a 1:3 volume ratio (collagen:ethanol). Each 1.0 μm PET microporous filter insert was coated with 400 μL of this solution and dried for >8 hours for complete evaporation of the solvent, at room temperature under sterile conditions. On collagen-coated microporous inserts, BBMVEC form well-organized confluent monolayers that express typical tight junctions.[59]

**Coculture of BBMVEC and RA:** Rat astrocytes were seeded onto a 6-well Poly-D-Lysine coated culture dish at a density of 2.4 x $10^5$ cells/well and incubated overnight (in a humidified atmosphere of 95% air, 5% $CO_2$, at 37 °C) to promote cell attachment. BBMVEC cells were then seeded onto collagen-coated 1.0 μm PET porous inserts at a density of 4x$10^5$ cells/mL and suspended in the 6-well culture dishes containing rat astrocytes. BBMVEC and RA were cocultured for 12 days after which the confluent BBMVEC layer was ready for the BBB permeability experiments.

***In vitro* study to assess BBB permeability of compounds:** 10 mL stock solutions of the test compound were prepared in Ringer-HEPES buffer (pH 7.4, 150 mM NaCl, 5.2 mM KCl, 2.2 mM $CaCl_2$, 0.2 mM $MgCl_2$, 6 mM $NaHCO_3$, 2.8 mM Glucose, 5 mM HEPES in nanopure $H_2O$). 2.5 mL Ringer-HEPES buffer was added to each well of several sterile, untreated 6-well plates (the receiver compartment). Microporous filter inserts (the donor chamber) containing confluent monolayers of BBMVEC were rinsed gently and thoroughly with PBS and nanopure $H_2O$ and then placed inside the 6-well plates containing Ringer-HEPES. 1.5 mL of the compound solution (100 μM of test compound or 50 μM in the case of Lucifer Yellow) was added to microporous filters containing the BBMVEC monolayer and to microporous filters containing no cells and the plates were covered and placed on a rocking shaker and incubated at 37˚C. The filters were transferred every 15 minutes to new wells containing fresh Ringer-HEPES to minimize back diffusion of the compound from the lower chamber into the upper compartment. Three filters

containing confluent BBMVEC monolayers and three filters with no cells were assayed for each compound. 50 μL aliquots were withdrawn from the receiver compartments at the 15, 30, 45, and 60 minute time points and 50 μL aliquots were taken from the donor chamber at 0 min and 60 minutes. These aliquots were pipetted into a UV-Vis transparent 96-well plate and analyzed spectrophotometrically using a plate reader (SpectraMax 190, Molecular Devices, LLC). The amount of compound in each well was calculated using a standard calibration curve.

**Data Analysis and Calculations**

In this assay, the amount of compound that crossed into the receiver compartment during incubation is converted into the cleared volume in order to obtain a concentration-independent parameter, as described by Siflinger-Birnboim *et al.*,[80] using the following equation:

$$V = \frac{[\text{compound}]_{\text{receiver compartment}}}{[\text{compound}]_{\text{donor chamber}}} \times V_{\text{receiver compartment}} \qquad \text{Equation 2.1}$$

The average cumulative cleared volume was plotted vs. time and the slope was calculated by linear regression analysis (Origin 7.0, Microcal, Inc.). The slope of the clearance curve of the filters with no cells and the filters containing a monolayer of BBMVEC is equal to $PS_f$ and $PS_t$, respectively, where PS refers to the permeability surface area product. The PS value for the endothelial monolayer, $PS_e$, was calculated using the following equation:

$$\frac{1}{PS_e} = \frac{1}{PS_t} - \frac{1}{PS_f}$$ Equation 2.2

To calculate the endothelial permeability coefficient, $P_e$ (cm/min), the $PS_e$ value is divided by S, the surface area (4.5 $cm^2$) of the filter insert:

$$P_e = \frac{PS_e}{S}$$ Equation 2.3

## 2.5 Additional Figures

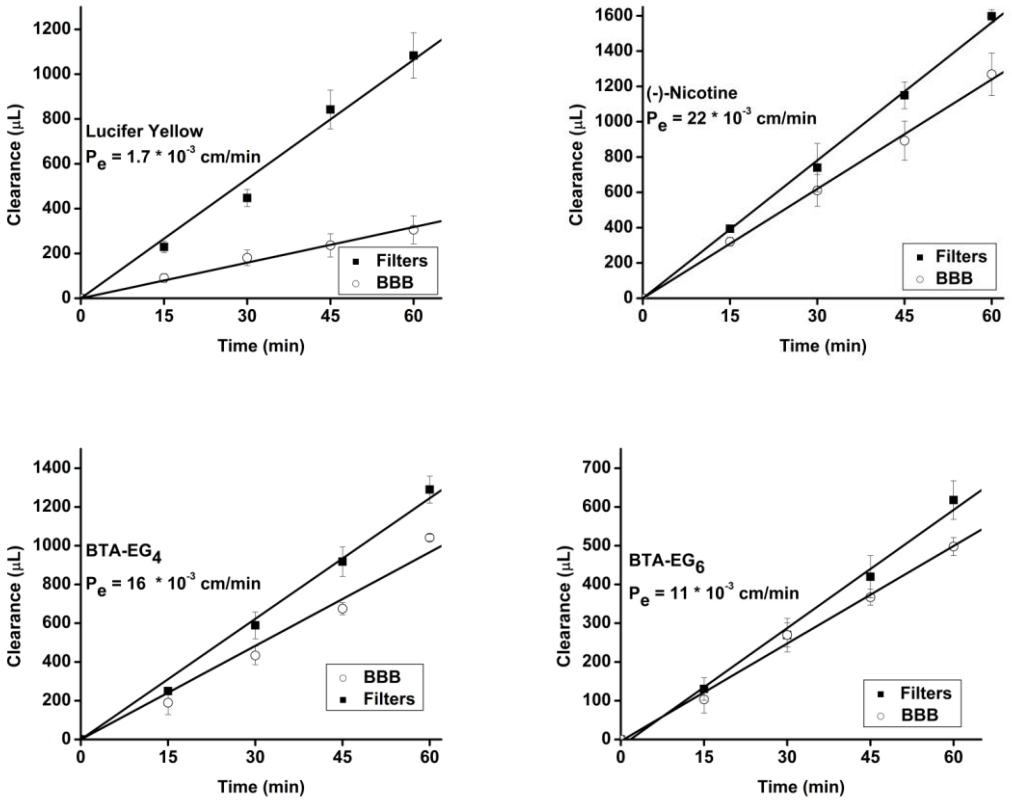


*Figure 2.7. Clearance curves of the compounds tested in the in vitro BBB assay*

## Notes about this Chapter

All work pertaining to the *in vitro* BBB assay outlined in this chapter was carried out by me. I would like to thank Vivisource Laboratories for carrying out the pre-clinical *in vivo* mouse studies and Dr. Lila K. Habib for analyzing and computing the log(BB) values.

# Chapter 3

# An ELISA-based Method to Quantify the Association of Small Molecules with Aggregated Aβ Amyloid Peptides

## 3.1 Introduction

Alzheimer's Disease (AD) is a progressive neurodegenerative disorder characterized by the deposition of senile plaques (along with neurofibrillary tangles) in the brain.[9] These senile plaques are primarily comprised of a 40-42 amino acid peptide called β-amyloid (Aβ) peptide. Currently, AD is diagnosed through the clinical evaluation of symptoms, but it can only be confirmed post mortem by the presence of amyloid deposits in brain tissue.[9] Methods for both early diagnosis and for monitoring the progression of AD are critical for the development of effective

treatments to combat this debilitating disease.[81] The clinical development of PET (positron emission tomography) and SPECT (single photon emission computed tomography) imaging agents that target deposits of aggregated Aβ peptides *in vivo* show tremendous promise for detecting changes in the accumulation of senile plaques in living patients.[36,60-62,82] These imaging techniques, therefore, provide a potentially useful means to follow the pathological progression of AD.

Methods to rapidly identify and quantify the association of small molecules to aggregated Aβ are critical for the development of new and improved imaging agents for diagnosing and monitoring AD. Currently, the association of small molecules with aggregated Aβ is usually quantified by radioactivity- or fluorescence-based assays.[83-85] However, these analytical methods limit the type of molecules that can be developed to those that are either inherently fluorescent or to those that are labeled with a radioisotope. Here, I describe a new ELISA-based assay to quantify the binding of small molecules to aggregated forms of Alzheimer's-related Aβ peptides. This method has the advantage that it does not require inherent radioactivity or fluorescent properties of the molecules being analyzed, consequently making it possible to quantify the binding of Aβ to a significantly more diverse set of molecules compared to current methods.

We previously reported a protein inhibition assay that could be used to qualitatively identify whether a small molecule could associate with aggregated forms of Aβ.[86] Since the molecules and antibodies were not introduced under competitive conditions in these previous studies, this inhibition assay, while simple,

rapid, and inexpensive, was not capable of revealing quantitative information on interaction between the small molecules and Aβ. In order to generate a similarly accessible assay that could be used for quantification of dissociation constants, I developed an ELISA-based competition assay that prevents significant denaturation of Aβ upon adsorption to hydrophobic ELISA plates, which can be an inherent general problem with quantitative ELISA assays.[87,88]

Many binding interactions between small molecules and Aβ are dependent on the secondary structure of Aβ. It is widely accepted that the β-sheet secondary structure common to amyloids is necessary for binding of histological agents such as Thioflavin T.[89] The conformation of the peptide is, therefore, an important consideration in assays that attempt to quantify the interaction between small molecules and aggregated Aβ peptides.

Since a typical ELISA protocol includes the deposition of a protein (here, aggregated Aβ) to the hydrophobic surface of a polystyrene 96-well plate, I developed a protocol that accounts for the effect of the surface on the conformation of Aβ. The influence of hydrophobic and hydrophilic surfaces on the conformation of Aβ peptide has been reported previously.[90-92] Giacomelli *et al.*,[93,94] for instance, found that aggregated Aβ adsorbed to hydrophilic surfaces retained the β-sheet conformation that is typically characteristic of Aβ aggregates in aqueous solution; adsorption of aggregated Aβ on hydrophobic surfaces generally lead to an increase in the α-helix content of aggregated Aβ. Based on these observations, I hypothesized that we would need to use hydrophilic materials in the development of a quantitative

ELISA protocol in order to mimic an aqueous solution environment and maintain the desired native conformation of the Aβ aggregates during analysis of small molecule-amyloid interactions.

Here, I investigated the conformation of Aβ aggregates on hydrophobic and hydrophilic surfaces and the association of small molecules to Aβ aggregates adsorbed to hydrophilic and hydrophobic surfaces.

## 3.2 Results and Discussion

ELISA assays routinely employ hydrophobic 96-well plates made from polystyrene (PS). I examined the influence of PS on the secondary structure of pre-aggregated Aβ(1-42) by dissolving a PS ELISA plate in toluene, spin-coating the PS onto a gold surface, evaporating the residual solvent from the PS, and examining aggregated Aβ peptides deposited on this thin film of PS by specular FTIR.

The amide I region of the IR spectrum (1600-1700 $cm^{-1}$) is associated with the C=O stretching vibration and, thus, can reveal information on the backbone conformation (e.g., β-sheet content) of the peptide.[95-99] Figure 3.1A shows the FTIR spectrum (black line) of Aβ(1-42) adsorbed on PS. Two major peaks of similar intensity centered at 1633 $cm^{-1}$ and 1676 $cm^{-1}$ appear in the amide I region of this spectrum. Second derivative spectral analysis of the amide I region[98,100] resolved the overlapping bands and revealed component bands centered at 1630 (red line), 1660 (green line), 1680 (blue line), and 1695 (cyan line) $cm^{-1}$, which correspond approximately to the relative abundance of β-sheet, α-helix/unordered, β-turns, and antiparallel β-sheet content, respectively.[101] The bands at 1695 $cm^{-1}$ may also

contain absorbance contributions from the Arg, Asn, and Gln sidechains. Subtracting the absorbance contribution of PS (at 1601 $cm^{-1}$ corresponding to the C=C stretch of the aromatic ring of PS) prior to peak fitting analysis and subsequent peak integration of the component band centered at 1630 $cm^{-1}$ revealed that the aggregated Aβ(1-42) adsorbed to PS contained ~37% β-sheet content. This value is significantly lower than the percentage of β-sheet content that is typically found in solution samples of aggregated Aβ peptides.[101,102]

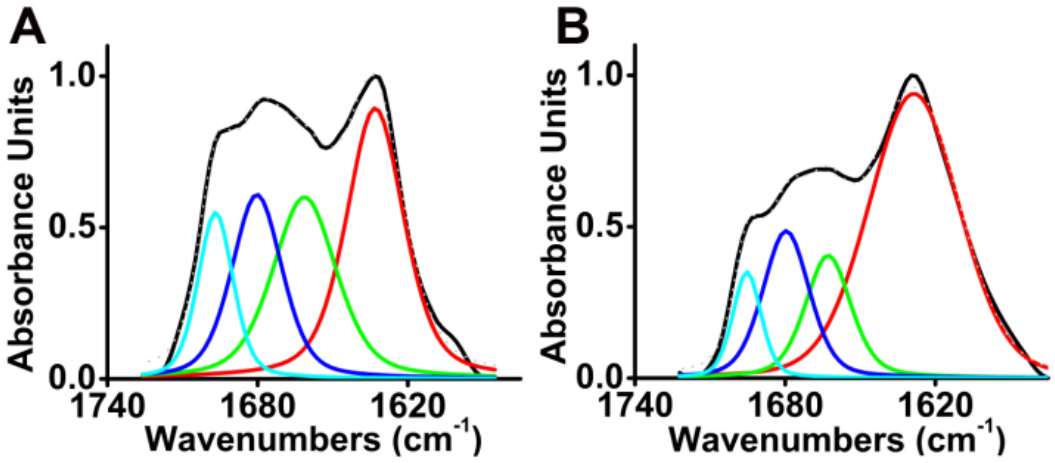


*Figure 3.1. The FTIR spectrum of aggregated Aβ(1-42) adsorbed on polystyrene (A) or on plasma oxidized polystyrene (B). The black lines denote the raw FTIR spectra. The red, green, blue, and cyan lines denote the β-sheet, α-helix/unordered, β-turns, and antiparallel β-sheet content, respectively, as estimated by second derivative spectral analysis.*[101]

In order to evaluate the effects of a hydrophilic material on the secondary structure of aggregated Aβ(1-42), I subjected the PS to an air plasma treatment to render the PS more hydrophilic.

Plasma treatment is routinely used to modify hydrophobic material into hydrophilic material.[103,104] Known as the fourth state of matter, everyday examples

of plasma include modern television sets, lightning, and the sun. Plasma consists of partially ionized gases made of electrons, positive ions, and neutral atoms or molecules. In our system, in order to generate a plasma, a radiofrequency (RF) oscillating electric field is applied to oxygen gas (from background air) under partial vacuum (<1800 mTorr) (Figure 3.2). Molecules of oxygen gas are accelerated in this electric field and gain enough kinetic energy to surmount the first ionization threshold required to strip an electron from a neutral atom or molecule. The energy of plasma is sufficient to ionize neutral atoms, break molecules apart to form reactive radical species, and generate excited states in atoms or molecules.[103,104] These reactive oxygen species, in turn, bombard the polystyrene surface, resulting in the oxidation of the exposed atomic layers of polystyrene and, ultimately, a more hydrophilic surface (Figure 3.3, left).[105,106]

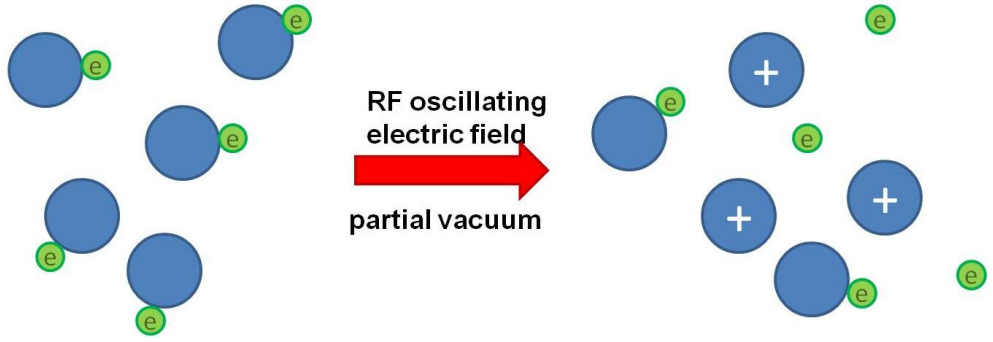


*Figure 3.2. A schematic of the generation of plasma by a RF field.*

Figure 3.3 shows the behavior of water droplets on a thin film of plasma-modified polystyrene (PMPS, left) and on untreated polystyrene (right). Water

droplets spread out on hydrophilic surfaces, whereas on untreated hydrophobic PS, water droplets bead together to minimize interaction with the hydrophobic surface.

*Figure 3.3. Water droplets on PMPS (left) and on PS (right)*

I incubated Aβ(1-42) on PMPS to evaluate the influence of this hydrophilic surface on the conformation of Aβ. Figure 3.1B shows the FTIR spectrum of Aβ(1-42) adsorbed on plasma-modified PS (PMPS). Second derivative spectral analysis revealed that aggregated Aβ(1-42) adsorbed on PMPS contained a β-sheet content of ~61%,which is consistent with the approximate β-sheet content that is typically found in solution samples of native aggregated Aβ peptides.[101,102] Thus, we conclude that deposition of the peptide on PMPS plates would result in better retention of the desired β-sheet secondary structure of aggregated Aβ(1-42), and, thus, might be more suitable for development of an ELISA protocol for quantifying dissociation constants between small molecules and aggregated Aβ peptides.

Figure 3.4 shows the IR spectra of aggregated Aβ(1-42) adsorbed on PS (green line) and on PMPS (blue line) as well as the IR spectra of PS (black line) and PMPS (red line). The IR spectrum of polystyrene shows the typical absorbance bands at 1601 $cm^{-1}$, 1493 $cm^{-1}$, and 1452 $cm^{-1}$. The absorbance band at 1601 $cm^{-1}$ corresponds to the C=C stretch of the aromatic ring, the band at 1493 $cm^{-1}$

corresponds to the in-plane bending mode of the aromatic ring, and the band at 1452 $cm^{-1}$ corresponds to C-H bending of the (-$CH_2$-) chain and to the in-plane bending mode of the aromatic ring.[107] Its important to note that while PMPS became more hydrophilic after plasma treatment, its IR spectrum was unaltered. Since plasma can only react with the exposed surface layer of the thin film, the bulk properties of the polystyrene film remain unmodified.[108,109] I created ultrathin films of PS (<100 nm thickness)[110] such that there would be minimal interference from the IR absorbances of PS with respect to the IR absorbances of Aβ(1-42).

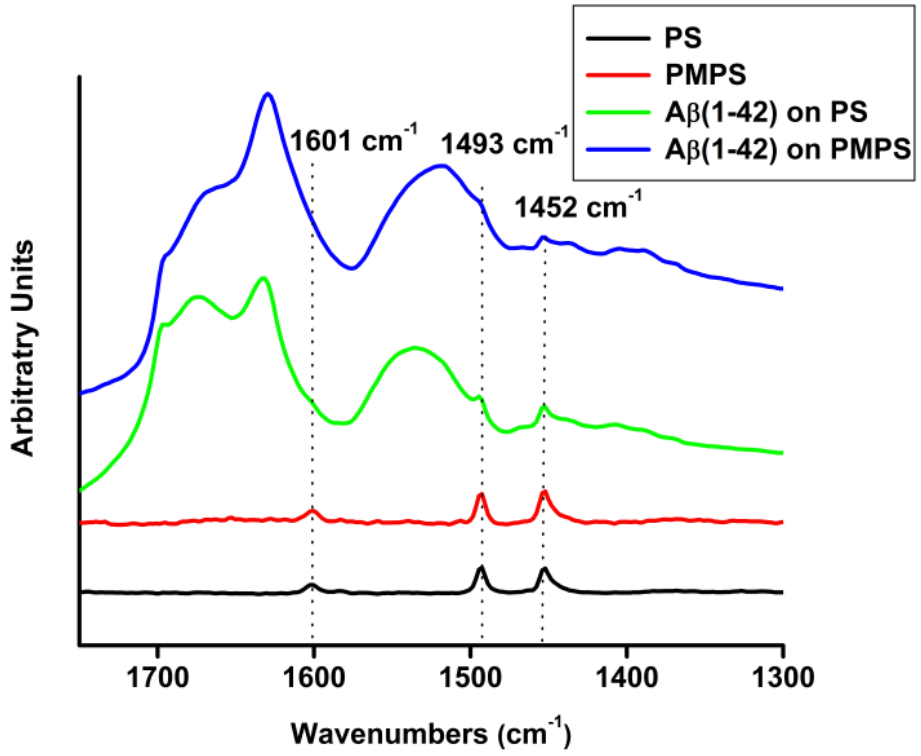


*Figure 3.4. The FTIR spectrum of PS (black line), PMPS (red line), Aβ(1-42) on PS (green line) and Aβ(1-42) on PMPS (blue line).*

Figure 3.5 outlines a general procedure for a modified quantitative ELISA protocol that can be used to estimate dissociation constants (here, reported as $K_i$'s since they are derived from a competition assay) for the binding of small molecules to aggregated Aβ(1-42) peptides. In this assay, the binding of small molecule to Aβ(1-42) is determined by its competition with a monoclonal anti-Aβ IgG (clone 6E10, $K_d$ = 340 nM[111]). We previously reported that this antibody effectively competes with multiple, different binding sites for small molecules along the aggregated Aβ(1-42) peptide surface.[86] I estimated the binding constants ($K_i$'s) of small molecules to aggregated Aβ peptides from the $IC_{50}$'s obtained directly from the ELISA assay using the Cheng-Prusoff equation:[112]

$$K_i = \frac{IC_{50}}{1+\frac{[C]}{K_c}} \qquad \text{Equation 3.1}$$

where C is the concentration of anti-Aβ IgG used in this assay and $K_c$ is the dissociation constant of the competing anti-Aβ IgG.

In order to provide a comparison for the $K_i$ values obtained from this assay, I evaluated the binding of five molecules whose binding constants to aggregated Aβ(1-42) had previously been reported in the literature[56,83,85,89,113,114] (Table 3.1). I performed the ELISA assay on both air plasma treated and untreated PS plates to examine whether treating the plates with air plasma was necessary for accurate estimation of $K_i$'s.

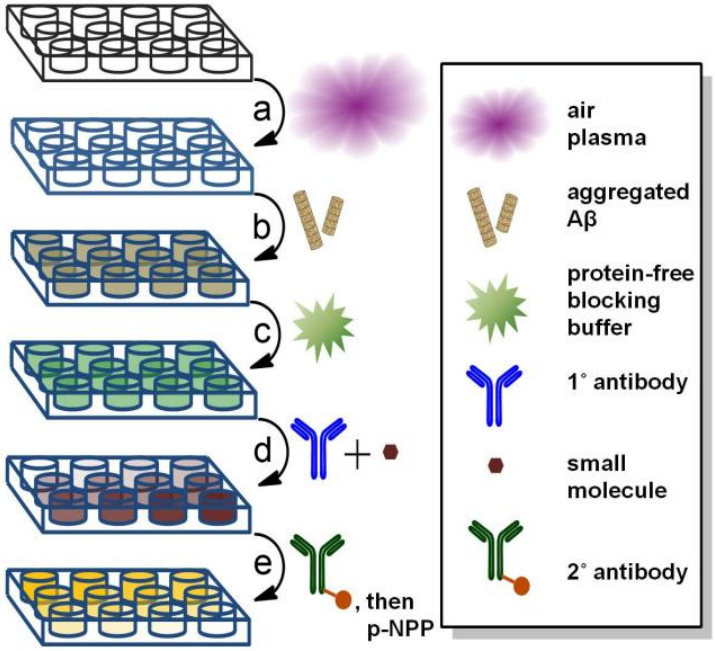


*Figure 3.5. Schematic representation for the experimental steps in a quantitative ELISA protocol for estimating competitive inhibition constants ($K_i$'s) for the interaction of small molecules with aggregated Aβ peptides. (a) We treat a commercial polystyrene 96 well plate with a 60 sec exposure to air plasma. (b) We deposit pre-aggregated Aβ(1-42) peptides into the wells. (c) We incubate the wells with a protein-free blocking buffer to minimize non-specific adsorption of the IgGs to the wells. (d) We co-incubate the wells with a fixed concentration of anti-Aβ IgG and increasing concentrations of small molecules. (e) After removal of all excess primary (1°) antibody, we incubate the wells with a secondary (2°) antibody conjugated to alkaline phosphatase followed by introduction of para-nitrophenyl phosphate (p-NPP). We quantify the relative abundance of 2° antibody remaining in each well using a UV-Vis microplate reader.*

The measured $K_i$'s for compound **1-5** are given in Table 3.1. In the case of fluorescent molecules Thioflavin T (**1**, ThT) and Congo Red (**2**), the $K_i$'s obtained from this ELISA assay on PMPS plates were similar to previously reported literature values obtained from fluorescence-based[56,83,85,89,113,114] or radioligand assays.[85,89,113,115,116] On untreated PS plates, compounds **1-5** exhibited a much lower

affinity for aggregated Aβ than they did on PMPS plates. These results suggest that air plasma treatment of PS was necessary to afford reliable estimations of $K_i$ values, which can be partly attributed to the ability of the plasma-modified surface to conserve the native secondary structure of aggregated Aβ.

*Table 3.1. Summary of the $K_i$ values obtained for compounds 1-5 for binding to Aβ(1-42) peptides using a quantitative ELISA format on polystyrene (PS) or plasma-modified polystyrene (PMPS). A) The structures of compounds **1-5**. B) Table of $K_i$ values obtained by a quantitative ELISA protocol on PS and PMPS or values.*

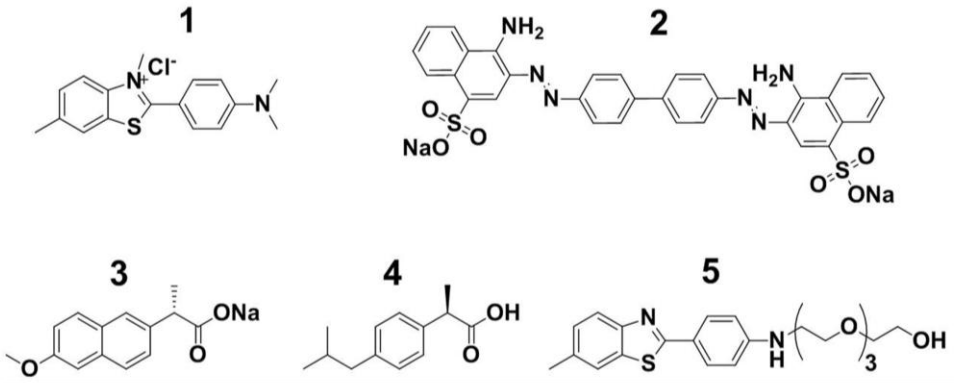


| Compound # | Name | $K_i$ (μM) on PS | $K_i$ (μM) on PMPS | Literature Values ($K_d$ or $K_i$, μM) |
|---|---|---|---|---|
| 1 | Thioflavin T | 164 ± 59 | 1.7 ± 0.2 | 2[b,d]<br>0.75[b,d] |
| 2 | Congo Red | 3.1 ± 0.6 | 0.45 ± 0.14 | 1.1[b,h]<br>1.5[b,e] |
| 3 | *(S)*-Naproxen Na | No Binding | 4.1 ± 2.2 | 0.0057[c,e,g]<br>>20[c,d,f]<br>>15[c,d] |
| 4 | *(R)*-Ibuprofen[a] | No Binding | 2.3 ± 1.4 | 44[c,e,g]<br>>15[c,d] |
| 5 | BTA-$EG_4$ | >1000 | 0.020 ± 0.008 | 0.02[b,d]<br>0.13[b,d] |

[a]2.5% DMSO in buffer; [b]$K_d$; [c]$K_i$; [d]determined by fluorescence assay; [e]determined by radioactivity assay; [f]10% EtOH used as a cosolvent; [g]1% EtOH used as a cosolvent; [h]measured by UV-Vis

Table 3.1 also summarizes the $K_i$ values of two non-fluorescent amyloid-binding molecules, *(S)*-Naproxen (**3**) and *(R)*-Ibuprofen (**4**).[83,85,116] I included these

molecules in the initial development of this ELISA protocol since their $K_i$'s for binding to Aβ(1-42) peptides had previously been reported from competition assays using known radiolabeled or fluorescent amyloid-binding molecules. Surprisingly, the literature $K_i$ value for *(S)*-Naproxen binding to aggregated Aβ varied significantly (by ~ 4 orders of magnitude), presumably due to the use of different formats for analysis (i.e., fluorescence- vs radioactivity-based competition assays) or due to the significant difference in the structures of molecules used as competitors in these previously reported assays. This discrepancy in reported $K_i$ values highlights the need for developing novel and general platforms for the quantitative and comparative study of small molecules that bind to aggregated amyloid peptides. I demonstrated that the quantitative ELISA protocol on PMPS could be used to estimate $K_i$ values for **3** and **4**, even though these molecules are not inherently fluorescent or radioactive. The $K_i$ value of 4.1 μM for *(S)*-Naproxen that I measured is in better agreement with the low micromolar values reported by Lockhart *et al.*[113] and Levine[83] compared to the low nanomolar $K_i$ value reported by Agdeppa *et al.*[116] Additionally, the low micromolar $K_i$ value that I estimated for (*R*)-Ibuprofen was also similar (within an order of magnitude) to the reported literature values.[83,116] Lastly, I estimated the $K_i$ for BTA-$EG_4$ (**5**) using this ELISA protocol, an amyloid-targeting molecule with potential therapeutic applications for AD.[58] The 20 nM $K_i$ value that we measured for **5** is comparable to the $K_i$ values reported for a number of benzothiazole aniline (BTA) derivatives (low to mid nM range).[56,83]

The accuracy of this new ELISA-based method for quantifying the interaction of small molecules with amyloid targets is based on at least the following two assumptions: 1) The method assumes that the small molecules exhibit a 1:1 stoichiometry with the anti-Aβ IgGs that compete for overlapping binding sites for Aβ. This same assumption is made for previously reported competition assays used to estimate the binding constants of amyloid-targeting molecules.[83,85,113,116] Deviations from this 1:1 binding stoichiometry (e.g., if it requires more than one small molecule to competitively displace an antibody from the amyloid surface) could lead to reported $K_i$ values that were weaker than the true value. The similar values between the $K_i$'s estimated for **1** and **2** and the literature $K_d$ values for these molecules (which were not obtained through competition, and therefore, do not require the assumption of a 1:1 binding stoichiometry with a competitor), however, suggests that making the rough approximation of a 1:1 stoichiometry between the small molecules and the IgG leads to reasonably accurate values for binding constants. 2) The method assumes that the small molecules do not significantly interact with the monoclonal anti-Aβ IgG during the co-incubation step (step d in Figure 3.5) of the ELISA protocol, and, therefore, do not affect the estimation of $K_i$ values. I did not observe a change in the absorbance or emission spectrum of ThT (**1**) when it was incubated with the anti-Aβ IgG alone in solution, suggesting that ThT (and, presumably, molecules **2-5**) does not significantly interact in a non-specific manner with the IgG (Figure 3.7) to affect the accuracy of the ELISA assay.[89,117,118]

## 3.3 Conclusions

I have, thus, developed a simple and accessible method for quantifying the binding of small molecules to aggregated Aβ peptides. We demonstrate that this ELISA method can estimate binding constants of small molecules from the low nanomolar to the low micromolar range, regardless of the inherent physical properties (i.e., spectroscopic properties) of the molecules. A key step in this assay is the air plasma treatment of the polystyrene surface of the ELISA plates, which helps maintain the native β-sheet content of the amyloid peptides during analysis. The relatively large size of the IgG[119] makes it possible for it to compete with multiple, different binding sites for small molecules along the surface of the amyloid,[86] thus, making it a general competitor for many classes of molecules. This ELISA assay addresses the major limitation of previously reported binding assays by making it possible to evaluate small molecule-amyloid binding interactions without any obvious restrictions on the molecules that can be analyzed. This assay only requires access to a UV-Vis microplate reader and an air plasma generator (both common and relatively inexpensive laboratory equipment), can be carried out with minimal training of laboratory personnel, and should be readily translatable to amyloidogenic peptides other than Aβ. This assay should, therefore, serve as a valuable tool in both industry and academic laboratories for developing novel diagnostics[36,37,60-62] (and possibly therapeutics[58]) for amyloid-associated neurodegenerative diseases.

## 3.4 Materials & Methods

### 3.4.1 Materials

Sodium chloride, sodium dihydrogen phosphate monohydrate; potassium chloride and sodium hydroxide were purchased from Baker; Congo Red, *(S)*-Naproxen sodium, and magnesium chloride were from Sigma-Aldrich; diethanolamine and p-nitrophenyl phosphate were purchased from Fluka; Thioflavin T was purchased from MP Biomedical; *(R)*-Ibuprofen was from Biomol; All reagents were used without further purification. BTA-$EG_4$ was synthesized as previously described.[57]

Water (18.2 μΩ/cm) was filtered through a NANOPure DiamondTM (Barnstead) water purification system before use. Buffers were prepared fresh for each experiment.

Protein-Free Blocking Buffer was purchased from Piercenet (Catalog # 37572).

As primary IgGs against Aβ, monoclonal anti-Aβ IgG (clone 6E10, mouse, derived from residues 3-8 of Aβ peptide as antigens,) was obtained from Covance Signet (Cambridge, MA, Lot 08BC00306). The secondary anti-mouse IgG (anti-mouse IgG H+L conjugated with alkaline phosphatase, polyclonal, from rabbit) was purchased from Abcam (Lot # 588335).

Aβ(1-42) peptide was obtained from Biopeptide, Inc.

96-well polystyrene plates were from Thermo Scientific (Catalog #269620).

Gold-coated silicon wafers were purchased from Sigma-Aldrich (Catalog # 643262).

Reagent-grade toluene was from Sigma-Aldrich.

## 3.4.2 Experimental Methods

**Growth of aggregated Aβ**:

Aβ aggregates were grown from synthetic Aβ(1-42) peptides by reconstituting the lyophilized peptide in ultrapure $H_2O$ (final concentration 111 μM) and incubating the peptides at 37 °C for 72 h. Aβ aggregates were characterized by circular dichroism (CD) for the presence of β-sheet secondary structure. We previously reported that this procedure produces mostly fibrillar structures.[120,121] CD measurements were performed on an AVIV spectropolarimeter at room temperature. Spectra were recorded from 260 nm to 190 nm in a 1-mm cuvette pathlength, 1 nm stepsize (Figure 3.6).

**Air plasma treatment of polystyrene plates**:

Polystyrene plates were treated with air plasma for a duration of 60 seconds, rendering them hydrophilic. The air plasma was generated under partial vacuum (<1800 mTorr) in a Harrick Plasma Cleaner/Sterilizer (Model PDC- 32G). Plates were used in the assay immediately after treatment. Hydrophilicity was assessed qualitatively, by observing the behavior of water at the surface. Water droplets spread out on hydrophilic surfaces, whereas on untreated hydrophobic PS, water droplets bead together to minimize interactions with the hydrophobic surface.

**Procedure for quantitative ELISA:**

All incubation steps were done at 25°C unless stated otherwise. Phosphate buffered saline (PBS, 10 mM sodium phosphate, 138 mM sodium chloride, 2.7 mM potassium chloride, pH 7.4) was prepared fresh for each experiment.

**ELISA protocol for competition of anti-Aβ IgG-Aβ interactions using small molecules**:

The wells of air plasma-treated or untreated 96-well plates were coated with aggregated Aβ peptide by incubating each well for 6 h with 50 μL of a 1.4 μM solution of aggregated Aβ in PBS. After removal of solutions containing excess Aβ, 300 μL of protein-free blocking buffer was added to each well and incubated for 1 h. The blocking buffer was removed and the wells were washed three times with PBS. The wells were then incubated for 12 h at 4˚C with 50 μL solutions containing various concentrations of small molecule (obtained by diluting a stock solution) and a fixed concentration of anti-Aβ IgG (clone 6E10, Lot 08BC00306, 1 nM in Protein-Free Blocking Buffer). The amount of bound monoclonal IgGs was quantified by removing the excess solution, washing the wells three times with 300 μL of PBS buffer, and incubating for 45 min with 50 μL of a polyclonal secondary rabbit IgG (anti-mouse IgG, 6.8 nM in Protein-Free Blocking Buffer) conjugated with alkaline phosphatase. The wells were then washed five times with 300 μL of PBS buffer. The relative amount of secondary IgG bound in each well was quantified by adding 50 μL of a solution containing *p*-nitrophenyl phosphate (*p*-NPP, 2.7 mM, in 0.1 M diethanol amine/ 0.5 mM magnesium chloride, pH 9.8) to each well. The plates

were incubated until a color change was observed under visual inspection. The concentration of *p*-nitrophenoxide was quantified at 405 nm using a UV-Vis microplate reader. Note: the color change upon developing the PMPS plates should not take more than one hour.

Each data point (Figures 3.8 and 3.9) from this assay represents the average of four independent measurements. Error bars represent standard deviations. Graphs were normalized, plotted, and fitted with the sigmoidal curve fitting option in Origin 7.0 (Microcal Software, Inc., Northhampton, MA) to obtain $IC_{50}$ values. $K_i$ values for these compounds were calculated using the Cheng-Prusoff equation for competitive binding:[112]

$$K_i = \frac{IC_{50}}{1+\frac{[C]}{K_c}} \qquad \text{Equation 3.1}$$

where [C] is the concentration of anti-Aβ IgG used in this assay and $K_c$ is the dissociation constant of the anti-Aβ IgG to Aβ). The conversion of $IC_{50}$ to $K_i$ for estimating the binding of small molecules to Aβ in competition assays is the same as reported by others.[85,113]

In order to evaluate whether a 12 h incubation period was sufficient to reach equilibrium for competitive binding of small molecules and the anti-Aβ IgG, we incubated the small molecules and IgG with the aggregated Aβ in the wells for 3 h instead of the 12 h incubation period. We found that the $K_i$ values obtained from this quantitative ELISA protocol was the same with either the 3 h or 12 h incubation periods, suggesting that 3 h was a sufficient duration of time to reach equilibrium.

For the data shown in Table 3.1, we reported values for $K_i$ using an incubation time of 12 h for consistency.

**Determination of the binding constant ($K_c$) of anti-Aβ IgG (clone 6E10) to aggregated Aβ:**

The determination of $K_c$ was based on an ELISA assay according to Friguet *et al.*[122] Various concentrations of Aβ aggregates (16.4 μM -30.9 pM) were incubated with anti-Aβ IgG (clone 6E10, 0.59 nM) in 1% BSA/PBS buffer for 2 hours. Each well of a 96-well plate was coated for 3 hours with 50 μL of a 1.3 μM solution of Aβ in PBS buffer. Solutions in the wells were discarded and the wells were blocked with 300 μL of 1% BSA/PBS for 30 minutes, followed by washing the wells twice with 300 μL PBS buffer. 50 μL of the various solutions containing Aβ and anti-Aβ IgGs were incubated in the wells for one hour. 50 μL of various concentrations of anti-Aβ IgG (2.3 nM – 2.2 pM in 1% BSA/PBS) were incubated at the same time as a concentration standard. The solutions were then removed and the wells washed twice with 300 μL of PBS buffer. The amount of bound anti-Aβ IgG was quantified with an alkaline phosphatase conjugated secondary antibody as outlined in the assay above. The dissociation constant ($K_c$) was fitted using a Scatchard analysis and was determined to be 340 ± 7 nM.

**Procedure for Preparation of Samples for Surface IR measurements**

**Procedure for spin-coating thin films of polystyrene on gold:**

Gold-plated silicon wafers (1000 Å Au layer thickness) were rinsed with acetone, water, 3:1 $H_2SO_4$: 30% $H_2O_2$, water, and then ethanol. The wafers were then dried overnight in a dessicator under vacuum.

Ultrathin films of PS were generated according to Hall *et al.*[110] Briefly, a 2% (w/v) polystyrene (PS) solution was made by dissolving 2 g of a polystyrene ELISA plate in 100 mL reagent-grade toluene. 4 mL of the 2% PS solution was deposited onto a gold-plated silicon wafer. The initially stationary wafer was accelerated (~2-3 seconds) on a spincoater and rotated at 2000 rpm for 60 seconds to give a uniform PS film thickness of approximately 100 nm. Spun films were dried overnight under vacuum.

The PS-coated wafers were scored and cut into 1 cm x 1 cm squares. Immediately prior to the surface studies, a portion of these PS-coated squares were subjected to air plasma treatment, similar to the procedure above for ELISA plates, to render them hydrophilic (plasma-modified polystyrene, PMPS).

**Incubation of aggregated Aβ on air plasma treated and untreated polystyrene surfaces:**

Aβ aggregates were prepared as previously described.[120] 100 uL of aggregated Aβ(1-42) in nanopure $H_2O$ was deposited onto PS-coated wafers and on PMPS-coated wafers. 100 μL nanopure $H_2O$ was deposited onto the PS and PMPS surface to serve as controls and as reference spectra. The squares were covered and

incubated for 6 hours. After incubation, excess water was removed under a flow of dry nitrogen. IR spectra were recorded on a Magna-IR 550 spectrophotometer (Nicolet) equipped with a liquid nitrogen-cooled MCT detector and an ATR accessory (Spectratech, ATR Magna 60 FTIR Accessory). Each spectrum was recorded at 4 $cm^{-1}$ resolution and is an average of at least 256 scans. The reference IR spectrum (PS incubated with $H_2O$ or PMPS incubated with $H_2O$) was subtracted from the corresponding spectrum of aggregated Aβ incubated on PS or PMPS. The spectra were then baseline corrected between 1720 $cm^{-1}$ and 1580 $cm^{-1}$ and smoothed at a 9 $cm^{-1}$ resolution. Second derivative analysis was applied using the Savitsky-Golay algorithm to resolve conformational structure bands.[98] We performed a least square iterative curve fitting using a mix of Gaussian and Lorentzian line shapes on the spectra between 1700 and 1600 $cm^{-1}$. The percentage of each secondary structure motif was determined by calculating the areas of each component band with respect to the total area of the original spectrum between 1700-1600 $cm^{-1}$. Baseline correction, reference subtraction, data smoothing, second derivative analysis, peak fitting, and peak integrations were all carried out using Omnic software (version 7.3). Additional data analysis was completed using Origin 7.0 (Microcal Software, Inc., Northhampton, MA). All experiments were repeated at least 3 times.

**Control Study to assess nonspecific binding of Thioflavin T to the anti-Aβ IgG (clone 6E10):**

A 40 μM solution of Thioflavin T (ThT) in PBS was incubated with a solution of 1.4 μM aggregated Aβ(1-42) or 1.4 μM Anti-Aβ IgG to give a final concentration of 20 μM ThT and 0.7 μM of protein. Solutions containing only 0.7 μM ThT or only 0.7 μM protein were also incubated in PBS. The solutions were mixed and then 100 μl of each solution was pipetted into a cuvette (ultramicrocuvette,10-mm light path, Hellma®, Müllheim, Germany). Fluorescence, indicative of ThT binding,[83] was determined at 450 nm excitation and 485 nm emission with a spectrofluorometer (Photon Technology International, Inc., Birmingham, NJ), using a solution of ThT alone as a reference (i.e., blank). Graphs were plotted using Origin 7.0 software (Microcal Software, Inc., Northhampton, MA).

## 3.5 Additional Figures

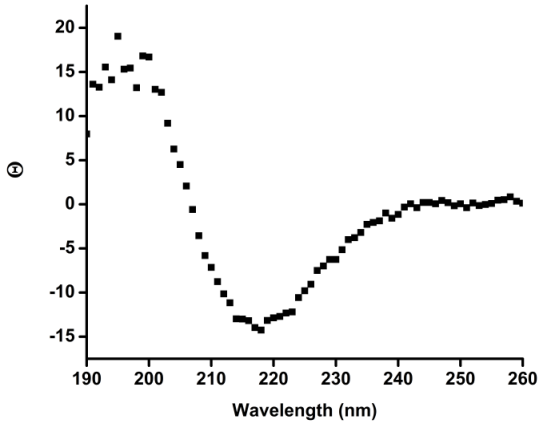


*Figure 3.6. CD spectrum of 111 μM Aβ(1-42) in nanopure $H_2O$ indicating significant β-sheet content for the amyloid.*[123]

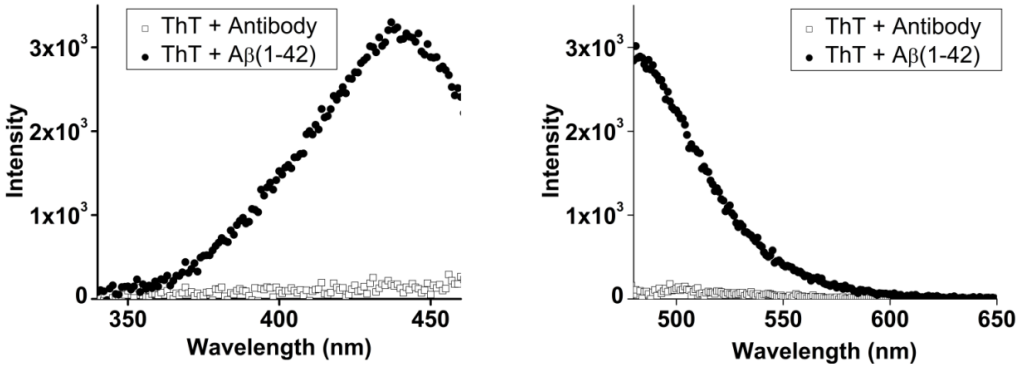


*Figure 3.7. The excitation (left) and emission (right) spectra of Thioflavin T (ThT) that was incubated alone with the anti-Aβ antibody (□) or alone with Aβ(1-42) (●). The excitation and emission spectrum from a solution of ThT alone was used as a blank reference for these spectra to better highlight any spectral changes induced by interaction of ThT with the proteins. The lack of significant spectral changes in the excitation and emission spectra of ThT upon incubation with the anti-Aβ antibody suggests that ThT does not significantly interact non-specifically with the antibody. This result is in contrast to the expected large spectral change observed for the interaction of ThT with the aggregated Aβ peptides (●).*

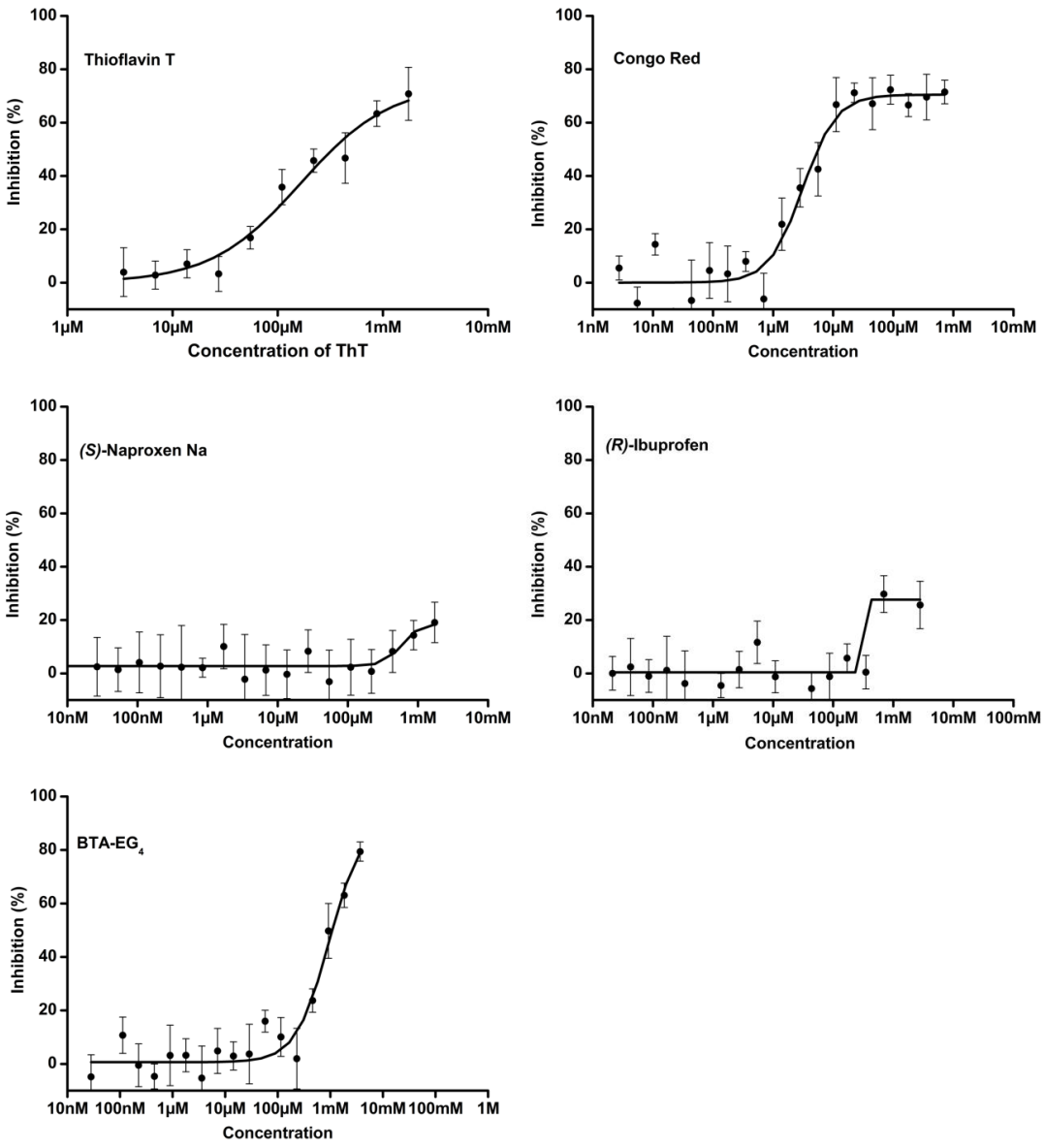


*Figure 3.8. The inhibition curves for compounds **1**-**5** in the competitive ELISA protocol using untreated polystyrene plates.*

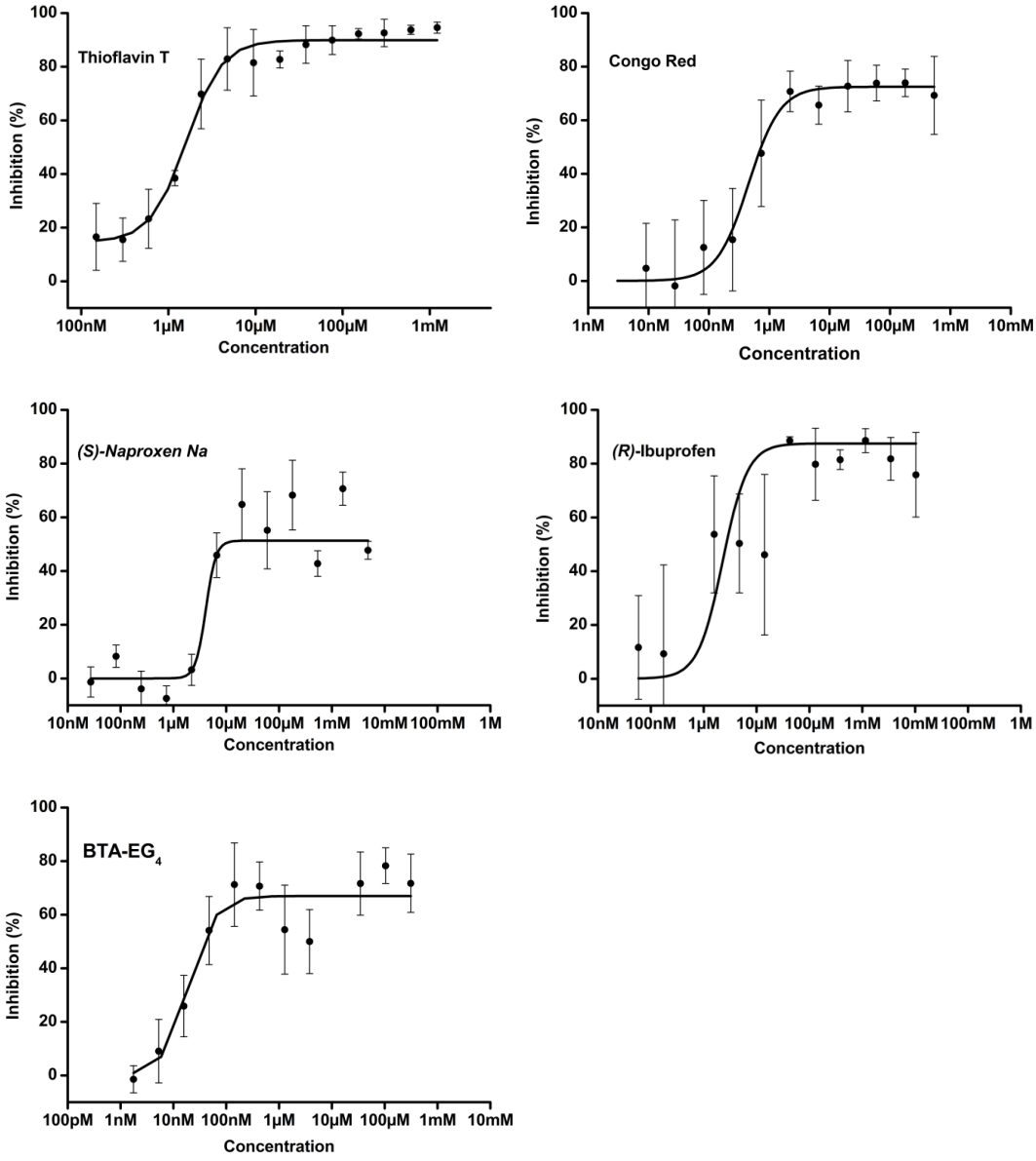


*Figure 3.9. The inhibition curves for compound **1-5** in the competitive ELISA protocol using plasma-modified polystyrene plates.*

## Notes about this Chapter

I would like to thank Dr. Petra Inbar for determining the binding constant of the anti-Aβ IgG (clone 6E10) to Aβ aggregates. Aside from this, all work presented in this chapter was carried out by me. This chapter contains material that has been

submitted for publication: “An ELISA-based Method to Quantify the Association of Small Molecules with Aggregated Aβ Peptide.” Capule, C.; Yang, J. I am the primary author of this pending manuscript.

# Chapter 4

# Rational Design of Amyloid-binding Agents based on the Molecular Rotor Motif

## 4.1 Introduction

Alzheimer's disease (AD) is characterized by a progressive loss of cognitive function and constitutes the most common and fatal neurodegenerative disorder.[124,125] Genetic and clinical evidence supports the hypothesis that accumulation of amyloid deposits in the brain plays an important role in the pathology of the disease. This event is associated with perturbations of biological functions in the surrounding tissue leading to neuronal cell death, thus contributing to the disease process. The deposits are comprised primarily of amyloid (Aβ) peptides, a 39–43 amino acid sequence that self aggregates into a fibrillar β-pleated sheet motif. While the exact three-dimensional structure of the aggregated Aβ

peptides is not known, a model structure that sustains the property of aggregation has been proposed.[126,127] This creates opportunities for *in vivo* imaging of amyloid deposits that can not only help evaluate the time course and evolution of the disease, but can also allow the timely monitoring of therapeutic treatments.[128-130]

Historically, Congo Red (CR) and Thioflavin T (ThT) have provided the starting point for the visualization of amyloid plaques and are still commonly employed in post mortem histological analyses (Figure 4.1).[131,132] However, due to their charge these probes are unsuitable for *in vivo* applications.[133] To address this issue, several laboratories developed probes with noncharged, lipophilic (log*P* = 0.1–3.5) and low-molecular weight chemical structures (MW<650) that facilitate crossing of the blood–brain barrier.[134] Further functionalization of these compounds with radionuclides led to a new generation of *in vivo* diagnostic agents (Figure 4.1) that target plaques and related structures for imaging with positron emission tomography (PET) and single-photon emission computed tomography (SPECT).[135-137] Despite these advances, there is a pressing need for the design and development of new amyloid-targeting molecules with improved physical, chemical, and biological characteristics.[138,139] At present, identification of new amyloid sensing molecules is based mainly on modification of existing dyes[140,141] and/or screening of libraries of dyes.[142,143]

Examination of the chemical structures shown in Figure 4.1 reveals that the majority of these probes contain an electron-donor unit in conjugation with an electron acceptor (D-π-A motif). This motif is a typical feature in molecular rotors, a

family of fluorescent probes known to form twisted intramolecular charge-transfer (TICT) complexes in the excited state producing a fluorescence quantum yield that is dependent on the surrounding environment.[144,145] Following photoexcitation, this motif has the unique ability to relax either via fluorescence emission or via an internal nonradiative molecular rotation. This internal rotation occurs around the σ-bonds that connect the electron-rich π-system with the donor and acceptor groups, and can be modified by altering the chemical structure and microenvironment of the probe.[146] Hindrance of the internal molecular rotation of the probe by increasing the surrounding media rigidity, or by reducing the available free volume needed for relaxation, leads to a decrease in the nonradiative decay rate and consequently an increase in fluorescence. In contrast, relaxation proceeds mainly via nonradiative pathways in environments of low viscosity or of high free volume. Due to these properties, molecular rotors have been used to study polarity, free volume, and viscosity changes in solvents and organized assemblies,[147,148] such as liposomes,[149] cells,[148,150,151] and polymers.[152,153]

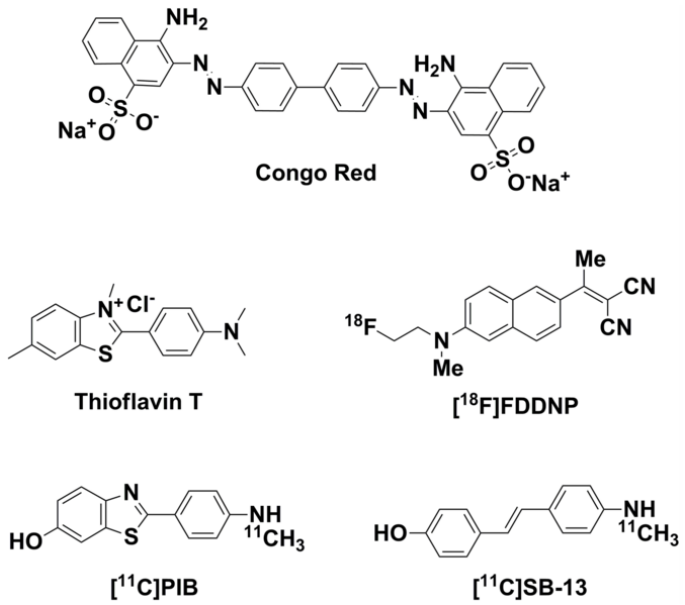


*Figure 4.1. Structures of selected amyloid imaging agents*

Intrigued by these observations, we asked whether we could design amyloid-binding agents based on the molecular rotor motif. We envisioned that π-conjugation of a dialkyl amino group, as the electron donor (D), with a 2-cyano acrylate unit as the electron acceptor (A), would produce Aβ-binding molecules with inherent fluorescence properties.[154,155] Interestingly, the fluorescence properties of such a motif could be fine-tuned by modifying the electronic density and extent of conjugation between the donor and acceptor units. The solubility of these amyloid-binding agents in aqueous media can be achieved by the introduction of water solubilizing groups (WSG), such as esters of triethylene glycol monomethyl ether (TEGME) or of glycerol. The design concept is shown in Figure 4.2.

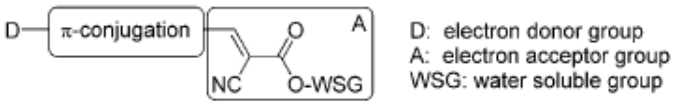


*Figure 4.2. Design of amyloid-binding agents based on the structure of a molecular rotor (D-π-A motif).*

## 4.2 Results and Discussion

Molecular rotors **JS-1** – **JS-7** (Figure 4.3) were synthesized using a key Knövenagel condensation of the appropriate aldehyde with the appropriate malonic acid derivative (see methods section of this chapter for additional details).

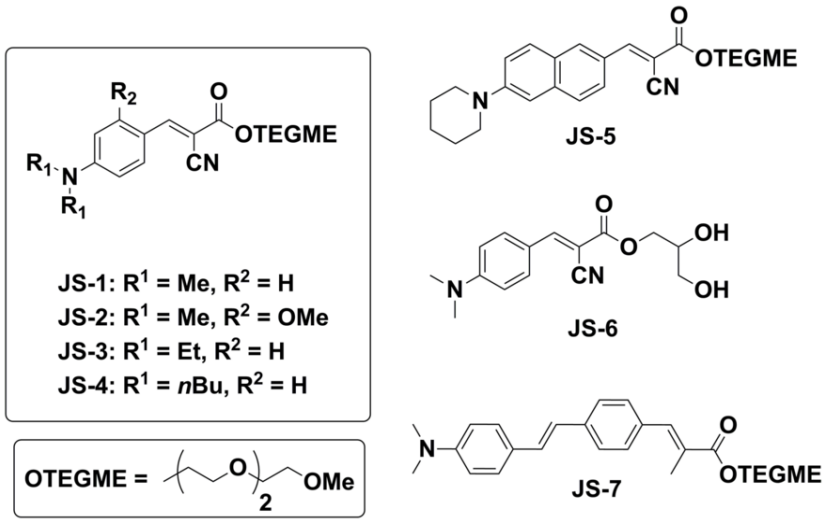


*Figure 4.3. Structures of molecular rotors*

An initial study to determine whether a probe can associate with aggregated Aβ is to compare its fluorescence spectra before and after mixing with the Aβ aggregates.[140-143] Typically, a fluorescent amyloid-binding agent displays a significant fluorescence intensity increase after binding to Aβ aggregates as compared to its native fluorescence in solution.[156] Along these lines, we measured

the fluorescent properties of each probe at 4 μM before and after mixing with preaggregated Aβ(1–42) peptides (5 μM, aggregated in PBS buffer for 3 days at 25 ˚C).

*Table 4.1. Table of fluorescence profile and related values for the interaction of the synthesized probes with aggregated Aβ(1-42) peptides.*

| Compound | Excitation Maximum[a] (nm) | | Emission Maximum[a] (nm) | | Fold | $K_d$ | $R^2$ | $I_{max}$[b] | $IC_{50}$[b] | Log *P* |
|---|---|---|---|---|---|---|---|---|---|---|
| | before | after | before | after | increase | (μM) | | (%) | (μM) | |
| JS-1 | 439 | 435 | 476 | 470 | 1.8 | 2.6 | 0.93 | 81 | 129 | 1.74 |
| JS-2 | 442 | 444 | 478 | 469 | 1.3 | 5.3 | 0.99 | 92 | 1.2 | 1.54 |
| JS-3 | 445 | 442 | 478 | 470 | 4.2 | 4.8 | 0.96 | 98 | 11.4 | 2.49 |
| JS-4 | 432 | 440 | 466 | 468 | 9.4 | 4.4 | 0.95 | 91 | 90.6 | 4.62 |
| JS-5 | 445 | 440 | 462 | 538 | 9.3 | 2.5 | 0.98 | 58 | 74.3 | 3.81 |
| JS-6 | 437 | 434 | 476 | 467 | 2.2 | 3.3 | 0.99 | 79 | 82.1 | 1.07 |
| JS-7 | 312 | 319 | 658 | 638 | 2.3 | 1.4 | 0.98 | 40 | 33.6 | 4.30 |

[a] Before or after binding [b] Maximum percent inhibition ($I_{max}$) and $IC_{50}$ values were determined by ELISA assay.

In all cases, a 1.3- to 9.4-fold fluorescence intensity increase was observed in the presence of aggregated Aβ, indicating that these compounds bind to the peptide (Table 4.1). In most cases a modest blue shift (6–20 nm) was observed upon binding. Only in the case of the naphthalene-based probe **JS-5** was a significant red shift of 76 nm observed upon binding to preaggregated Aβ (Figure 4.4c and d). Interestingly, this binding was accompanied with a 9.3-fold intensity increase. A similar intensity increase has been observed with FDDNP[157] and may be explained by the ability of the naphthalene motif to create excimers upon binding to its target.[158,159] Probes **JS-1** and **JS-2** exhibited similar fluorescence characteristics suggesting that addition of a methoxy group on the phenyl group does not alter the binding properties of the probe. On the other hand, it is worth noting that increasing the size of the alkyl groups of the nitrogen leads to a significant increase in the fluorescence intensity after binding (Table 4.1, **JS-1**, **JS-3**, **JS-4**). This is likely a

result of the decreased rotational freedom of the molecules upon binding to the aggregated forms of Aβ peptide.[160,161]

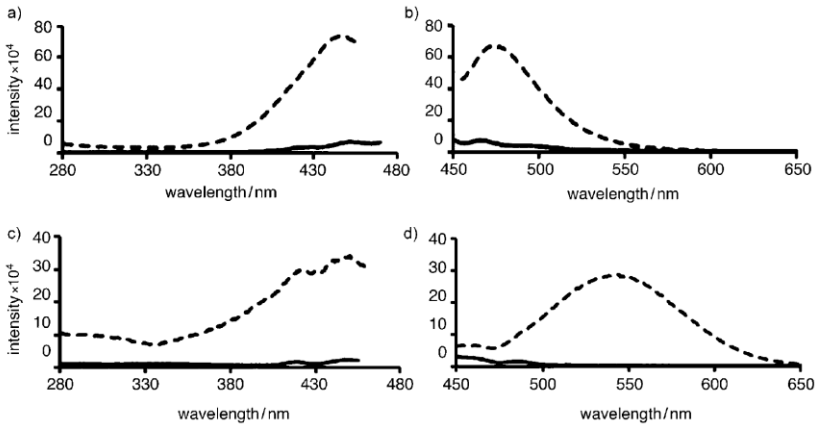


*Figure 4.4. Fluorescence excitation (a,c) and emission spectra (b,d) of probes **JS-4** (a,b) and **JS-5** (c,d) in PBS(—) and in the presence of aggregated Aβ peptides (---).*

Interestingly, no increase of fluorescence intensity was observed upon mixing of these probes with monomeric Aβ peptide (see section 4.5 Additional Figures). This supports the notion that these probes bind selectively to aggregated forms of Aβ. The fluorescence profile of **JS-4** (excitation and emission) is shown in Figure 4.4a and b.

We also measured the apparent binding constants ($K_d$) of the probes (in concentrations of 10, 5, 2.5 and 1.25 μM) to 5.0 μM preaggregated Aβ(1–42) peptide. The $K_d$ can be measured from the double reciprocal of the fluorescence maximum ($F_{max}$) and the concentration of the probe.[156] All $K_d$ values were measured between 1.4 and 5.3 μM (Table 4.1). It is remarkable that, despite the structural differences, these probes display similar $K_d$ values suggesting that they bind in a similar fashion to aggregated Aβ. Moreover, these values are similar to the reported

$K_d$ values for ThT (2 μM).[85,156,162,163] The double reciprocal plot of fluorescence intensity versus concentration of probes **JS-4** and **JS-5** are shown in Figure 4.5. The $K_d$ corresponds to the -1/(x-intercept) of the linear regression.[156]

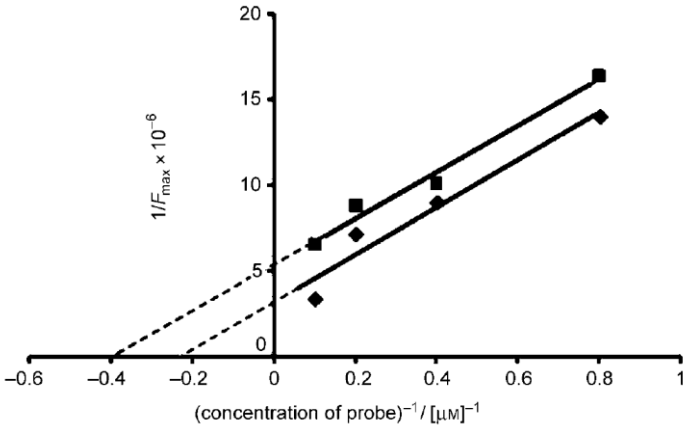


*Figure 4.5. Determination of the apparent binding constant ($K_d$) of probes **JS-4** (♦;$R^2$ = 0.95) and **JS-5** (■;$R^2$ = 0.98) to preaggregated Aβ peptide.*

The association of the synthesized compounds with aggregated Aβ peptides was tested using a semi-quantitative ELISA-based assay developed by Yang and co-workers.[57,86,121] The assay is based on screening for molecules that inhibit the interaction of the aggregated Aβ peptide with a monoclonal anti-Aβ IgG raised against residues 1–17 of Aβ. Table 4.1 shows the concentrations of the probes corresponding to 50% inhibition ($IC_{50}$) of the IgG-Aβ interactions as well as the maximal percentage of IgG inhibited from binding to the aggregated peptide. All probes exhibited $IC_{50}$ values at micromolar levels, the lowest value being measured for compound **JS-2** ($IC_{50}$ = 1.2 μM). The maximum inhibition ($I_{max}$), a measure of the extent of surface coating of the aggregated peptide by the probes,[57,86,121] was determined to be between 40–98% (Table 4.1). Comparison of these data indicates that the surface coating increases by decreasing the size of the probe or the extent of

the π system. Specifically, while the maximum inhibition is between 81–98% for the phenyl compounds, it decreases to 58% for the longer naphthalene compound **JS-5** and to 40% for the more conjugated stilbene **JS-7**. Representative graphs for **JS-4** and **JS-5** are shown in Figure 4.6.

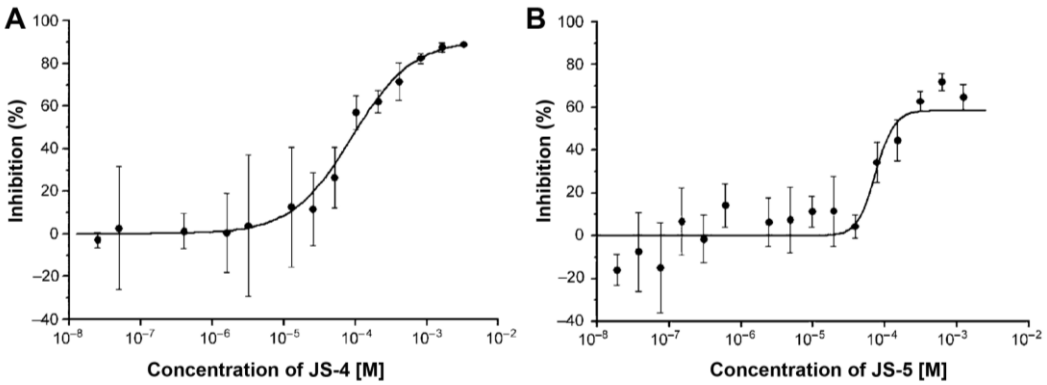


*Figure 4.6. Inhibition of IgG-Aβ interactions with probes A)* ***JS-4*** *($I_{max}$ = 91%, $IC_{50}$ = 91 μM) and B)* ***JS-5*** *($I_{max}$ = 58%, $IC_{50}$ = 74 μM.)*

The logP values for all the compounds were calculated to be between 1.07 and 4.62 (Table 4.1)[164] indicating that most of these probes meet the solubility criteria and should be able to cross the blood–brain barrier.[57,86,121,165] Finally, all compounds showed little or no cytotoxicity against human neuroblastoma cells at concentrations up to 100 μM (Figure 4.7). These properties represent significant advantages for further *in vivo* evaluation.

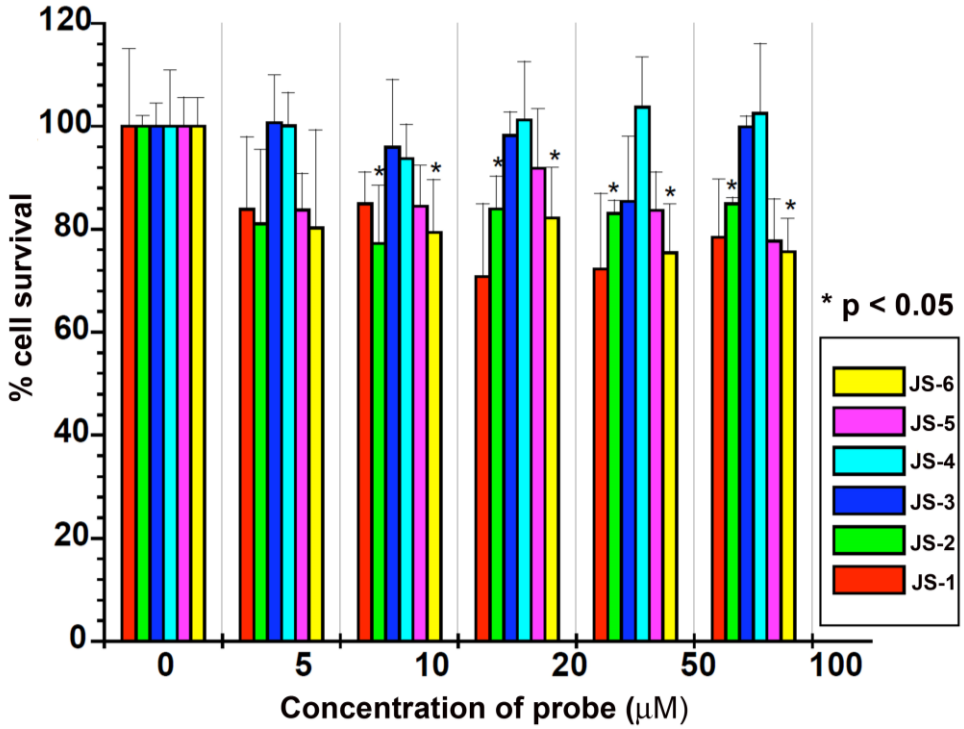


*Figure 4.7. Cytotoxicity data of probes **JS-1** – **JS-6** on SHSY-5Y human neuroblastoma cells as determined by MTT assay*

## 4.3 Conclusion

In conclusion, inspired by the structures of the currently used amyloid-binding agents, we have evaluated the possibility to design new Aβ-binding fluorescent probes based on the molecular rotor motif. We found that the molecular rotors, designed based on the concept shown in Figure 4.2, bind to aggregated Aβ peptide with low micromolar affinity. We hypothesize that this binding is a result of hydrophobic interactions between the rotor and the amyloid peptide. This binding reduces the free volume around the rotor, resulting in an increased fluorescence emission.[166,167] A similar effect has been reported for the binding of molecular rotors

to actin, albumin, and other proteins.[168,169] We have demonstrated that these molecules can be readily synthesized and have no significant cytotoxicity. In addition, we have shown that both the physical properties and fluorescence profile of these probes can be fine-tuned by modifying their chemical structure. Notably, substituent changes in the electron donor group can affect the intensity of fluorescence emission, while changes in the π-system can affect the emission wavelength. These effects can be implemented for the construction of multicolored dyes and can lead to potential applications for *in vitro* and *in vivo* imaging.[170] Interestingly, a recent report describes the identification of CRANAD-2,[171] a small molecule containing two electron-donating groups connected simultaneously via π-conjugation to a single difluoroboronate acceptor. This probe has a high affinity for Aβ aggregates ($K_d$=38.0 nM) and suitable near-infrared fluorescence properties for *in vivo* imaging, further validating our proposed concept of exploring the molecular rotor motif for the development of new amyloid-imaging probes. These findings demonstrate that the D-π-A motif of molecular rotors, presented in Figure 4.2, is a privileged scaffold and represents an important first step for the rational design of new diagnostic tools for Alzheimer's disease and related amyloid-based neurodegenerative disorders.

## 4.4 Materials and Methods

### 4.4.1 Materials

All the reagents were obtained (Aldrich, Acros) at highest commercial quality and used without further purification except where noted. Air- and moisture-sensitive

liquids and solutions were transferred via syringe or stainless steel cannula. Organic solutions were concentrated by rotary evaporation below 45 °C at approximately 20 mm Hg. All non-aqueous reactions were carried out under anhydrous conditions.

Reactions were monitored by thin-layer chromatography (TLC) carried out on 0.25 mm E. Merck silica gel plates (60F-254) and visualized under UV light and/or developed by dipping in solutions of 10% ethanolic phosphomolybdic acid (PMA) or p-anisaldehyde and applying heat. E. Merck silica gel (60, particle size 0.040-0.063 mm) was used for flash chromatography. Preparative thin-layer chromatography separations were carried out on 0.25 or 0.50 mm E. Merck silica gel plates (60F-254).

NMR spectra were recorded on Varian Mercury 300 or 400 MHz instruments and calibrated using the residual non-deuterated solvent as an internal reference. (HRMS) were recorded on a VG 7070 HS mass spectrometer under electron spray ionization (ESI) or electron impact (EI) conditions.

Fluorescence spectroscopy data were recorded on a MD-5020 Photon Technology International Spectrophotometer at 25 °C.

## 4.4.2 Experimental Methods

**General procedure for the preparation of fluorescence probes.**

To a round bottom flask containing a solution of aldehyde (5.0 mmol) and 2-(2-(2 methoxyethoxy)ethoxy)ethyl 2-cyanoacetate (5.5 mmol) in 20 ml of tetrahydrofuran (THF) was added 0.50 mmol of piperidine and the mixture was heated at 50 °C. The reaction was monitored by TLC and was completed within 21

hours. The crude mixture was concentrated under reduced pressure and the product was purified via flash chromatography (10-30% ethyl acetate in hexane).

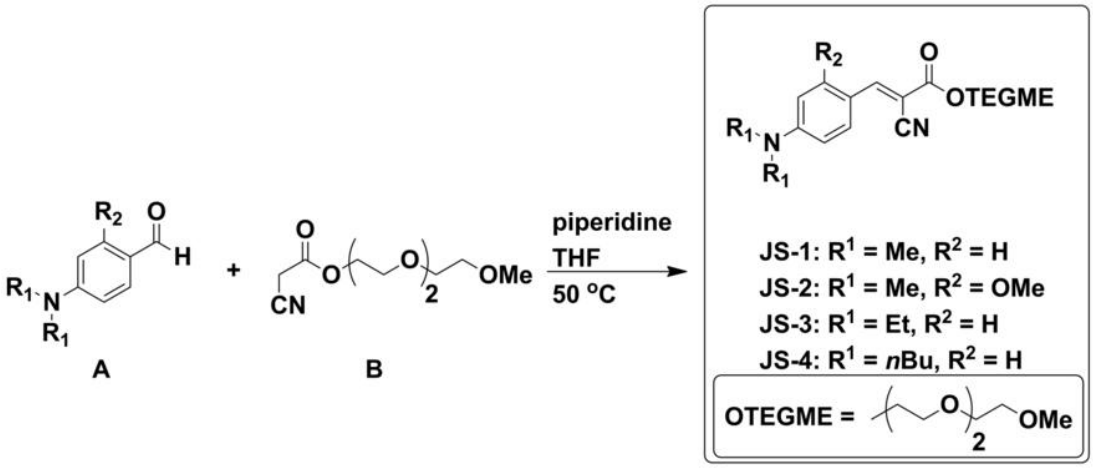


*Figure 4.8. Schematic for the synthesis of probes **JS-1** – **JS-4***

**(E)-2-(2-(2-methoxyethoxy)ethoxy)ethyl 2-cyano-3-(4 (dimethylamino)phenyl) acrylate (JS-1).** 98% ; yellow solid; $^{1}$H NMR (400 MHz, $CDCl_3$): δ = 8.07 (s, 1H), 7.93 (d, 2H, *J*= 9.0 Hz), 6.69 (d, 2H, *J*= 9.1 Hz), 4.41 (m, 2H), 3.81-3.79 (m, 2H), 3.73-3.65 (m, 6H), 3.56-3.54 (m, 2H), 3.37 (s, 3H), 3.10 (s, 6H); $^{13}$C NMR (100 MHz, $CDCl_3$): δ = 164.2, 154.7, 153.6, 134.1, 119.3, 117.4, 111.4, 93.6, 71.9, 70.8, 70.6, 70.5, 68.9, 65.0, 59.0, 40.0; HRMS calc for $C_{19}H_{26}N_2O_5$ $(M)^+$ 362.1836; found 362.1841.

**(E)-2-(2-(2-methoxyethoxy)ethoxy)ethyl2-cyano-3-(4-(dimethylamino)-2-methoxyphenyl)acrylate (JS-2).** 98% yield; yellow solid; $^{1}$H NMR (400 MHz, $CDCl_3$): δ = 8.64 (s,1H), 8.39 (d, 1H, *J*= 9.2 Hz), 6.63 (dd, 1H, *J*= 2.3 Hz, *J*= 9.2 Hz), 6.01 (s, 1H), 4.40 (m, 2H), 3.87 (s, 3H), 3.81-3.78 (m, 2H), 3.73-3.65 (m, 6H), 3.56-3.53 (m, 2H), 3.36 (s, 3H), 3.10 (s, 6H); 13C NMR (400 MHz, $CDCl_3$): δ =

165.0, 162.2, 155.9, 148.5, 131.3, 118.4, 109.7, 105.4, 93.0, 92.0,72.2, 71.1, 70.9, 70.8, 69.2, 65.1, 59.3, 55.6, 40.4; HRMS calc for $C_{20}H_{28}N_2O_6$ $(M+Na)^+$ 415.1840; found 415.1836.

**(Z)-2-(2-(2-methoxyethoxy)ethoxy)ethyl-2-cyano-3-(4-(diethylamino)phenyl) acrylate (JS-3).** 90% yield; orange liquid; $^1$H NMR (400 MHz, $CDCl_3$): δ = 8.05 (s, 1H), 7.92 (d, 2H, *J*= 9.1 Hz), 6.67 (d, 2H, *J*= 9.2 Hz), 4.42 (m, 2H), 3.82-3.79 (m, 2H), 3.73-3.72 (m, 2H), 3.69-3.65 (m, 4H), 3.57-3.54 (m, 2H), 3.45 (q, 4H, *J*= 7.1 Hz), 3.37 (s, 3H), 1.23 (t, 6H, *J*= 7.1 Hz); $^{13}$CNMR (100 MHz, $CDCl_3$): δ = 164.7, 154.8, 151.9, 134.8, 119.0, 117.8, 111.4, 93.0, 72.2, 71.1, 70.9, 70.8, 69.2, 65.2, 59.3, 45.0, 12.8; HRMS calc for $C_{21}H_{30}N_2O_5$ $(M+Na)^+$ 413.2047; found 413.2053.

**(Z)-2-(2-(2-methoxyethoxy)ethoxy)ethyl-2-cyano-3-(4-(dibutylamino)phenyl) acrylate (JS-4).** 78% yield; yellow liquid; $^1$HNMR (400 MHz, $CDCl_3$): δ = 8.00 (s, 1H), 7.87 (d, 2H, *J*= 9.0 Hz), 6.60 (d, 2H, *J*= 9.2 Hz), 4.38 (m, 2H), 3.78- 3.76 (m, 2H), 3.71-3.69 (m, 2H), 3.66-3.62 (m, 4H), 3.53-3.51 (m, 2H), 3.34- 3.30 (m, 7H), 1.57 (m, 4H), 1.34 (m, 4H), 0.94 (t, 6H, *J*= 7.3 Hz); $^{13}$CNMR (100 MHz, CDCl3): δ = 164.7, 154.7, 152.2, 134.6, 118.9, 117.9, 111.5, 92.8, 72.1, 71.0, 70.8, 69.1, 65.2, 59.2, 51.1, 29.5, 20.4, 14.1; HRMS calc for $C_{25}H_{38}N_2O_5$ $(M+Na)^+$ 469.2673; found 469.2677.

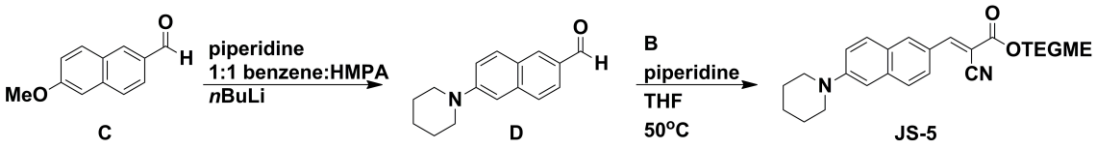


*Figure 4.9. Schematic for the synthesis of probe **JS-5**.*

**6-(piperidin-1-yl)-2-naphthaldehyde (C)**. To a 50 ml round bottom flask containing benzene (3 mL), hexamethylphosphoramide (HMPA, 3 mL) and piperidine (1.65 ml, 16.7 mmol), n-butyllithium (n-BuLi, 1.6 M in hexane, 10.4 mL, 16.7 mmol) was added via syringe, at 0 °C. After stirring for 15 min, the reaction mixture was treated with a solution of 6-methoxy-2-naphthaldehyde (390 mg, 2.09 mmol) in benzene:HMPA 1:1 (2 ml). The reaction mixture was warmed to room temperature, left stirring for 12 hours and then it was poured into cold 5% aqueous NaCl (30 ml). The mixture was extracted with diethyl ether (3 x 20 mL), dried over anhydrous magnesium sulfate (anh. $MgSO_4$) and concentrated. The product was purified via flash chromatography (20% EtOAc in hexanes) to give compound **C**. **C**: 35% yield, yellow solid; $^1$H NMR (300 MHz, $CDCl_3$): δ = 10.02 (s, 1H), 8.14 (s, 1H), 7.88-7.73 (m, 2H), 7.67 (d, 1H, *J*= 8.6 Hz), 7.32 (dd, 1H, *J*= 2.5 Hz, *J*= 9.1 Hz), 7.08 (d, 1H, *J*= 2.4 Hz), 3.42-3.32 (m, 4H), 1.85-1.57 (m, 6H); $^{13}$C NMR (100 MHz, $CDCl_3$): δ = 192.2, 152.2, 138.8, 134.7, 131.6, 130.7, 127.5, 126.5, 123.6, 119.7, 109.0, 49.8, 25.8, 24.6; HRMS calc for $C_{16}H_{17}NO$ $(M+H)^+$ 240.1383; found 240.1387.

**(E)-2-(2-(2-methoxyethoxy)ethoxy)ethyl-2-cyano-3-(6-(piperidin-1-yl) naphthalen-2-yl)acrylate (JS-5).** 82% yield; red liquid; $^1$H NMR (400 MHz, $CDCl_3$): δ = 8.30 (s, 1H), 8.22 (d, 1H, *J*=1.2 Hz), 8.10 (dd, 1H, *J*= 1.8 Hz, *J*= 8.8 Hz), 7.76 (d, 1H, *J*= 9.2 Hz), 7.65 (d, 1H, *J*= 8.8 Hz), 7.29 (dd, 1H, *J*= 2.4 Hz, *J*= 9.2 Hz), 7.05 (d, 1H, *J*= 2.2 Hz), 4.47 (m, 2H), 3.85-3.82 (m, 2H), 3.74-3.66 (m, 6H),

3.57-3.54 (m, 2H), 3.42-3.38 (m, 4H), 3.37 (s, 3H), 1.74- 1.67 (m, 6H); $^{13}$C NMR (100 MHz, $CDCl_3$): δ = 163.4, 155.5, 151.9, 137.8, 134.7, 130.6, 127.3, 126.4, 126.0, 125.7, 119.3,116.4, 108.4, 98.7, 71.9, 70.8, 70.6, 70.5, 68.8, 65.4, 59.0, 49.4, 25.5, 24.3; HRMS calc for $C_{26}H_{32}N_2O_5$ $(M+H)^+$ 453.2384; found 453.2390.

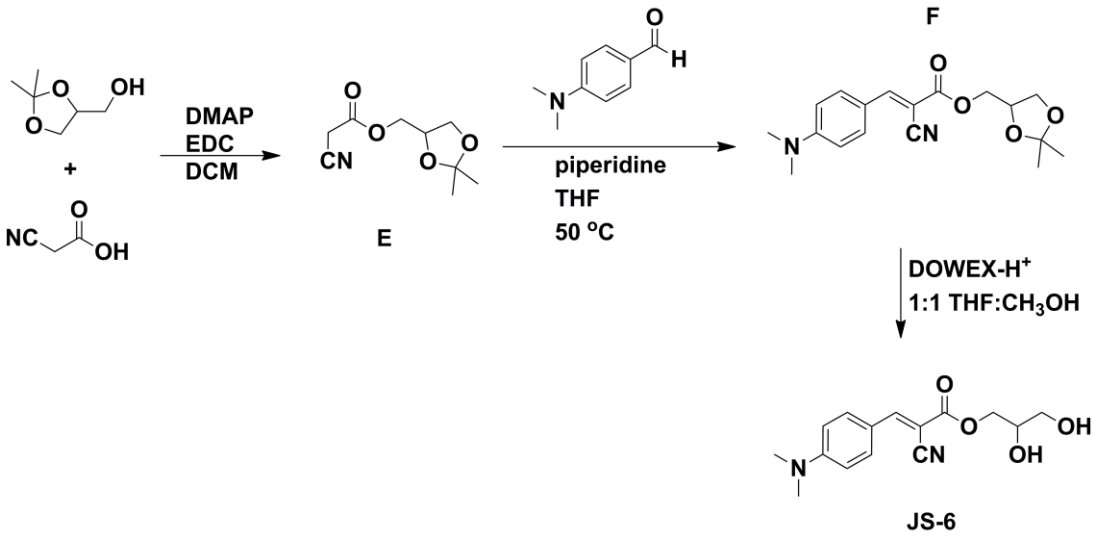


*Figure 4.10. Schematic for the synthesis of probe **JS-6**.*

**(2,2-dimethyl-1,3-dioxolan-4-yl)methyl 2-cyanoacetate (E).** To a solution of 2-cyanoacetic acid (1.02 g, 12 mmol), the acetal (2,2-dimethyl-1,3-dioxolan-4-yl)methanol (1.32 g, 10 mmol) in 5 mL of DCM and DMAP (61 mg, 0.50 mmol) was added dropwise at 0 °C. Finally, EDC 1.86 g (12 mmol) was added and the reaction mixture was stirred at 0 °C for 6 hours. The reaction was diluted with 15 mL of DCM and the formed dicyclohexyl urea (DCU) was filtered off. The filtrate was dried over anhydrous $MgSO_4$ and the solvents were removed under reduced pressure. The residue was purified by flash chromatography (Hex: EtOAc; 10:1) to give compound **E**. **E**: 71% yield; colorless liquid; $^1$H NMR (400 MHz, $CDCl_3$): δ = 4.34-

4.32 (m, 1H), 4.28-4.17 (m, 2H), 4.07 (dd, 1H, *J*= 6.5 Hz, *J*= 8.5 Hz), 3.75 (dd, 1H, *J*= 5.8 Hz, *J*= 8.5 Hz), 3.51 (s, 2H), 1.41 (s, 3H), 1.34 (s, 3H); HRMS calc for $C_9H_{13}NO_4$ $(M+H)^+$ 200.0923; found 200.0931.

**(E)-(2,2-dimethyl-1,3-dioxolan-4-yl)methyl2-cyano-3-(4-(dimethylamino)phenyl) acrylate (F).** To a round bottom flask containing a solution of 4-(dimethylamino)benzaldehyde (0.75 g, 5.0 mmol) and compound **E** (1.2 g, 5.5 mmol) in 20 ml of THF was added 0.50 mmol of piperidine and the mixture was heated at 50 °C. The crude mixture was concentrated under reduced pressure and the product was purified via flash chromatography (10-30% ethyl acetate in hexane) to give compound **F**. **F**: 91% yield; yellow solid; $^1$H NMR ( 400 MHz, $CDCl_3$): δ = 8.08 (s, 1H), 7.94 (d, 2H, *J*= 9.0 Hz), 6.69 (d, 2H, *J*= 9.2 Hz), 4.42- 4.29 (m, 3H), 4.13 (dd, 1H, *J*= 6.2 Hz, *J*= 8.6 Hz), 3.89 (dd, 1H, *J*= 5.9 Hz, *J*= 8.5 Hz), 3.11 (s, 6H), 1.46 (s, 3H), 1.38 (s, 3H); $^{13}$CNMR (400 MHz, $CDCl_3$): δ = 164.3, 155.3, 153.9, 134.5, 119.5, 117.5, 111.7, 110.1, 93.3, 73.7, 66.7, 65.6, 40.3, 26.9, 25.7; HRMS calc for $C_{18}H_{22}N_2O_4$ $(M+H)^+$ 331.1658; found 331.1691.

**(E)-2,3-dihydroxypropyl 2-cyano-3-(4-(dimethylamino)phenyl)acrylate (JS-6).** Compound **F** (0.5 g, 1.5 mmol) was dissolved in a mixture of THF/MeOH (1:1) and DOWEX-$H^+$ resin (0.10 g) was added and the heterogeneous mixture was stirred for 20 hours. The DOWEX-$H^+$ resin was removed by filtration and triethylamine (50 mg, 0.5 mmol) was added and the solvent was removed under reduced pressure. The residue was purified by flash chromatography (100% ether) to give compound **JS-6**. **JS-6**: 75% yield; bright yellow solid; $^1$H NMR (400 MHz, $CDCl_3$): δ = 8.08 (s, 1H),

7.94 (d, 2H, *J*= 9.1 Hz), 6.69 (d, 2H, *J*= 9.2 Hz), 4.42-4.32 (m, 2H), 4.05 (m, 1H), 3.80-3.70 (m, 2H), 3.12 (s, 6H); $^{13}$C NMR (100 MHz, $CDCl_3$): δ = 199.0, 164.8, 155.5, 154.0, 134.6, 119.4, 117.9, 111.8, 111.7, 92.8, 70.3, 70.2, 66.9, 66.8, 63.6, 63.5, 40.3, 40.2; HRMS calc for $C_{15}H_{18}N_2O_4$ $(M+H)^+$ 291.1345; found 291.1361.

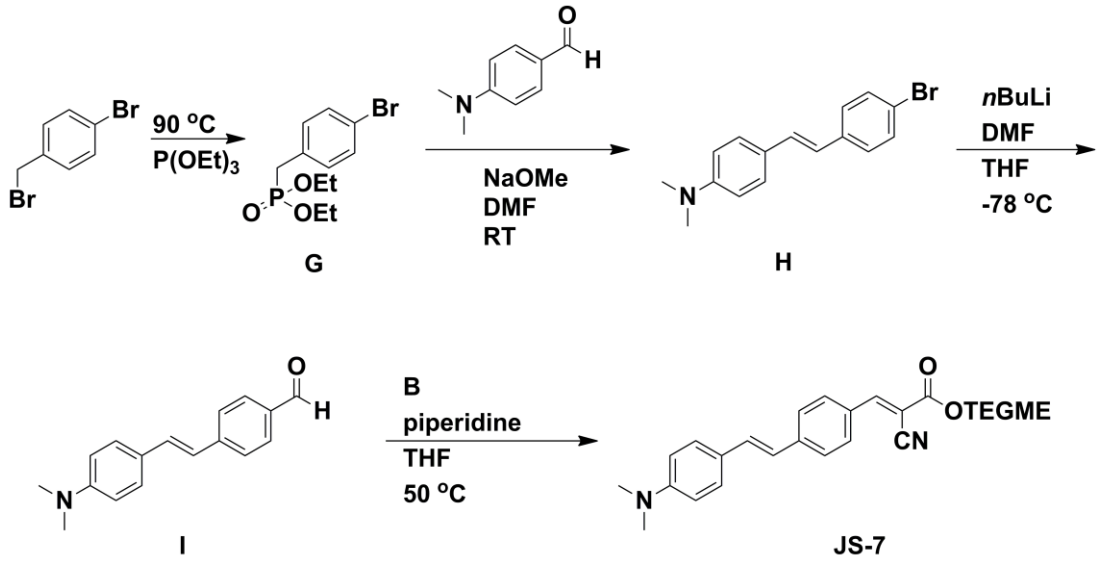


*Figure 4.11. Schematic for the synthesis of probe **JS-7.***

**Diethyl 4-bromobenzylphosphonate (G).** 1-bromo-4-(bromomethyl) benzene (5.0 g, 20 mmol) and triethyl phosphite (51 mL, 300 mmol) were mixed in a round bottom flask and refluxed at 90˚C for 19 hours. Excess triethyl phosphite was removed under reduced pressure and the product purified by flash chromatography (1:1 Hexane/ EtOAc) to give compound **G**. **G**: 98 % yield; colorless liquid; $^1$H NMR (400 MHz, $CDCl_3$): δ = 7.30 (d, 2H, *J*= 7.5 Hz), 7.05 (d, 2H, *J*= 7.6 Hz), 3.99-3.88 (m, 4H), 2.99 (s, 1H), 2.94 (s, 1H), 1.12 (t, 6H, *J*= 6.9 Hz); $^{13}$C NMR (100 MHz, $CDCl_3$): δ = 131.7, 131.6, 131.5, 121.0, 62.3, 34.0, 32.0, 16.5; HRMS calc for $C_{11}H_{16}BrO_3P$ $(M+H)^+$ 307.0097; found 307.0093.

**(E)-4-(4-bromostyryl)-N,N-dimethylaniline (H).** DMF (anhydrous) (10.5 mL) was added to sodium methoxide (176 mg, 3.26 mmol) and the color was changed to pink. To the above solution diethyl 4-bromobenzylphosphonate (1.0 g, 3.26 mmol) in DMF (6.5 ml) was added dropwise over 2 minutes, followed by 4 (dimethylamino)benzaldehyde (486 mg, 3.26 mmol). The reaction mixture was stirred at room temperature for 24 hours. Deionized water (17 mL) was added. The product was filtered out through vacuum filtration and recrystallized with DCM/hexane to give compound **H**. **H**: 74%. Yield; tan solid; $^{1}$H NMR (400 MHz, $CDCl_3$): δ = 7.47- 7.32(m, 6H), 7.04 (d, 1H, *J*= 12.5 Hz), 6.83 (d, 1H, *J*= 16.3 Hz), 6.71 (d, 2H, *J*= 8.9 Hz), 2.99 (s, 6H); $^{13}$C NMR (100 MHz, $CDCl_3$): δ = 150.5, 137.4, 136.1, 132.1, 131.8, 129.7, 128.3, 128.2, 127.9, 127.7, 125.5, 123,2, 120.3, 112.6, 40.7; HRMS calc for $C_{16}H_{16}BrN$ 302.0541; found 302.0539.

**4-(4-(dimethylamino)styryl)benzaldehyde (I).** To a round bottom flask compound **H** (300 mg, 1 mmol) was transferred followed by THF (5 mL). The heterogeneous solution was cooled at –78 °C and n-BuLi (1.6M in hexane, 1 mmol) was added dropwise over 5 min, followed by DMF (1.5 mL). The reaction mixture was stirred at –78 °C for 3 hours then it was quenched by water (1 mL) and the mixture was extracted with ether (2 x 25 mL). The combined organic extracts were washed with brine, dried over $MgSO_4$ and concentrated under reduced pressure to give compound **I**. **I**: 60% yield; yellow powder; $^{1}$H NMR (400 MHz, $CDCl_3$): δ = 9.96 (s, 1H), 7.83 (d, 2H, *J*= 8.2 Hz), 7.60 (d, 2H, *J*= 8.2 Hz), 7.44 (d, 2H, *J*= 8.8 Hz), 7.22 (d, 1H, *J*=

16.2 Hz), 6.94 (d, 1H, *J*= 16.2 Hz), 6.72 (d, 2H, *J*= 8.8 Hz), 3.01 (s, 6H); $^{13}$C NMR (100 MHz, $CDCl_3$): δ = 191.8, 150.8, 144.7, 134.7, 134.6, 132.7, 130.4, 128.4, 126.4, 124.9, 122.8, 112.4, 40.5; HRMS calc for $C_{17}H_{17}NO$ 252.1384; found 252.1383.

**(E)-2-(2-(2-methoxyethoxy)ethoxy)ethyl-cyano-3-(4(4(dimethylamino)styryl) phenyl)acrylate (JS-7).** 97% yield; red solid; $^1$H NMR (400 MHz, $CDCl_3$): δ = 8.20 (s, 1H), 7.98 (d, 2H, *J*= 8.4 Hz), 7.57 (d, 2H, *J*= 8.4 Hz), 7.45 (d, 2 H, *J*= 8.7 Hz), 7.20 (d, 1H, *J*= 16.2 Hz), 6.92 (d, 1H, *J*=16.2 Hz), 6.72 (d, 2H, *J*= 8.7 Hz) , 4.47 (m, 2H), 3.84-3.82 (m, 2H), 3.74-3.72 (m, 2H), 3.70-3.66 (m, 4H), 3.57-3.55 (m, 2H), 3.37 (s, 3H), 3.02 (s, 6H); $^{13}$C NMR (100 MHz, $CDCl_3$): δ = 154.9, 133.0, 132.2, 128.6, 128.5, 126.7, 122.7, 112.4, 72.2, 71.1, 70.8, 69.0, 65.8, 59.3, 40.6, 40.5, 29.9, 28.2; HRMS calc for $C_{27}H_{32}N_2O_5$ $(M+Na)^+$ 487.2203; found 487.2201.

**Fluorescence studies with aggregated Aβ peptides:** Aggregated Aβ peptide was prepared by dissolving Aβ(1-42) in PBS pH 7.4 to a final concentration of 100 μM. This solution was magnetically stirred at 1200 rpm for 3 days at room temperature. The 100 μM Aβ(1-42) stock solution in PBS was aliquoted and frozen at –80 °C for up to 4 weeks without noticeable change in its property. 150 μL of pre-aggregated Aβ(1-42) was added to 2.85 mL of probe to attain a final concentration of 5 μM Aβ(1-42) and 4 μM of probe. The solution was transferred to a 3 mL cuvette and the fluorescence was measured at 25 °C.

**Determination of the probe binding constant ($K_d$) to Aβ(1-42):** Pre-aggregated Aβ(1-42) (5 μM final concentration) was mixed with various concentrations of

probes (10, 5, 2.5, 1.25 μM) in PBS buffer (pH 7.4) and their fluorescence was measured. The negative inverse of the x-intercept of the linear regression, that was drawn between the double reciprocal of the fluorescence intensity maximum and concentration of the probe, represents the probe binding constant ($K_d$) to Aβ(1-42).

**Determination of $K_d$'s from fluorescence measurements:** In order to quantify the dissociation constants ($K_d$'s) for the binding of fluorescent probes with aggregated β-amyloid peptides, we used the method described by LeVine.[156] This method is similar to the method described by Benesi-Hildebrand.[172] Here, the fluorescence of the probe was measured with and without the addition of the aggregated peptides in solution. The relative fluorescence enhancement of the probe upon binding to aggregated β-amyloid peptides was determined by taking the difference between $F$ (fluorescence after the addition of aggregated peptides) and $F_O$ (fluorescence before the addition of aggregated peptides).

In order to estimate the binding constant ($K_d$) for the probe-Aβ complexes from the fluorescence studies, we made the following assumptions:

1. All probes are completely in solution and free of any significant competing binding process such as self-aggregation.
2. The concentration of unbound probes can be approximated as close to the total concentration of the probes.

3. The binding sites in the aggregated Aβ peptides are not completely occupied at the concentration of Aβ binding probes used for the fluorescence studies (i.e., the experiments are carried out under non-saturated binding conditions).

According to the Beer-Lambert law,[173] we can obtain two expressions that relate the concentration of bound probe ([*HG*]), free probe ([*G*]), and free binding sites on the amyloid peptides ([*H*]) with either 1) the measured fluorescence of the probe in solution before the addition of the aggregated peptides ($F_O$), or 2) the measured fluorescence of the probe in the presence of the amyloid peptides (*F*):

$$F_O = \varepsilon_G l[G_O] \qquad \text{Equation 4.1}$$

$$F_O = \varepsilon_{HG} l[HG] + \varepsilon_H l[H] + \varepsilon_G l[G] \qquad \text{Equation 4.2}$$

where

$l$ = path length

$[G_O]$ = total concentration of probes

$\varepsilon_G$ = absorption coefficient of the probes

$[G]$ = unbound probe concentration

$\varepsilon_{HG}$ = absorption coefficient of probe-Aβ complex

$[HG]$ = probe-Aβ complex concentration

$\varepsilon_H$ = absorption coefficient of *H*

$[H]$ = concentration of free binding sites on the aggregated peptide

$[H_O]$ = total concentration of binding sites on the Aβ peptides

Substituting $[G_{O]} = [G] + [HG]$ into equation 4.1, and making the approximation that $\varepsilon_{HG} l[HG] + \varepsilon_G l[G] \gg \varepsilon_H l[H]$, we can arrive at a simplified expression for the relative fluorescence of bound probe (DF):

$$\Delta F = F - F_o = \varepsilon_{HG} l[HG] + \varepsilon_G l[G] - \varepsilon_G l[G] - \varepsilon_G l[HG] \qquad \text{Equation 4.3}$$

or $$\Delta F = \Delta\varepsilon l[HG] \qquad \text{Equation 4.4}$$

where $\Delta\varepsilon = \varepsilon_{HG} - \varepsilon_G$

In order to obtain a relationship between the change in measured fluorescence of the probe ($\Delta F$) with the binding constant of the probe to aggregated β-amyloid peptides ($K_d$'s), we used the standard equation for a binding isotherm to obtain a relationship between [*HG*] and $K_d$:

$$[HG] = \frac{[H_O][G]}{K_d + [G]} \qquad \text{Equation 4.5}$$

Combining equations 4.4 and 4.5, we obtained a relationship between $\Delta F$ and $K_d$:

$$\Delta F = \frac{[H_O][G]}{K_d + [G]} \Delta\varepsilon l \qquad \text{Equation 4.6}$$

In order to estimate the $K_d$ of the probe bound to aggregated Aβ peptides from the measured change in fluorescence, we take the reciprocal of the equation 4.6 to give:

$$\frac{1}{\Delta F} = \frac{K_d}{\Delta \varepsilon l [H_O]} \frac{1}{[G]} + \frac{1}{\Delta \varepsilon l [H_O]} \qquad \text{Equation 4.7}$$

Equation 4.7 suggests that a double reciprocal plot of $\Delta F$ and [$G$] should yield a straight line with the x-intercept equal to -1/$K_d$. Figure 4.5 and figure 4.10 show double reciprocal plots of the measured fluorescence versus total concentration of probe [$G_O$]. Assuming that [$G$] can be approximated as close to [$G_O$] (assumption 2), we can obtain estimates for the $K_d$'s of the probe-Aβ complexes from the x-intercept of the linear fits of the data for each probe. The estimated $K_d$'s for all probes are given in Table 4.1.

**ELISA assay:** Aggregated Aβ peptides were generated from synthetic Aβ(1-42) peptides by dissolving 30 μg of peptide in 90 μL of nanopure water (pH 5-6) and incubating at 37 °C for ≥ 72 h without agitation. Each well of a 96-well plate (well volume 0.4 mL; clear, flat bottom polystyrene) was coated for 3 h at 25 °C with 50 μL of 1.3 $\mu$M solution of Aβ peptides in phosphate-buffered saline (PBS, 10 mM $NaH_2PO_4/Na_2HPO_4$, 138 mM NaCl, 2.7 mM KCl, pH 7.4). After removal of the excess sample, 50 μL solutions of probes in PBS buffer (various concentrations were obtained by diluting a stock solution with PBS buffer) were incubated in the wells for 12 h. Probes that did not dissolve in PBS buffer were dissolved in DMSO and diluted in PBS buffer to give a final solution of 5% DMSO in PBS buffer. The excess solutions were then removed and all wells were blocked for 30 min by adding 300 μL of a 1% (w/v) solution of bovine serum albumin in PBS buffer (BSA/PBS). On occasion, an additional blocking step was performed prior to incubation with

solutions of small molecules. The blocking solution was discarded and the wells were washed once with 300 μL of PBS buffer. Wells were incubated for 1h with 50 μL of a 1.1 nM solution (in 1% BSA/PBS, dilution 1:6000) of anti-Aβ IgG (clone 6E10, monoclonal, mouse), followed by removal of the solution. The wells were washed twice with 300 μL of PBS buffer and incubated for 60 min with 50 μL of the secondary IgG (anti- mouse IgG H+L, polyclonal, rabbit) conjugated with alkaline phosphatase (6.8 nM in 1% BSA/PBS, dilution 1:1000). The solution was discarded, and the wells were washed twice with 300 μL PBS buffer. Bound secondary IgGs were detected by the addition of 50 μL of a *p*-nitrophenyl phosphate solution (2.7 mM, in 100 mM diethanol amine/0.5 mM magnesium chloride, pH 9.8). Absorbance intensities were determined at 405 nm using a UV-vis spectroscopic plate reader (Sprectramax 190, Molecular Devices, Sunnyvale, CA). Each run was performed five times and averaged. Error bars represent standard deviations. Graphs were plotted and fitted with the sigmoid curve fitting function(Origin 7.0, Microcal).

**Fluorescence studies with monomeric Aβ:** Aβ (Biopeptide, Inc.) was initially solubilized in hexafluoroisopropanol at 1 mM concentration, vortexed, sonicated, and vortexed. The vial was covered in foil and was incubated for 21 hours at 25 °C on a shaker, with 3 times of vortexing throughout the incubation period. The solution was sonicated and vortexed again then diluted with cold nanopure water (2:1 H2O:HFIP), fractionated in desired amounts into small glass vials, and immediately frozen in a $CO_2$/acetone bath. Each fraction was covered with parafilm that was punctured to allow solvent vapors to escape. The fractions were lyophilized for 2

days to obtain monomeric Aβ (91% monomer by 12% Tris-bis PAGE gel analysis). 1.8 μL (8.42 μM) of this monomeric Aβ(1-42) was added to 3 μL of 4 μM concentration of small molecules that was prepared by dissolving in PBS buffer pH 7.4 to attain a final concentration of 5 μM of Aβ(1-42) and 4 μM of the probe. The solution was transferred to a 3 mL cuvette and the fluorescence was measured at 25 °C.

**Evaluation of fluorescent probes for cytotoxic activity against SH-SY5Y human neuroblastoma cells (MTT assay):** SH-SY5Y human neuroblastoma cells, MTT (3-(4,5-dimethylthiazol-2-yl)-2,5-diphenyltetrazolium bromide) cell proliferation kit, Eagle's Minimum Essential Medium (EMEM), Ham's F12 nutrient mixture, and Fetal Bovine Serum (FBS) were all purchased from ATCC (Manassas, VA). Briefly, SH-SY5Y cells (in 1:1 EMEM:Ham's F12 with 10% FBS) were seeded on 96-well plates at a density of 5x104 cells/well. Plates were incubated overnight (in a humidified atmosphere of 95% air, 5% $CO_2$, at 37 °C) to promote attachment of cells to the wells. Cells were then treated with various concentrations of compound **JS-1**, **JS-2**, **JS-3**, **JS-4**, **JS-5**, or **JS-6** and incubated for 24 hours (humidified atmosphere of 95% air, 5% $CO_2$, at 37 °C). MTT reagent (20 μL) was added to the medium and incubated for an additional 4 hours. After incubation, 100 μL of detergent reagent was added and the plates were covered with aluminum foil and left at room temperature overnight. The amount of solubilized MTT formazan was measured by spectrophotometric absorbance at 570 nm (Spectramax 190, Molecular Devices, Sunnyvale, CA). MTT assay was not performed on compound **JS-7** due to its poor

solubility in aqueous media. All data are presented as the mean ± S.D, N= 3 for each concentration. The Student's *t*-test was employed for all statistical analyses. A *p*-value of < 0.05 was considered statistically significant compared to control cells.

## 4.5 Additional Figures

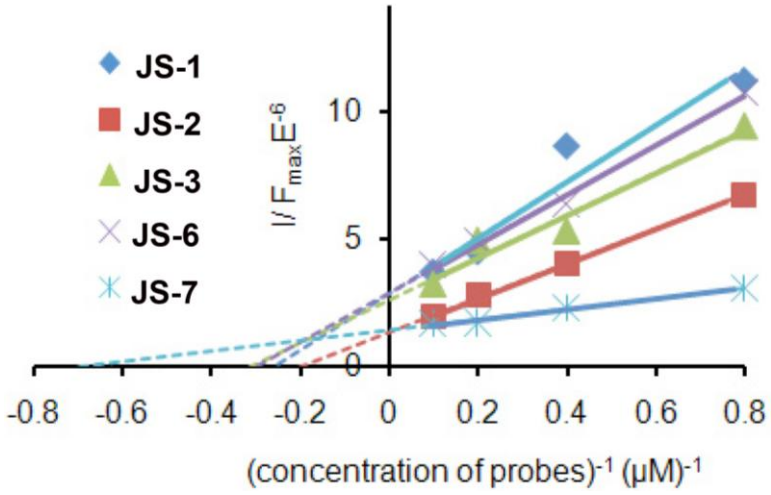


*Figure 4.12. Double reciprocal of fluorescence maxima and concentration of compounds **JS-1**, **JS-2**, **JS-3**, **JS-6**, and **JS-7**.*

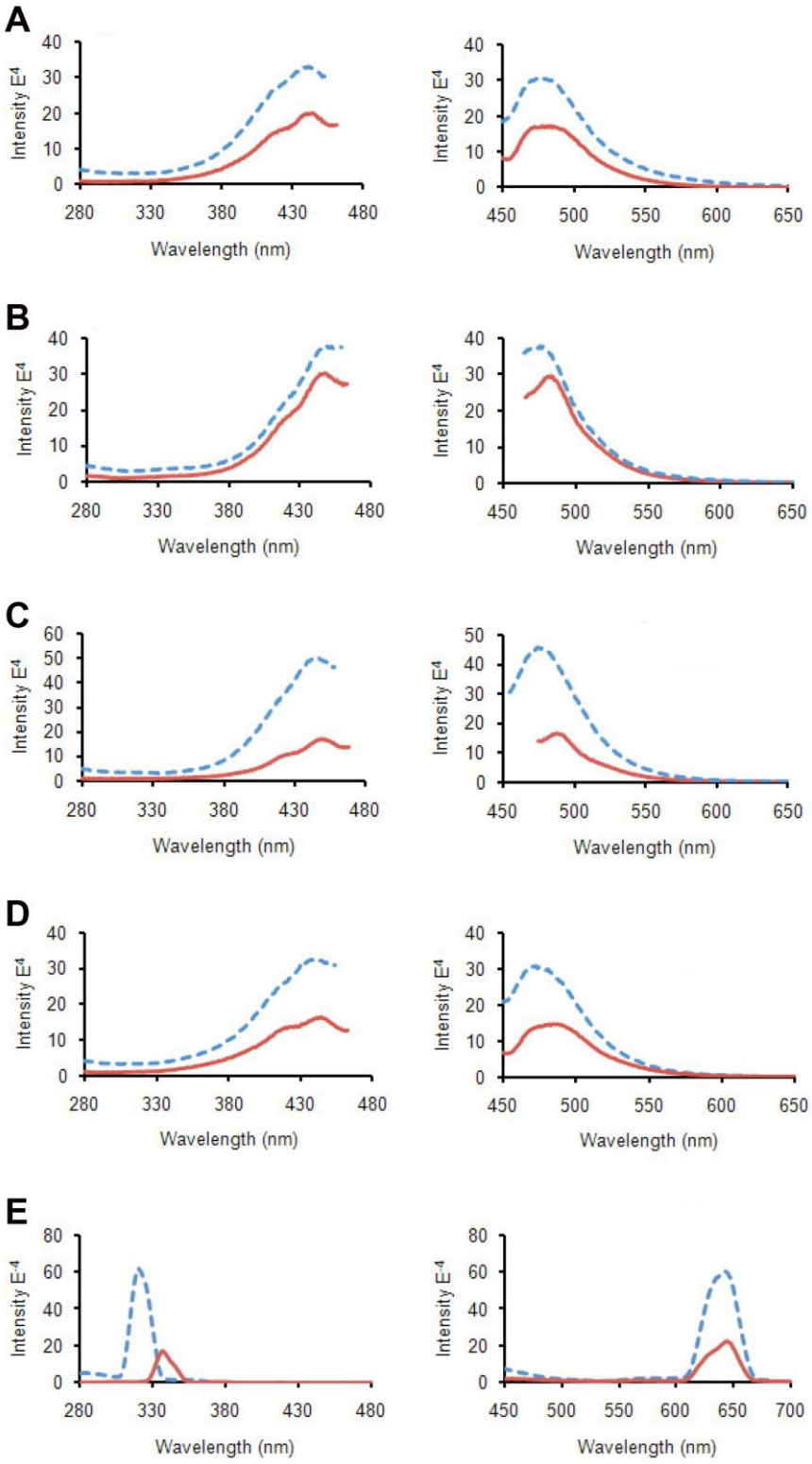


*Figure 4.13. Fluorescence excitation spectra (left) and emission spectra (right) for **JS-1** (A),**JS-2** (B), **JS-3** (C),**JS-6** (D), and **JS-7** (E) in PBS(—) and in the presence of aggregated Aβ peptides (---).*

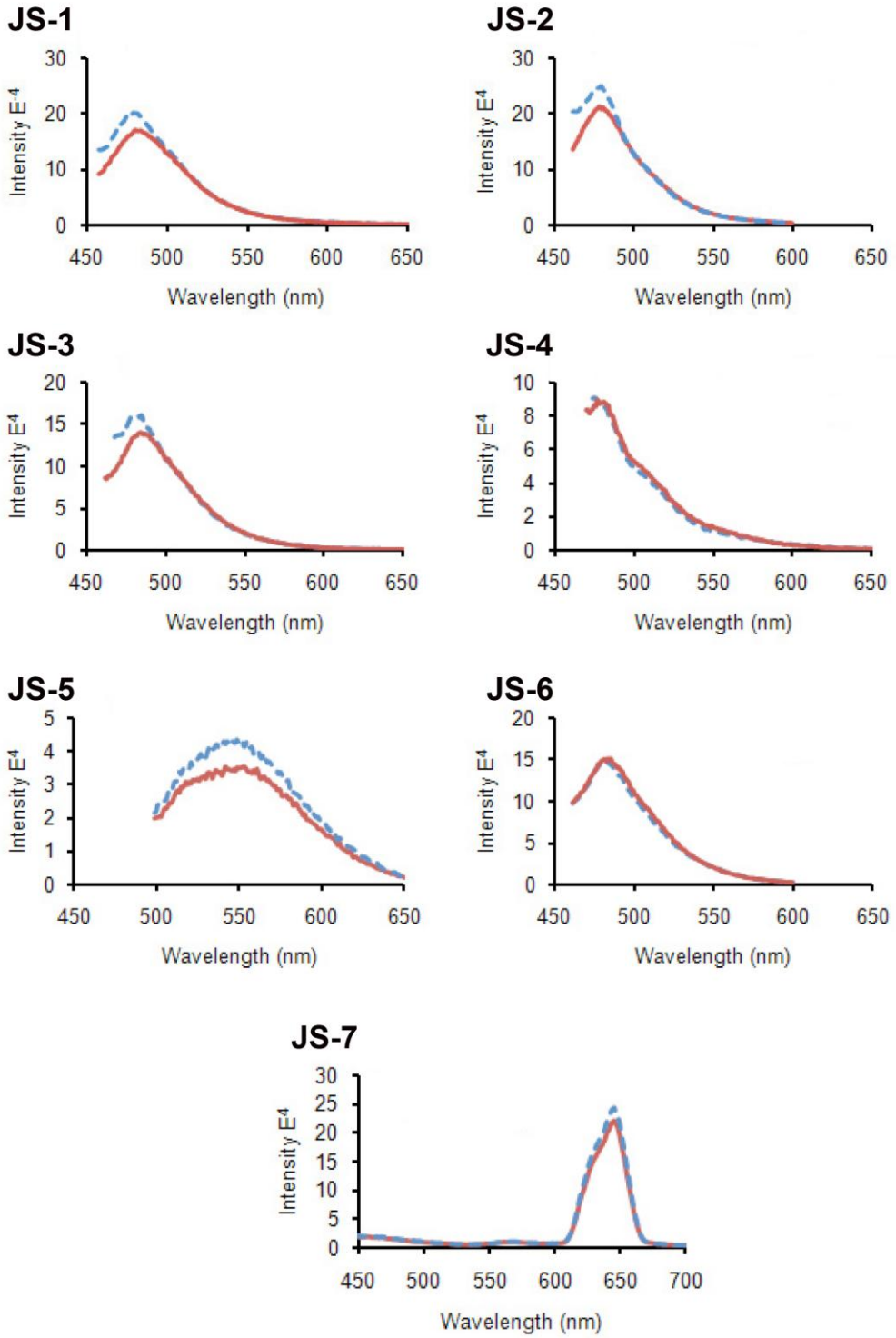


*Figure 4.14. Fluorescence emission spectra for probes **JS-1**- **JS-7** in PBS(—) and in the presence of monomeric Aβ peptides (---).*

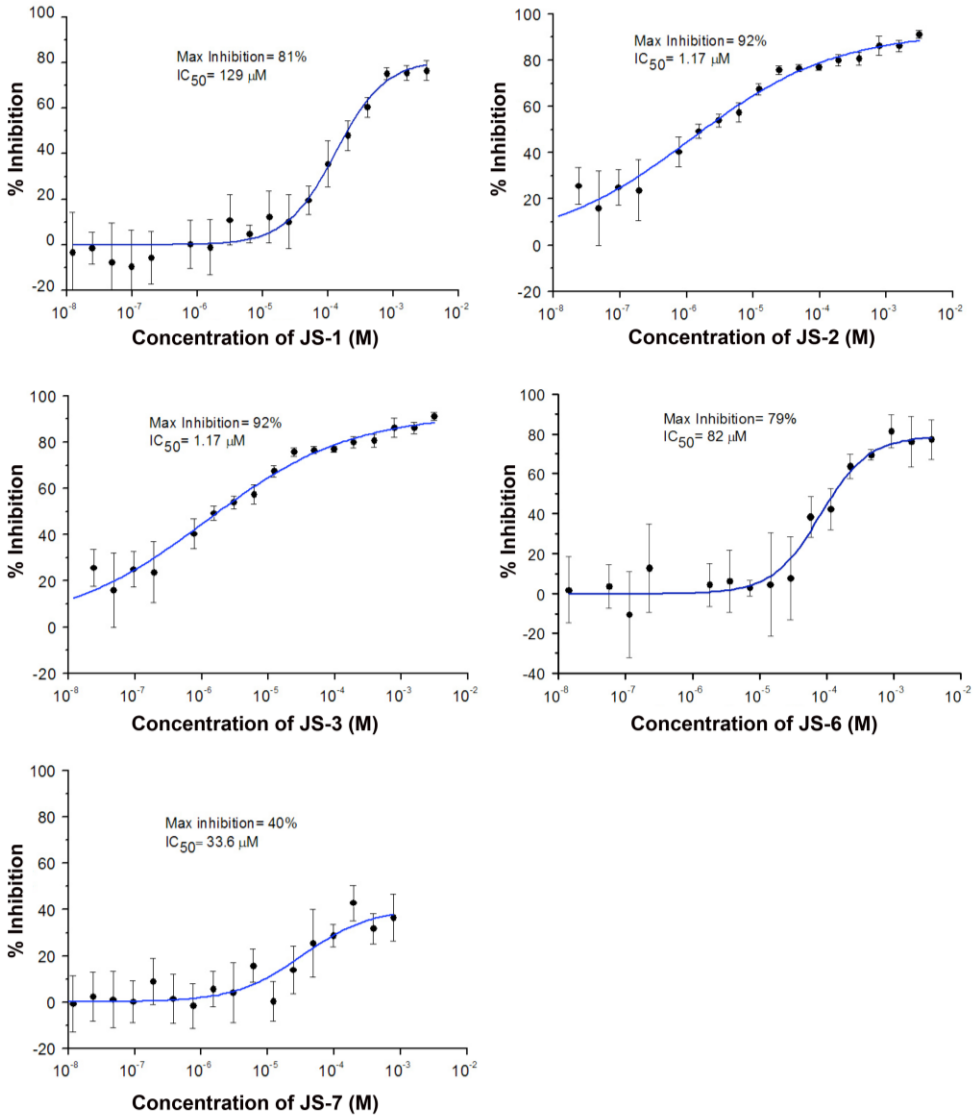


*Figure 4.15. Inhibition curves for **JS-1**,**JS-2**, **JS-3**, **JS-6**, and **JS-7**.*

## Notes about this Chapter

This chapter is based on material that appears in "Rational Design of Amyloid-binding Agents based on the Molecular Rotor Motif." Sutharsan, J.; Dakanali, M.; Capule, C. C.; Haidekker, M. A.; Yang, J.; Theodorakis, E. A.

*Chemmedchem* **2010**, *5*, 56-60. Jeyanthy Sutharsan was the first author of this work and generated a significant portion of the data. I am a co-author on this publication. My contributions focused on the cellular MTT assay, technical aspects of the inhibition assay and the fluorescence measurements, data analysis of the inhibition assay as well as the fluorescence studies.

# Chapter 5

# ANCA: A Family of Fluorescent Probes that Bind and Stain Amyloid Plaques in Human Tissue

## 5.1 Introduction

Alzheimer's Disease (AD) is characterized by a progressive impairment of episodic memory and language deficits.[174] Pathologically, AD is characterized by the accumulation of amyloid-β (Aβ) deposits in the brain. The major component of these deposits are Aβ40 and Aβ42 peptides that are derived from Amyloid Precursor Protein after cleavage by β- and γ-secretases.[175] To date, the late-stage diagnosis of

AD is achieved using functional memory and behavioral tests;[176] early stage asymptomatic diagnosis, however, remains a challenge. Along these lines, recent efforts have targeted the visualization of amyloid deposits *in vivo*. Moreover, the structure of a model amyloidogenic peptide that sustains the property of aggregation has been proposed.[177,178] In turn, this paves the way for a rational design of amyloid-binding molecules that can potentially be used for *in vivo* and *ex vivo* imaging. Such molecules can not only help evaluate the time course and evolution of the disease, but can also allow for the timely monitoring of therapeutic treatment.[179-181]

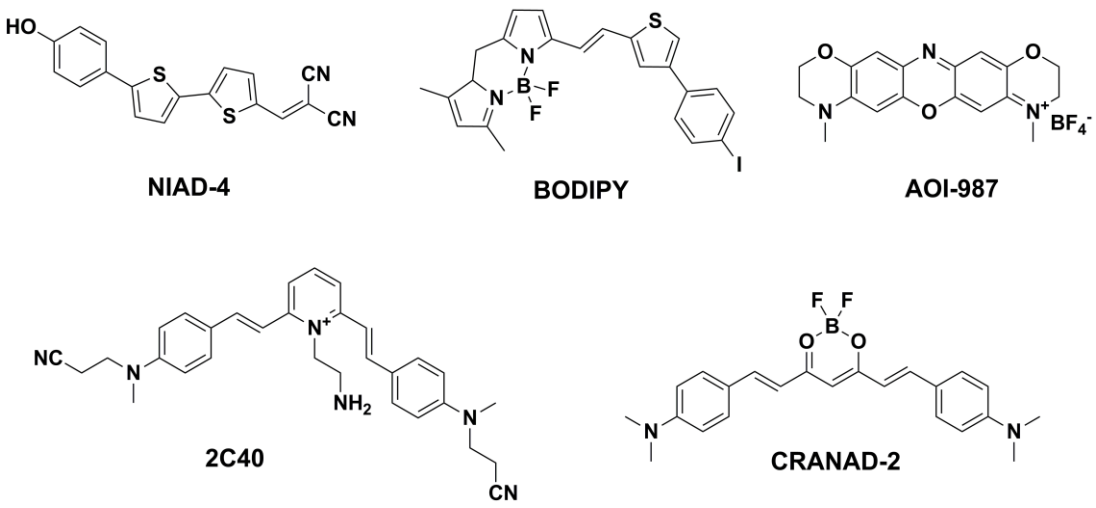


*Figure 5.1. Examples of fluorescent probes that stain Aβ deposits in tissue.*

Over the past few years a number of probes have been developed for the specific labelling and imaging of the Aβ plaques. These probes rely on techniques such as Magnetic Resonance Imaging (MRI),[182,183] Positron Emission Tomography (PET),[34,136,184,185] and Single Photon Emission Computed Tomography

(SPECT).[186,187] In addition, fluorescent probes that can stain Aβ deposits have gained increasing interest as potential tools for monitoring the progression of AD *in vitro* and *in vivo*. In principle, such fluorescent probes are advantageous over PET/SPECT methods since they provide real-time, non-radioactive, and high-resolution imaging both *in vivo* and *ex vivo*. Figure 5.1 illustrates representative structures of such probes that, to-date, have found limited use as fluorescent labelling agents of Aβ deposits in small animal studies.[188-193] Reliable methods to fine-tune the optical and biocompatible properties of these amyloid-targeting agents and to improve their selectivity and affinity to amyloid deposits in tissue could further advance this optical strategy for AD monitoring and diagnosis. In general, an appropriate fluorescent probe for amyloids should have the following properties:[34,189,192] a) molecular mass less than 600 Da, b) emission wavelength above 450 nm to minimize background fluorescence from brain tissue,[23] c) high quantum yield, d) appropriate lipophilicity (log*P* value between 1-3), e) specificity to Aβ plaques, f) sufficient binding affinity to aggregated amyloid peptides, g) straight forward synthesis and h) upon binding to Aβ deposits, a significant change in fluorescent properties should be observed.

Recently, we reported the rational design of a new class of amyloid-binding agents based on the molecular rotor motif.[194,195] This motif contains an electron-donor unit in conjugation with an electron acceptor, and produces a fluorescent quantum yield that is dependent on the surrounding environment. Hindrance of the internal molecular rotation of the probe, by increasing the surrounding media rigidity

or by reducing the available free volume needed for relaxation, leads to a decrease in the non-radiative decay rate and consequently an increase of fluorescent emission. Closer evaluation of the data led to the identification of 6-aminonapthalenyl-2-cyano-acrylate (ANCA) as a motif with potentially useful spectroscopic properties for fluorescent labelling of aggregated amyloid peptides (Figure 5.2). Specifically, compound **WMC-1**, referred to as ANCA-11, possesses a long emission wavelength and large increase in fluorescence intensity upon binding to Aβ fibrils.[194] In order to validate the ANCA scaffold as a general motif that can bind to aggregated Aβ peptides, we sought to examine whether structural changes at its periphery, including alterations at the water solubilizing groups or at the nitrogen substitution, can affect the binding and fluorescent properties of the probe. The synthesis and the optical properties of a small family of compounds based on the ANCA motif is discussed in this chapter. The *ex vivo* staining of amyloid plaques in human tissue by these novel fluorescent probes is also presented in this chapter.

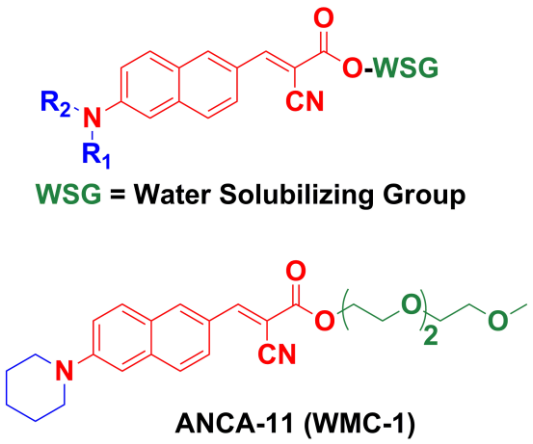


*Figure 5.2. General motif of the ANCA probes. The ANCA scaffold is shown in red. Substitutions at the nitrogen and the WSG sites are shown in blue and green, respectively.*

## 5.2 Results and Discussion

A general strategy for the synthesis of all ANCA-based probes is depicted in Figure 5.3. Commercially available methyl 6-bromonaphthalene-2-carboxylate (**A**) was converted to the corresponding naphthaldehyde **B** by reduction of the ester to the primary alcohol using diisobutylaluminum hydride (DIBALH) and oxidation of the resulting alcohol to the desired aldehyde upon treatment with pyridinium chloro chromate (PCC).[196] The transformation of the bromide to the appropriate amine demanded the use of novel chemistry to improve the yield and apply the method in bigger scale. To this end, treatment of bromide **B** in the presence of palladium using Buchwald and Hartwig conditions produced aldehydes **C**-**F** in excellent yield for most cases.[197-199] Knövenagel condensation of aldehydes **C**-**F** with the appropriate cyanoester **G** concluded the synthesis of the final probes **WMC-1** and **WMC-2** – **WMC-6**, as a single stereoisomer (E isomer).[30] Deprotection of the acetal group of **WMC-6** using acidic resin yielded the final dye **WMC-7**.

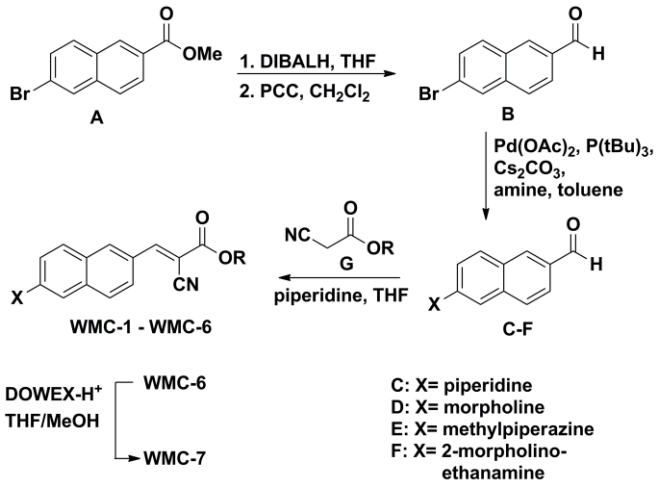


*Figure 5.3. General strategy for the synthesis of probes **WMC-1** – **WMC-7**.*

Table 5.1 summarizes the R and X combinations of the final products. Based on their chemical structures, the synthesized probes can be separated in two subgroups: compounds **WMC-1**, **WMC-5**, and **WMC-7** (group A) that contain an identical piperidine donor group and differ only in the WSG area (triethylene glycol monomethyl ether, tetraethylene glycol monomethyl ether and propane 1,2-diol motif, respectively) and compounds **WMC-1**, **WMC-2**, **WMC-3**, and **WMC-4** (group B) that contain an identical WSG motif (triethylene glycol monomethyl ether) but differ in the nitrogen substitution.

*Table 5.1. Structures of ANCA-based Aβ-binding probes.*

| Compound | X | R |
|---|---|---|
| **WMC-1** | 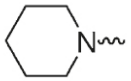 | 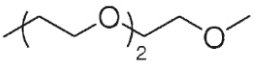 |
| **WMC-2** | 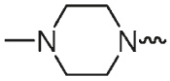 | 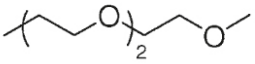 |
| **WMC-3** | 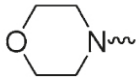 | 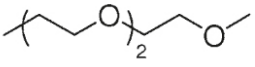 |
| **WMC-4** | 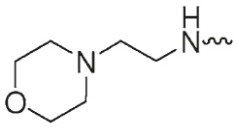 | 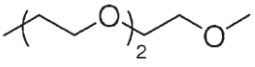 |
| **WMC-5** | 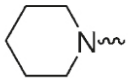 | 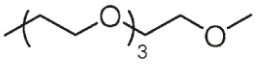 |
| **WMC-6** | 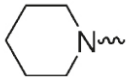 | 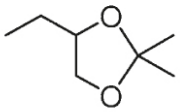 |
| **WMC-7** | 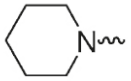 | 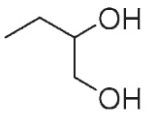 |

*Table 5.2. Fluorescence profile, $K_d$, and logP values of the synthesized probes with aggregated Aβ(1-42) peptides.*

| | exc. max (nm) | | em. max (nm) | | | | |
|---|---|---|---|---|---|---|---|
| cmpd no. | before | after | before | after | fold increase | $K_d$ ($\mu$M) | log $P^a$ |
| **WMC-1** | 415 | 410 | 590 | 545 | 7.7 | $1.4 \pm 0.2$ | 3.81 |
| **WMC-2** | 400 | 385 | 570 | 530 | 5.0 | $4.6 \pm 1.3$ | 2.79 |
| **WMC-3** | 400 | 380 | 530 | 525 | 5.1 | $13.8 \pm 3.1$ | 2.74 |
| **WMC-4** | 430 | 430 | 570 | 540 | 2.9 | $6.7 \pm 2.1$ | 2.53 |
| **WMC-5** | 420 | 410 | 590 | 550 | 8.4 | $1.6 \pm 0.9$ | 3.60 |
| **WMC-7** | 410 | 410 | 545 | 535 | 6.6 | $1.6 \pm 0.2$ | 3.14 |

[a] Log *P* values were calculated with Molinspiration Cheminformatics Software.

To be useful, a fluorescent amyloid-binding probe should display a significant increase in fluorescence emission upon binding with the aggregates as compared to the emission of the free probe in solution.[200] To test whether the ANCA family of probes possessed these desirable fluorescence properties, we compared the fluorescent properties of all free probes in aqueous solution to their fluorescence properties in the presence of aggregated Aβ42 peptides. We chose to evaluate the binding of probes to Aβ42 instead of Aβ40, since Aβ42 is the major amyloid species found in AD plaques.[2,197-199] Specifically, we evaluated the fluorescent properties of each probe at a final concentration of 4 μM in nanopure water, before and after mixing with aggregated Aβ42 peptide (final concentration peptide = 5 μM). As shown in Table 5.2, in all cases we observed a significant increase (2.9 to 8.4-fold) in the intensity of the emission spectra of the probes upon association with the aggregated amyloid peptides.[201] This intensity increase was

also accompanied with a blue shift in the emission spectra of around 5-50 nm. After binding, all compounds had excitation maxima between 380-430 nm and their emission maxima were between 525-550 nm, suggesting that small changes in the donor or acceptor part of the molecule do not alter significantly their fluorescent maxima. However, compounds **WMC-1**, **WMC-5**, and **WMC-7** (group A) that possess piperidine as the electron donor, showed higher increase in fluorescence intensity after binding (7.7-, 8.4- and 6.6-fold, respectively) as compared to probes containing piperazine (**WMC-2**), morpholine (**WMC-3**), or morpholino-ethanamine (**WMC-4**) groups as electron donors (group B). Figure 5.4 provides a representative example of the fluorescent properties of compound **WMC-2**.

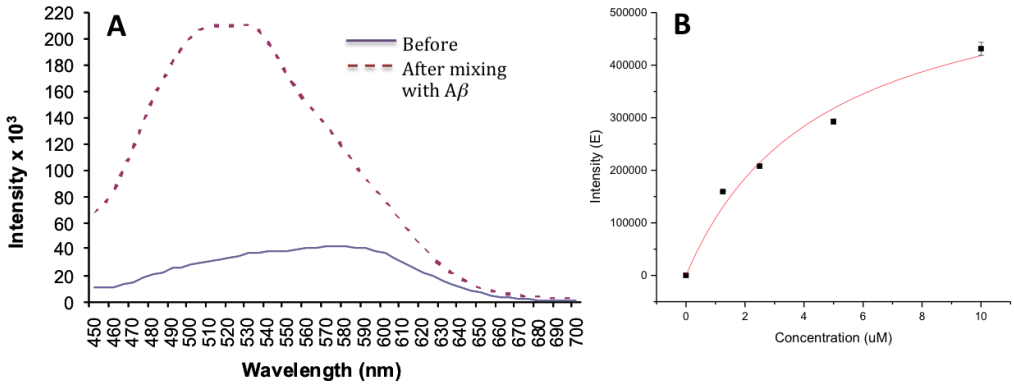


*Figure 5.4. A) Fluorescent emission of compound **WMC-2** before (blue solid line) and after (red dotted line) mixing with Aβ aggregates; B) Plot of the fluorescence intensity (at λ = 530 nm) as a function of the concentration of compound **WMC-2** in the presence of aggregated Aβ42 peptides (5 μM) in solution. Fitting this data to the equation: $y = B \cdot x/(K_d+x)$ revealed a $K_d$ of 4.6 ± 1.3 μM for association of compound WMC-2 to aggregated Aβ42 peptides.*

We also measured the apparent binding constants ($K_d$) of the probes to aggregated Aβ42 peptides. The fluorescent intensity of each probe was measured at concentrations of 1.25, 2.5, 5.0 and 10 μM in nanopure water, mixed with pre-aggregated Aβ42 peptides (final concentration of peptide = 5 μM).[202] In all cases, the $K_d$ values were between 1.4 and 13.8 μM. Interestingly, group A exhibited the highest affinity to aggregated Aβ peptides. The nearly identical $K_d$ values obtained for these dyes (1.4-1.6 μM) indicate that small chemical modifications within the water-solubilizing region of the ANCA motif do not affect significantly the binding of the probes to Aβ aggregates. On the other hand, a measurable change of the $K_d$ value was observed upon chemically altering the electron donor moiety of the ANCA motif. As shown in Table 5.2, compounds having piperidine as the electron donor were found to have lower $K_d$ values (1.4-1.6 μM) compared to those possessing piperazine, morpholine, or morpholino-ethanamine as electron donor (compounds **WMC-2**, **WMC-3**, and **WMC-4**, respectively).

Finally, the lipophilicity (log*P*) of the synthesized probes were calculated.[203] All compounds were found to have log*P* values between 2.5 and 3.8, suggesting that most of them possess the desirable properties for biocompatibility and can potentially cross the blood-brain barrier.[38]

In order to assess whether this family of ANCA-based fluorescent probes could stain amyloid deposits in brain tissue, we exposed sections of frozen human brain tissue (derived from the cerebral cortex of AD cases) to solutions containing the fluorescent probes. Figure 5.5 shows representative examples of fluorescence

micrographs of these tissue samples incubated with each probe. As can be seen in Figure 5.5, all tissue samples exposed to the ANCA probes contained small regions within the tissue that exhibited a significant concentration of fluorescence. As a negative control, we exposed frozen tissue sections from healthy human cases to probes **WMC-1**, **WMC-2** – **WMC-5**, **WMC-7** and did not observe such concentrated areas of fluorescence (data not shown).

More interestingly, inspection of the images from these staining experiments (Figure 5.5) reveal a trend of increased fluorescent labelling of amyloid plaques using probes **WMC-2** and **WMC-3** compared to all other probes (Figure 5.5G). This trend can be seen by increased fluorescence contrast between the plaques and surrounding tissue in Figures 5.5B,C (corresponding to tissue samples stained with compounds **WMC-2** and **WMC-3**) compared to the weaker observed contrast between the plaques and the surrounding tissue shown in Figures 5.5A,D-F (corresponding to tissue samples stained with compounds **WMC-1**, **WMC-4**, **WMC-5**, and **WMC-7**). We hypothesize that the improved contrast of amyloid deposits stained with probes **WMC-2** and **WMC-3** may be attributed to their increased hydrophilicity compared to **WMC-1**, **WMC-4**, **WMC-5**, and **WMC-7**. The increased hydrophilic properties of **WMC-2** and **WMC-3** could reduce the amount of non-specific staining by these probes to the brain tissue. This effect would result in the observed trend for increased fluorescence contrast between the plaques and surrounding tissue when using the more hydrophilic fluorescent probes.

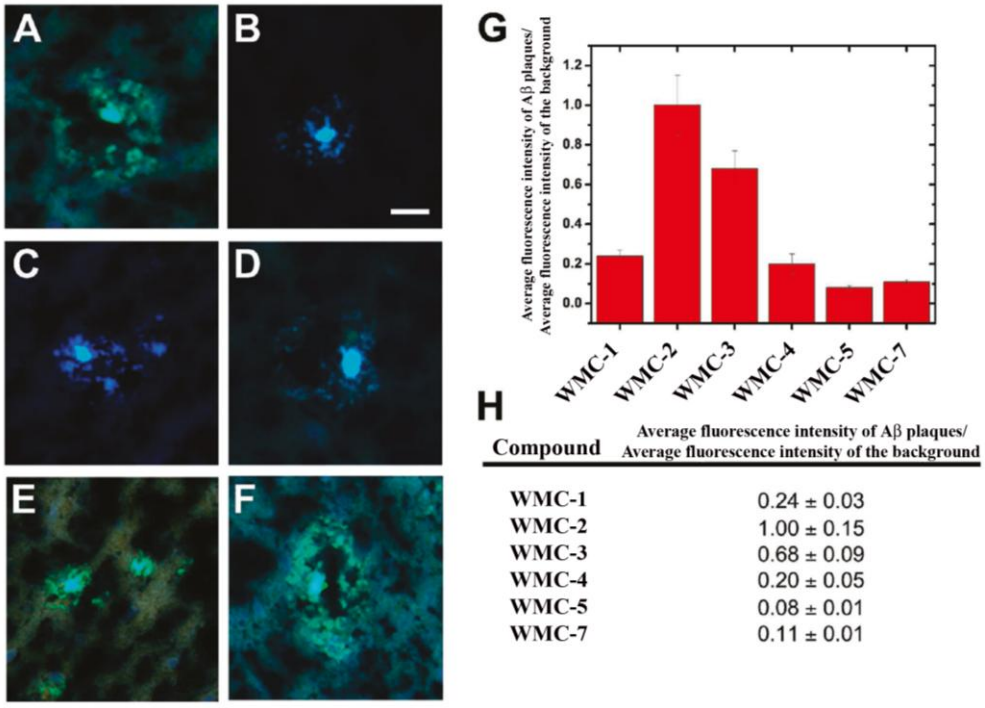


H

| Compound | Average fluorescence intensity of Aβ plaques/ Average fluorescence intensity of the background |
|---|---|
| **WMC-1** | 0.24 ± 0.03 |
| **WMC-2** | 1.00 ± 0.15 |
| **WMC-3** | 0.68 ± 0.09 |
| **WMC-4** | 0.20 ± 0.05 |
| **WMC-5** | 0.08 ± 0.01 |
| **WMC-7** | 0.11 ± 0.01 |

*Figure 5.5. Staining of Aβ plaques in brain sections from an AD patient. Frozen brain sections mounted on glass slides were dried and briefly fixed in ethanol, immersed in PBS, exposed to a 60 µM solution of fluorescent probe in PBS for 30 min, washed with PBS and covered with a glass coverslip. Plaques from brain sections were stained with A) compound **WMC-1**, B) compound **WMC-2**, C) compound **WMC-3**, D) compound **WMC-4**, E) compound **WMC-5**, or F) compound **WMC-7**. Stained Aβ plaques were imaged using a Leica DM IRE2 inverted epi-fluorescence microscope equipped with a Hamamatsu camera. Images from the blue, red, and green filters were overlayed. G) Graphical representation of the average fluorescence intensity of the probes bound to amyloid plaques relative to the fluorescence intensity of the background. All data is presented relative to the fluorescence contrast for staining plaques with compound **WMC-2**. The data represents the mean relative fluorescence intensity ± SD (n = 10 measurements for each compound). H) Table of the average fluorescence intensity of the plaques in A-F relative background. All data were normalized to the average fluorescence intensity of plaques stained with compound **WMC-2** relative to background. Scale bar = 20 µm.*

In addition, Figure 5.6A-C shows representative fluorescence micrographs of a single formalin-fixed tissue sample from a human AD patient that was treated sequentially with a mouse monoclonal anti-human Aβ IgG (clone 82E1), a fluorescently-labelled polyclonal anti-mouse IgG, and a solution containing probe

**WMC-3**. The bright green areas in Figure 5.6A indicate the regions of tissue that are labelled by compound **WMC-3**, the bright red areas in Figure 5.6B indicates the regions of the tissue that are labelled by the anti-Aβ IgGs, and the bright yellow areas in Figure 5.6C represent the regions where probe **WMC-3** and the anti-Aβ IgGs overlap in the tissue. The images in Figure 5.6A-C reveal that the fluorescent ANCA probes label the amyloid deposits with good specificity in these human tissue sections. These staining experiments strongly support the notion that the ANCA-based probes are capable of marking the location of amyloid deposits within human brain tissue.

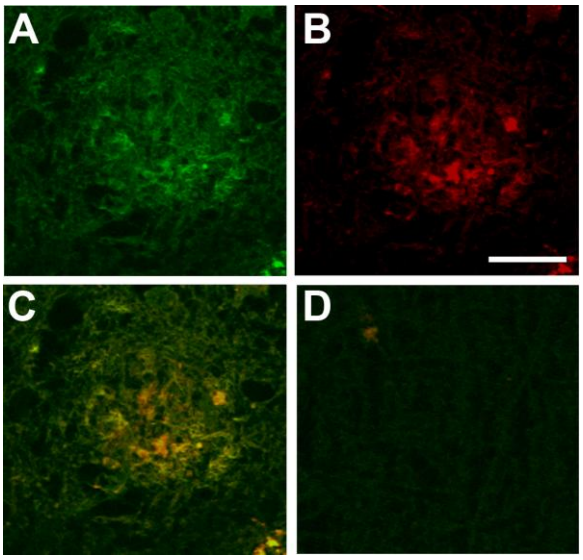


*Figure 5.6. Fluorescence micrographs of formalin-fixed brain sections from an AD patient revealing amyloid plaques that are labelled with A) probe **WMC-3** or B) a monoclonal anti-Aβ IgG (clone 82E1). C) A fluorescence micrograph representing regions of overlap (yellow) for the fluorescence labelling of tissue by probe **WMC-3** and the anti-Aβ IgG. No labelling was observed in the IgG isotype/DMSO stained isotype control section (D). Scale bar = 20 µm.*

## 5.3 Conclusion

In conclusion, we show that the aminonaphthalenyl-2-cyano-acrylate (ANCA) motif has appropriate fluorescence characteristics for the targeting and staining of Aβ deposits in tissue. Functionalization of this motif with water solubilizing groups does not affect the binding to Aβ but can help with the biocompatibility and water-solublizing properties of the compounds.[37, 39] On the other hand, changes in the nitrogen motif can significantly affect the binding affinity and specificity of the probes to Aβ deposits in tissue. Based on these results we can propose that the donor part of the molecule is most likely located within the binding pocket of the aggregated protein. Thus, any changes in that domain can affect the interactions between the small molecule and protein. Ongoing efforts in our lab are aiming to further support this hypothesis.

## 5.4 Materials & Methods

### 5.4.1 Materials

All reagents were purchased at highest commercial quality and used without further purification, except where noted. Air- and moisture-sensitive liquids and solutions were transferred via syringe or stainless steel cannula. Organic solutions were concentrated by rotary evaporation below 45 °C at approximately 20 mmHg. All non-aqueous reactions were carried out under anhydrous conditions.

Yields refer to chromatographically and spectroscopically ($^{1}$H NMR, $^{13}$C NMR) homogeneous materials, unless otherwise stated. Reactions were monitored

by thin-layer chromatography (TLC) carried out on 0.25 mm Dynamic Adsorbents, Inc. silica gel plates (60F-254) and visualized under UV light and/or developed by dipping in solutions of 10% ethanolic phosphomolybdic acid (PMA) and applying heat. Dynamic Adsorbents, Inc. silica gel (60, particle size 0.040-0.063 mm) was used for flash chromatography. NMR spectra were recorded on the Varian Mercury 400, 300 and/or Unity 500 MHz instruments and calibrated using the residual non-deuterated solvent as an internal reference. The following abbreviations were used to explain the multiplicities: s = singlet, d = doublet, t = triplet, q = quartet, m = multiplet, b = broad. High resolution mass spectra (HRMS) were recorded on a VG 7070 HS mass spectrometer under electron spray ionization (ESI) or electron impact (EI) conditions.

## 5.4.2 Experimental Methods

**6-bromo-2-naphthaldehyde (B).** To a solution of DIBAL-H (1.0 M in heptane, 34 mL, 34 mmol) at 0 °C under argon, a solution of **A** (3.0 g, 11 mmol) in anhydrous THF was added dropwise. The reaction mixture was allowed to warm up to room temperature and left stirring overnight. Upon completion, MeOH was added, followed by addition of a saturated sodium potassium tartrate solution and ethyl acetate. After the two phases were separated, the organic phase was washed with a saturated solution of ammonium chloride and brine, dried over $MgSO_4$ and concentrated under reduced pressure to yield 6-bromo-2-(hydroxymethyl) naphthalene. $R_f$ = 0.33 (EtOAc:Hexanes 3:7); $^1$H NMR (400 MHz, $CDCl_3$): δ = 7.99 (bs, 1H), 7.77 (bs, 1H), 7.74 (d, *J*= 8.5 Hz, 1H), 7.69 (d, *J*= 8.7 Hz, 1H), 7.55 (dd, *J*=

1.7, 8.7 Hz, 1H), 7.49 (dd, *J*= 1.7, 8.5 Hz, 1H), 4.84 (bs, 2H); $^{13}$C NMR (100 MHz, $CDCl_3$): δ = 138.8,133.9, 131.7, 129.7, 129.5, 129.5, 127.4, 126.1, 125.2, 119.8, 65.2.

To a suspension of pyridinium chlorochromate (2.4 g, 11 mmol) in anhydrous $CH_2Cl_2$ (60 mL) was added a solution of the above alcohol in anh. $CH_2Cl_2$, and the reaction was heated under reflux for 5 hours. Upon completion, it was cooled to room temperature and poured into diethyl ether. The solution was then filtered through a pad of silica and concentrated under reduced pressure to yield **B** (2.4 g, 95%). **B**: white solid; $R_f$ = 0.67 (EtOAc:Hexanes 3:7); $^1$H NMR (400 MHz, $CDCl_3$): δ = 10.15 (s, 1H), 8.31 (bs, 1H), 8.08 (bs, 1H), 7.98 (dd, *J*= 1.5, 8.5 Hz, 1H), 7.86 (m, 2H), 7.67 (dd, *J*= 1.5, 8.5 Hz, 1H); $^{13}$C NMR (100 MHz, $CDCl_3$): δ = 191.8, 137.3, 134.3, 134.1, 131.0, 131.0, 130.6, 130.2, 128.2, 124.0, 123.6.

**General procedure for the synthesis of 6-amino-substituted naphtaldehydes (C-F).**

In dry and degassed toluene (0.8 mL), were added $Pd(OAc)_2$ (0.022 mmol) and P(*t*Bu)3 (0.078 mmol). After stirring for 20 min, **B** (0.207 mmol), the appropriate amine (0.249 mmol) and cesium carbonate ($Cs_2CO_3$, 0.280 mmol) were added and the reaction left stirring for three days under reflux. After three days, the reaction was cooled at room temperature, diluted with $CH_2Cl_2$, filtered, concentrated under reduced pressure and purified via silica gel flash chromatography (hexanes/EtOAc 0-10%).

**6-(piperidin-1-yl)naphthalene-2-carbaldehyde (C).** 70% yield, yellow solid; $R_f$ = 0.61 (EtOAc:Hexanes 3:7); $^1$H NMR (400 MHz, $CDCl_3$): δ = 10.03 (s, 1H), 8.15 (s, 1H), 7.83 (m, 2H), 7.68 (d, *J*= 8.6 Hz, 1H) 7.32 (dd, *J*= 2.4, 9.1 Hz, 1H), 7.08 (d, *J*= 2.4 Hz, 1H), 3.38 (m, 4H), 1.78-1.63 (m, 6H); $^{13}$C NMR (100 MHz, $CDCl_3$): δ = 191.9, 151.9, 138.5, 134.4, 131.3, 130.4, 127.2, 126.3, 123.4, 119.5, 108.8, 49.6, 25.5, 24.3; HRMS calc for $C_{16}H_{18}NO$ $(M+H)^+$ 240.1383; found 240.1381.

**6-morpholinonaphthalene-2-carbaldehyde (D).** 79% yield, yellow solid; $R_f$ = 0.56 (EtOAc:Hexanes 3:7); $^1$H NMR (400 MHz, $CDCl_3$): δ = 10.06 (s, 1H), 8.20 (s, 1H), 7.88 (m, 2H), 7.73 (d, *J*= 8.4 Hz, 1H), 7.32 (m, 1H), 7.11 (d, *J*= 1.2 Hz, 1H), 3.92 (m, 4H), 3.36 (m, 4H); $^{13}$C NMR (100 MHz, $CDCl_3$): δ = 191.9, 151.3, 138.1, 134.2, 131.8, 130.6, 127.5, 127.0, 123.6, 118.7, 109.0, 66.7, 48.5; HRMS calc for $C_{15}H_{15}NO_2Na$ $(M+Na)^+$ 264.0995; found 264.0996.

**6-(4-methylpiperazin-1-yl)naphthalene-2-carbaldehyde (E).** 77% yield, yellow solid; $R_f$ = 0.36 (EtOAc:Hexanes 3:7); $^1$H NMR (300 MHz, $CDCl_3$): δ = 10.00 (s, 1H), 8.13 (s, 1H), 7.80 (m, 2H), 7.66 (d, *J*= 8.6 Hz, 1H), 7.28 (dd, *J*= 2.1, 9.2 Hz, 1H), 7.06 (d, *J*= 2.1 Hz, 1H), 3.36 (m, 4H), 2.57 (m, 4H), 2.33 (s, 3H); $^{13}$C NMR (100 MHz, $CDCl_3$): δ = 191.5, 151.0, 138.0, 134.0, 131.3, 130.2, 127.1, 126.4, 123.1, 118.7, 108.7, 54.5, 47.8, 45.7; HRMS calc for $C_{16}H_{19}N_2O$ $(M+H)^+$ 255.1492; found 255.1491.

**6-(2-morpholinoethylamino)naphthalene-2-carbaldehyde (F).** 33% yield, yellow solid; $R_f$ = 0.60 (2% MeOH in $CH_2Cl_2$); $^1$H NMR (400 MHz, $CDCl_3$): δ = 10.01 (s,

1H), 8.14 (s, 1H), 7.83 (dd, *J*= 1.6, 8.6 Hz, 1H), 7.76 (d, *J*= 8.9 Hz, 1H), 7.64 (d, *J*= 8.6 Hz, 1H), 6.98 (dd, *J*= 2.3, 8.9 Hz, 1H), 6.79 (d, *J*= 2.3 Hz, 1H), 4.88 (bs, 1H), 3.75 (m, 4H), 3.31 (dd, *J*= 5.1, 11.1 Hz, 2H), 2.72 (m, 2H), 2.51 (bs, 4H); $^{13}$C NMR (100 MHz, $CDCl_3$) δ 191.9, 148.8, 139.1, 134.6, 130.8, 130.7, 126.6, 126.0, 123.8, 118.7, 103.8, 66.9, 56.7, 53.3, 39.3; HRMS calc for $C_{17}H_{21}N_2O_2$ $(M+H)^+$ 285.1598; found 285.1600.

**General procedure for the synthesis of 2-cyanoacetates (G).**

To a solution of 2-cyanoacetic acid (2.72 mmol), the appropriate alcohol (2.27 mmol) in $CH_2Cl_2$ (2.5 mL) and DMAP (0.013 mmol) was added dropwise at 0 °C. Finally, DCC (2.72 mmol) was added and the reaction mixture was stirred at 0 °C for 6 hours. The reaction was diluted with $CH_2Cl_2$ and the formed dicyclohexyl urea (DCU) was filtered off. The filtrate was dried over $MgSO_4$ and concentrated under reduced pressure. The residue was purified by silica gel flash chromatography to yield 2-cyanoacetate **G**.

**2-(2-(2-methoxyethoxy)ethoxy)ethyl-2-cyanoacetate (G-1).** 86% yield; colorless liquid; $R_f$ = 0.45 (100% ether); $^1$H NMR (400 MHz, $CDCl_3$): δ = 4.29 (m, 2H), 3.67, (m, 2H), 3.59 (m, 6H), 3.50 (m, 2H), 3.49 (s, 2H), 3.32 (s, 3H); $^{13}$C NMR (100 MHz, $CDCl_3$): δ = 163.0, 113.0, 71.7, 70.4, 70.3, 68.3, 65.5, 58.8, 24.5; HRMS calc for $C_{10}H_{17}NO_5$: $(M+H)^+$ 232.1185; found 232.1199.

**2-(2-(2-(2-methoxyethoxy)ethoxy)ethoxy)ethyl-2-cyanoacetate (G-2).** 68% yield; colorless liquid; $R_f$ = 0.40 (100% ether); $^1$H NMR (400 MHz, $CDCl_3$): δ = 4.21 (bs, 2H), 3.61 (bs, 2H), 3.51 (m, 12H), 3.43 (m, 2H), 3.24 (bs, 3H) $^{13}$C NMR (100 MHz,

$CDCl_3$): δ = 163.0, 113.0, 71.4, 70.2, 70.1, 70.1, 70.0, 68.1, 65.3, 58.5, 24.2; HRMS calc for $C_{12}H_{22}NO_6$: $(M+H)^+$ 276.1447; found 276.1455.

**(2,2-dimethyl-1,3-dioxolan-4-yl)methyl 2-cyanoacetate (G-3).** 71% yield; colorless liquid; $R_f$ = 0.83 (100% EtOAc); $^1$H NMR (400 MHz, $CDCl_3$): δ = 4.35 (m, 1H), 4.29-4.19 (m, 2H), 4.09 (m, 1H), 3.76 (dd, *J*= 5.8, 8.6 Hz, 1H), 3.52 (s, 2H), 1.43 (s, 3H), 1.36 (s, 3H); $^{13}$C NMR (100 MHz, $CDCl_3$): δ = 162.8, 112.7, 110.1, 73.0, 66.8, 65.9, 26.6, 25.2, 24.6; HRMS calc for $C_9H_{13}NO_4$ $(M+H)^+$ 200.0923; found 200.0931.

**General procedure for the synthesis of fluorescent probes**

To a round bottom flask containing a solution of aldehyde (0.21 mmol) and the appropriate 2-cyanoacetate (0.23 mmol) in THF (0.8 mL), piperidine (0.02 mmol) was added and the mixture left stirring at 50 °C. The reaction was monitored by TLC and was completed within 21 hours. The crude mixture was concentrated under reduced pressure and the product was purified via flash column chromatography (10-30% EtOAc in hexanes).

**(E)-2-(2-(2-methoxyethoxy)ethoxy)ethyl 2-cyano-3-(2-(piperidin-1-yl)napthalen-6-yl) acrylate (WMC-1).** 90% yield; red liquid; $R_f$ = 0.44 (EtOAc:Hexanes 1:1); $^1$H NMR (400 MHz, $CDCl_3$): δ = 8.31 (s, 1H), 8.22 (bs, 1H), 8.10 (d, *J*= 8.8 Hz, 1H), 7.76 (d, *J*= 9.2 Hz, 1H), 7.65 (d, *J*= 8.8 Hz, 1H), 7.30 (dd, *J*= 2.1, 9.2 Hz, 1H), 7.05 (d, *J*= 2.1 Hz, 1H), 4.47 (m, 2H), 3.83 (m, 2H), 3.74-3.66 (m, 6H), 3.56 (m, 2H), 3.42-3.38 (m, 4H), 3.37 (s, 3H), 1.74 (m, 6H); $^{13}$C NMR (100 MHz, $CDCl_3$): δ = 163.3, 155.4, 151.9, 137.7, 134.7, 130.6, 127.2, 126.4, 125.9, 125.6, 119.2, 116.4,

108.3, 71.8, 70.7, 70.5, 70.5, 68.7, 65.3, 58.9, 49.3, 25.4, 24.3; HRMS calc for $C_{26}H_{32}N_2O_5Na$ $(M+Na)^+$ 475.2203; found 475.2197.

**(E)-2-(2-(2-methoxyethoxy)ethoxy)ethyl-2-cyano-3-(2-(4-methylpiperazin-1-yl) napthalen-6-yl)acrylate (WMC-2).** 85% yield; red liquid; $R_f$ = 0.71 (2% MeOH in $CH_2Cl_2$); $^1$H NMR (400 MHz, $CDCl_3$): δ = 8.31 (s, 1H), 8.23 (s, 1H), 8.10 (d, *J*= 8.6 Hz, 1H), 7.78 (d, *J*= 9.1 Hz, 1H), 7.67 (d, *J*= 8.6 Hz, 1H), 7.29 (d, *J*= 9.1 Hz, 1H), 7.06 (s, 1H), 4.46 (m, 2H), 3.83 (m, 2H), 3.73 (m, 2H), 3.67 (m, 4H), 3.55 (m, 2H) 3.42 (bs, 4H), 3.36 (s, 3H), 2.61 (bs, 4H), 2.37 (s, 3H); $^{13}$C NMR (100 MHz, $CDCl_3$): δ = 163.2, 155.4, 151.4, 137.5, 134.5, 130.6, 127.4, 126.9, 126.1, 126.1, 119.0, 116.2, 108.7, 99.3, 71.9, 70.8, 70.6, 70.5, 68.8, 65.4, 59.0, 54.8, 48.0, 46.1; HRMS calc for $C_{26}H_{34}N_3O_5$ $(M+H)^+$ 468.2493; found 468.2494.

**(E)-2-(2-(2-methoxyethoxy)ethoxy)ethyl-2-cyano-3-(2-morpholinonapthalen-6-yl) acrylate (WMC-3).** 83% yield; red liquid; $R_f$ = 0.76 (2% MeOH in $CH_2Cl_2$); $^1$H NMR (300 MHz, $CDCl_3$): δ = 8.31 (s, 1H), 8.24 (s, 1H), 8.11 (dd, *J*= 1.9, 8.8 Hz, 1H), 7.80 (d, *J*= 9.1 Hz, 1H), 7.69 (d, *J*= 8.8 Hz, 1H), 7.28 (m, 1H), 7.06 (d, *J*= 1.9 Hz, 1H), 4.47 (m, 2H), 3.90 (m, 4H), 3.83 (m, 2H), 3.70 (m, 6H), 3.55 (m, 2H), 3.35 (m, 7H); $^{13}$C NMR (100 MHz, $CDCl_3$): δ = 163.0, 155.2, 151.3, 137.2, 134.4, 130.6, 127.4, 127.0, 126.1, 126.0, 118.5, 116.1, 108.5, 99.4, 71.8, 70.7, 70.5, 70.4, 68.6, 66.5, 65.3, 58.9, 48.2; HRMS calc for $C_{25}H_{30}N_2O_6Na$ $(M+Na)^+$ 477.1996 found 477.1995.

**(E)-2-(2-(2-methoxyethoxy)ethoxy)ethyl-3-(2-(2-morpholinoethylamino) naphthalen-6-yl)-2-cyano acrylate (WMC-4).** 87% yield; red liquid; $R_f$ = 0.53 (2%

MeOH in $CH_2Cl_2$); $^1$H NMR (500 MHz, $CDCl_3$): δ = 8.28 (s, 1H), 8.19 (d, *J*= 1.6 Hz, 1H), 8.08 (dd, *J*= 1.9, 8.8 Hz, 1H), 7.69 (d, *J*= 8.9 Hz, 1H), 7.60 (d, *J*= 8.8 Hz, 1H), 6.95 (dd, *J*= 2.3, 8.8 Hz, 1H), 6.74 (d, *J*= 2.2 Hz, 1H), 4.96 (bs, 1H), 4.46 (m, 2H), 3.83 (m, 2H), 3.76-3.72 (m, 6H), 3.69-3.65 (m, 4H), 3.57-3.54 (m, 2H), 3.36 (s, 3H), 3.31 (s, 2H), 2.70 (m, 2H), 2.51 (s, 4H); $^{13}$C NMR (100 MHz, $CDCl_3$): δ = 163.4, 155.5, 149.0, 138.3, 135.0, 130.9, 126.6, 126.3, 126.2, 124.9, 118.9, 116.5, 103.6, 98.2, 71.9, 70.8, 70.6, 70.5, 68.8, 66.9, 65.3, 59.0, 56.6, 53.2, 39.2; HRMS calc for $C_{27}H_{36}N_3O_6$ $(M+H)^+$ 498.2599; found 498.2596.

**(E)-2-(2-(2-(2-methoxyethoxy)ethoxy)ethoxy)ethyl-2-cyano-3-(2-(piperidin-1-yl)napthalen-6-yl)acrylate (WMC-5).** 89% yield; red liquid; $R_f$ = 0.67 (2% MeOH in $CH_2Cl_2$); $^1$H NMR (400 MHz, $CDCl_3$): δ = 8.20 (s, 1H), 8.10 (s, 1H), 8.01(d, *J*= 8.5 Hz, 1H), 7.66 (d, *J*= 9.0 Hz, 1H), 7.55 (d, *J*= 9.0 Hz, 1H), 7.20 (d, *J*= 8.5 Hz, 1H), 6.95 (s, 1H), 4.39 (bs, 2H), 3.75 (bs, 2H), 3.65-3.54 (m, 10H), 3.45 (m, 2H), 3.31 (bs, 4H), 3.28 (s, 3H), 1.65-1.54 (m, 6H); $^{13}$C NMR (100 MHz, $CDCl_3$): δ = 163.2, 155.3, 151.8, 137.6, 134.6, 130.5, 127.1, 126.3, 125.8, 125.5, 119.1, 116.3, 108.2, 98.4, 71.7, 70.6, 70.4, 70.3, 68.6, 65.3, 58.8, 49.2, 25.3, 24.2; HRMS calc for $C_{28}H_{36}N_2O_6Na$ $(M+Na)^+$ 519.2466; found 519.2468.

**(E)-(2,2-dimethyl-1,3-dioxolan-4-yl)methyl-2-cyano-3-(2-(piperidin-1-yl) naphthalene-6-yl) acrylate (WMC-6).** 83% yield; red liquid; $R_f$ = 0.25 (EtOAc:Hexanes 4:6); $^1$H NMR (400 MHz, $CDCl_3$): δ = 8.29 (s, 1H), 8.19 (s, 1H), 8.09 (dd, *J*= 1.9, 8.8 Hz, 1H), 7.74 (d, *J*= 9.3 Hz, 1H), 7.63 (d, *J*= 8.8 Hz, 1H), 7.28 (dd, *J*= 2.8, 9.3 Hz, 1H), 7.03 (d, *J*= 1.9 Hz, 1H), 4.43 (m, 1H), 4.36 (m, 2H), 4.14

(dd, *J*= 6.0, 8.5 Hz, 1H), 3.90 (dd, *J*= 6.0, 8.5 Hz, 1H), 3.40 (m, 4H), 1.73-1.66 (m, 6H), 1.48 (s, 3H), 1.39 (s, 3H); $^{13}$C NMR (100 MHz, $CDCl_3$): δ = 162.9, 155.4, 151.5, 137.6, 134.6, 130.5, 127.0, 126.2, 125.6, 125.3, 119.0, 116.1, 109.6, 108.2, 98.0, 73.1, 65.9, 65.6, 57.1, 49.1, 45.5, 29.4, 26.4, 25.2, 24.0; MS $(M+H)^+$ 421.24.

**(E)-2,3-dihydroxypropyl2-cyano-3-(2-(piperidin-1-yl) naphthalene-6-yl)acrylate (WMC-7).** Compound **WMC-6** (50 mg, 0.12 mmol) was dissolved in a mixture of THF/MeOH (1:1) and DOWEX-$H^+$ resin (15 mg) was added and the heterogeneous mixture was stirred for 20 hours. The resin was removed by filtration and triethylamine was added and the solvent was removed under reduced pressure. The residue was purified by flash chromatography to give compound **WMC-7**. **WMC-7**: 38 mg, 84% yield; red liquid; $R_f$ = 0.55 (EtOAc:Hexanes 1:4); $^1$H NMR (400 MHz, $CDCl_3$): δ = 8.30 (s, 1H), 8.19 (s, 1H), 8.08 (d, *J*= 8.8 Hz, 1H), 7.74 (d, *J*= 9.1 Hz, 1H), 7.63 (d, *J*= 9.1 Hz, 1H), 7.29 (m, 1H), 7.03 (s, 1H), 4.46-4.36 (m, 2H), 4.09 (m, 1H), 3.81 (dd, *J*= 5.5, 11.3 Hz, 1H), 3.73 (dd, *J*= 5.5, 11.3 Hz, 1H), 3.41 (m, 4H), 1.74-1.67 (m, 6H); $^{13}$C NMR (100 MHz, $CDCl_3$): δ = 163.6, 156.0, 152.0, 137.9, 135.0, 130.7, 127.3, 126.3, 125.9, 125.5, 119.2, 116.6, 108.3, 97.8, 69.9, 67.0, 63.2, 49.3, 25.5, 24.3; HRMS calc for $C_{22}H_{25}N_2O_4$ $(M+H)^+$ 381.1809; found 381.1802.

**Fluorescence studies with aggregated Aβ peptides:** Aggregated Aβ peptide was prepared as described previously.[24] Briefly, we dissolved Aβ42 in PBS pH 7.4 to a final concentration of 100 μM. This solution was magnetically stirred at 1200 rpm for 3 days at room temperature. Aliquots of 15 μL of the pre-aggregated Aβ42 solution was added to 285 μL of the probe (5% DMSO in nanopure water) to attain a

final concentration of 5 μM Aβ42 and 4 μM of the probe. The solution was transferred to a 300 μL cuvette and the fluorescence was measured.

**Determination of the binding constant ($K_d$) of the probe to aggregated Aβ:** Pre-aggregated Aβ42 (5 μM final concentration) was mixed with various concentrations of probes (10, 5, 2.5, 1.25 μM) in 5% DMSO in nanopure water and their $K_d$'s were determined as described previously. [24]

**Patient samples.** AD cases were from the Alzheimer Disease Research Center (ADRC) at the University of California, San Diego (UCSD). Subjects came to autopsy between 1985 and 2006 and postmortem interval for the cases was under 12 h. Institutional board review was obtained from the UCSD Human Research Protections Program, in accordance with the Health Insurance Portability and Accountability Act. Written informed consent was obtained from all patients or their guardians.

**Staining of human tissue sections.** Frozen brain sections from patients diagnosed with AD were dried for 1 h, treated with 100%, 95%, and 70% ethanol for 5 min. each, and then rinsed in deionized water. The sections were equilibrated in phosphate-buffered saline (PBS) for 15 min. Fluorescent molecules were diluted in PBS (1:50, from stock solutions of 3 mM in PBS to give a final concentration of 60 μM), added to the brain sections, incubated for 30 min at room temperature, washed with PBS, and coverslipped.

**Co-staining with the Aβ antibody 82E1 and compound WMC-3.** Aβ and compound **WMC-3** co-staining was performed on a formalin-fixed brain section

from an AD case. Slides were deparaffinized, incubated for 5 min in 98% formic acid, and then washed in distilled water for 5 min. Sections were blocked with 10% goat serum and incubated with anti-Aβ antibody 82E1 (Immunobiological Laboratories) for 30 min. The slides were washed with PBS containing 0.2% tween and stained with antibody anti-mouse HRP (Jackson Immunolabs), washed in PBS-tween, and tyramide-Alexa Fluor 594 (Invitrogen™) for 30 min. After washing with PBS-tween, the slides were stained with 60 μM solutions of compound **WMC-3** for 30 min. Control sections were co-stained with the mouse isotype control antibody as the primary antibody, and the PBS control buffer that was used to generate stock solutions of compound **WMC-3**. Adjacent sections were singly stained with Aβ antibody 82E1 or compound **WMC-3**.

**Fluorescence microscopy.** The sample was excited using an Argon 488 nm laser on an Olympus FluoView FV1000 confocal microscope. The emission spectra of the probes bound to Aβ or background was collected in 5 nm increments from 450 – 645 nm. A minimum of 10 measurements were collected for probe bound to Aβ and for background. The peak intensity for the Aβ-bound probe was divided by an average of the background measurements to calculate the ratio of probe to background signal.

# 5.5 Additional Figures

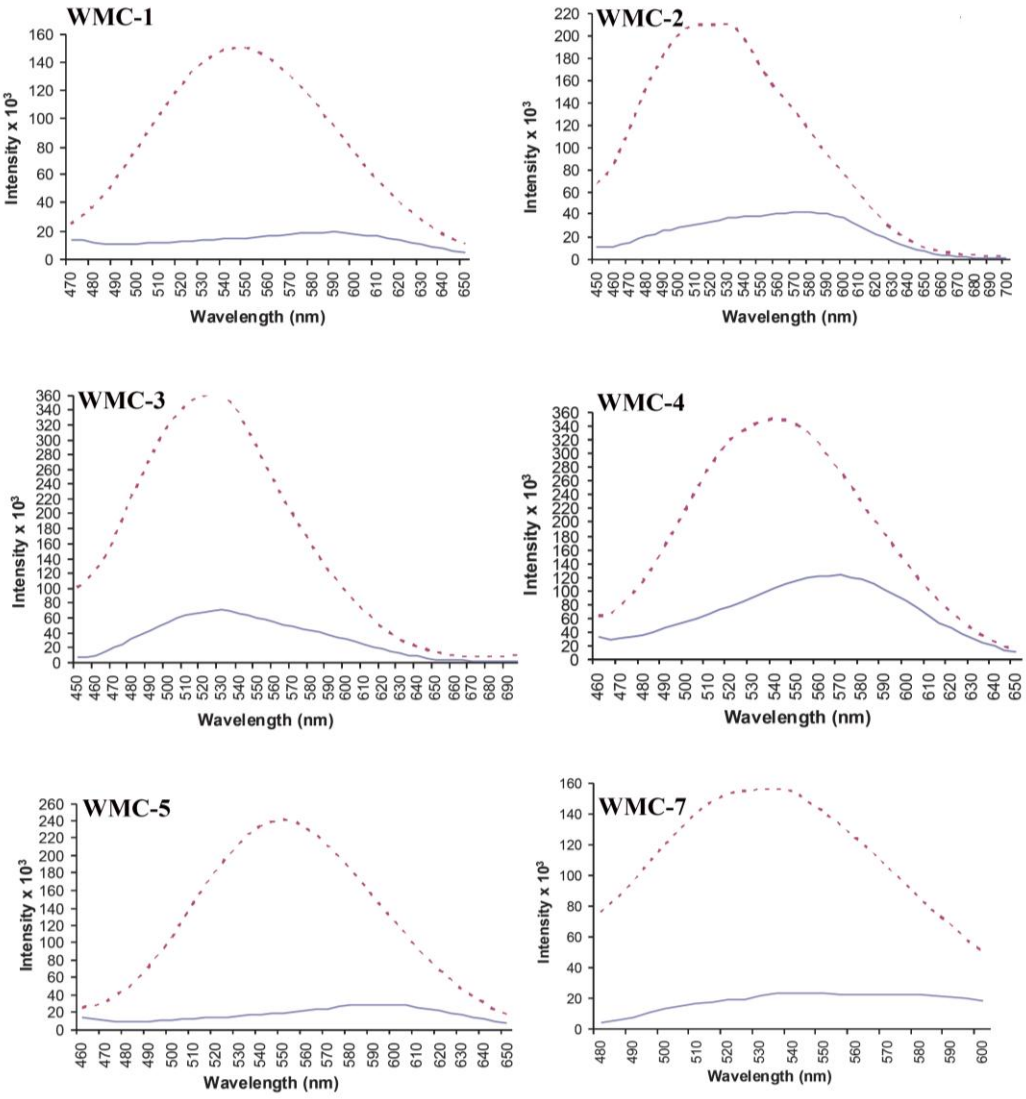


*Figure 5.7. Fluorescence emission spectra for probes in PBS(—) and in the presence of aggregated Aβ peptides (---).*

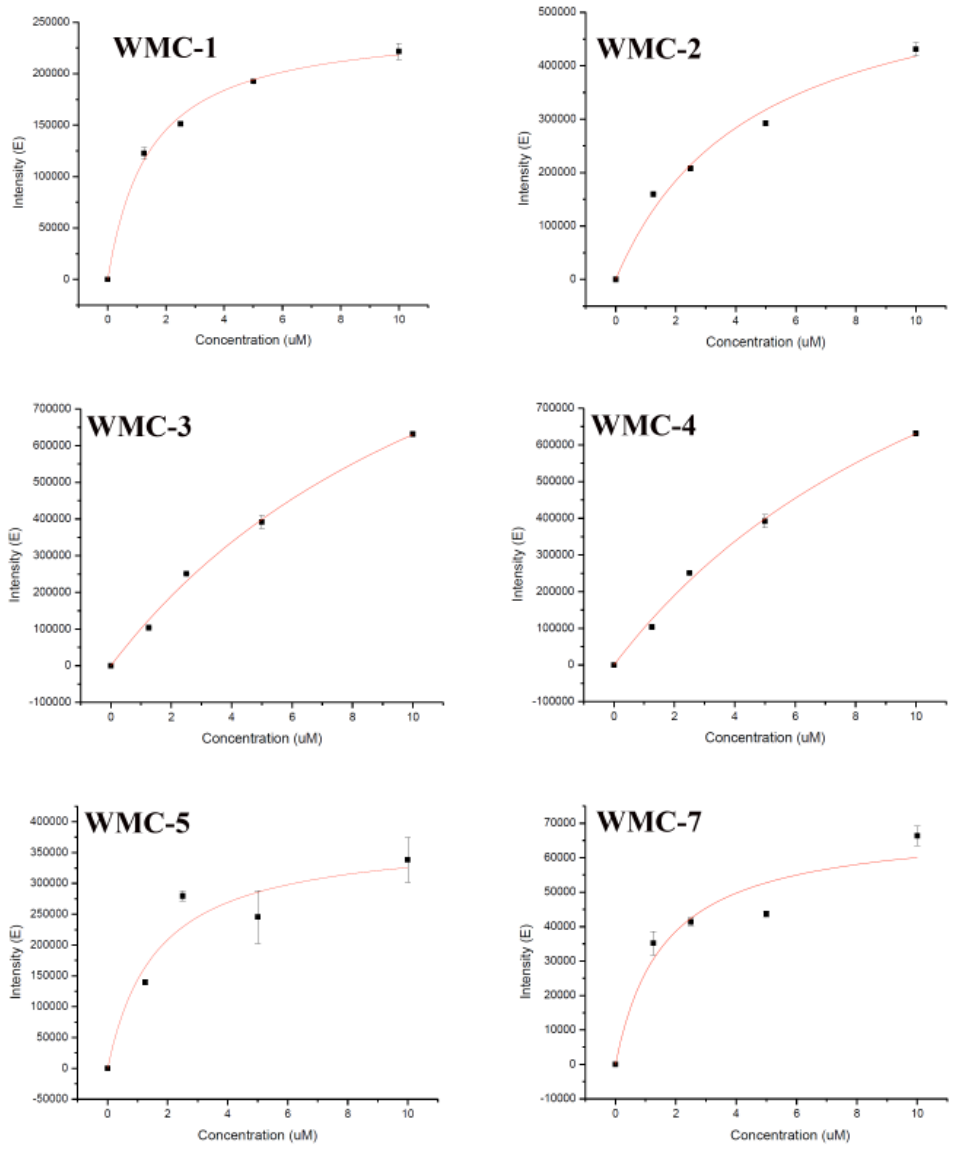


*Figure 5.8. Saturation binding curves of probes to aggregated Aβ42 peptide*

## Notes about this Chapter

This chapter is based on material that appears in "ANCA: A Family of Fluorescent Probes that Bind and Stain Amyloid Plaques in Human Tissue." Copyright (2011) American Chemical Socisety. Chang, W. M.; Dakanali, M.;

Capule, C. C.; Sigurdson, C. J.; Yang, J.; Theodorakis, E. A. *ACS Chem. Neurosci.* **2011**, *2*, 249-255. Willy M. Chang is the first author of this work and generated a significant portion of the data. I am a co-author on this publication. My contributions focused on the technical aspects of the fluorescence measurements, data analysis of the binding studies, and preliminary quantitative analysis of the fluorescence micrographs of stained brain tissue.

# Chapter 6

# Amyloid-binding Small Molecules Efficiently Block SEVI- and Semen-mediated Enhancement of HIV-1 Infection

## 6.1 Introduction

The global HIV-1 epidemic remains a pressing public health threat nearly 30 years after its identification. The vast majority of cases worldwide are acquired by heterosexual transmission, especially male to female.[46] Therefore, a microbicide that could limit the sexual transmission of HIV might provide an affordable and feasible way to decrease the spread of the virus, especially in developing countries.

Recently, Münch *et al.*[5] demonstrated that human semen can enhance HIV infection as a result of the presence of amyloid fibrils formed from a self-assembling peptide consisting of amino acid residues 248-486 of prostatic acid phosphatase

(PAP),[5] an abundant protein secreted into semen from the prostate. These fibrils, which Münch *et al.* termed the "semen-derived enhancer of virus infection" (SEVI), are highly cationic and enhance infectivity by at least two mechanisms. First, they decrease the electrostatic repulsion between the negatively charged surface of the virion and the target cell, and second, they bind virions and increase their rate of sedimentation onto the target cell surface, therefore enhancing the likelihood of receptor mediated viral entry.[204] The effect of SEVI fibrils is greatest with low levels of infectious virus,[5] similar to the conditions seen in a mucosal transmission of HIV, where relatively few virions must cross the mucosal barrier.[205]

Other amyloid fibrils, especially amyloid-β (Aβ), which is associated with Alzheimer's Disease,[206] have been well studied as potential therapeutic or diagnostic targets. One approach to target Aβ fibrils is the use of small molecules that bind the fibrils at a high density and thereby sterically inhibit their interactions with proteins.[57,58,121] The amyloid imaging agent, Thioflavin T (ThT) is one such molecule. Substituted 2-(4-aminophenyl)benzothiazoles (commonly referred to as "benzothiazole aniline" or BTA) are biocompatible analogues of ThT that bind to an increased number of sites along the Aβ fibril axis.[207] Specifically, the hexa(ethylene glycol) derivative of ThT, BTA-$EG_6$ (Figure 6.1), has been shown to bind to Aβ fibrils and to inhibit the interaction of Aβ fibrils with other proteins.[57,58] ThT and its derivatives are believed to bind to Aβ based on the β-sheet motif that is common to all amyloid fibrils.[63] Therefore, we investigated the ability of these small molecules to bind to SEVI and interfere with SEVI-mediated enhancement of HIV-1

infectivity.

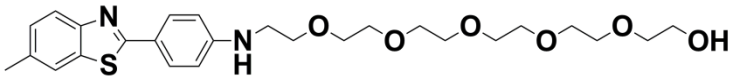


*Figure 6.1. The structure of BTA-EG$_6$*

We show here that BTA-EG$_6$ is capable of inhibiting both SEVI-mediated and semen-mediated enhancement of HIV-1 infectivity in a dose-dependent fashion. Furthermore, BTA-EG$_6$ exhibited no toxicity toward cervical cells. Taken together, these features show that BTA-EG$_6$ may be a useful candidate as an addition to potential microbicide formulations.

## 6.2 Results and Discussion

BTA-EG$_6$ has been previously shown to bind Aβ fibrils and interfere with the ability of Aβ-binding proteins to interact with the fibrils.[57,58,121] Based on these previous studies, and because SEVI shares the same β-sheet structural motif as aggregated Aβ, we hypothesized that BTA-EG$_6$ might also bind to SEVI fibrils. To test this hypothesis, we used fluorescence polarization to measure the ability of BTA-EG$_6$ to bind SEVI. Increasing concentrations of BTA-EG$_6$ were added to 50 μg/mL SEVI that had been preincubated with 16 μg/mL of fluorescein isothiocyanate-heparin (FITC-heparin), a known SEVI binder.[55] BTA-EG$_6$ was able to displace fluorescent heparin from the SEVI fibrils in a dose-dependent fashion (Figure 6.2), suggesting an interaction between these molecules and the fibrils.

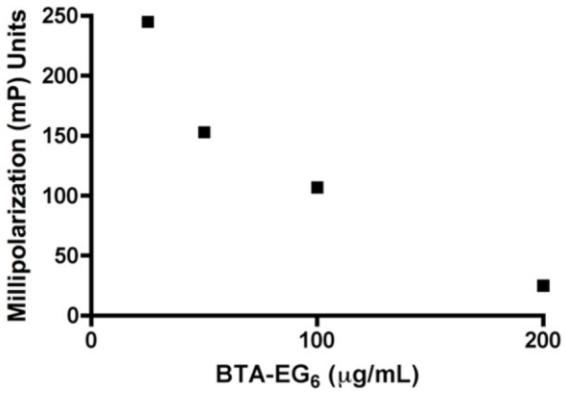


*Figure 6.2. BTA-$EG_6$ binds SEVI fibrils as measured by fluorescence polarization.*

To quantify the binding affinity of BTA-$EG_6$ to SEVI fibrils, I used a previously reported fluorescence-based assay to determine the $K_d$ between BTA-$EG_6$ and SEVI fibrils (Figure 6.3A).[83] Figure 6.3A shows the fluorescence intensity of BTA-$EG_6$ bound to SEVI fibrils as a function of exposure of the SEVI peptides to increasing concentrations of BTA-$EG_6$. Fitting the data with a one-site specific binding algorithm revealed a $K_d$ of 127 ± 22 nM. For comparison, I also measured the binding affinity of BTA-$EG_6$ toward Aβ fibrils (Figure 6.3B) and found that it exhibited a similar affinity for aggregated Aβ, with a $K_d$ of 111 ± 32 nM. These results suggest that BTA-$EG_6$ binds to these fibrils based on their shared structural features.

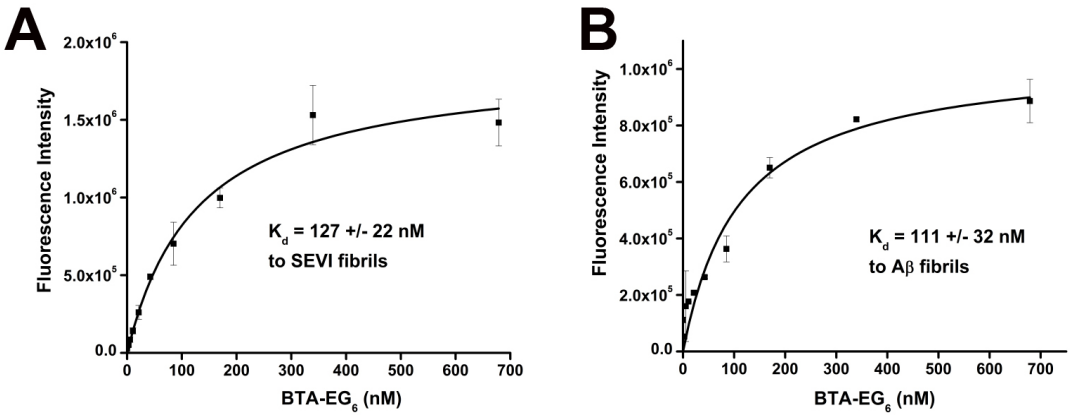


*Figure 6.3. A) The saturation binding curve of BTA-EG$_6$ to SEVI fibrils. B) The saturation binding curve of BTA-EG$_6$ to Aβ fibrils*

Given that BTA-EG$_6$ binds with similar affinity towards SEVI and Aβ fibrils, and based on what is known about the interactions of BTA-EG$_6$ with Aβ fibrils,[57,58] we hypothesized that BTA-EG$_6$ can densely coat the surface of SEVI and inhibit SEVI-HIV virion interactions, thereby neutralizing SEVI-mediated enhancement of HIV-1 infectivity. We evaluated the ability of BTA-EG$_6$ to inhibit SEVI-mediated enhanced infection of HIV-1 (strain IIIB) in CEM-M7 cells as a function of BTA-EG$_6$ concentration. CEM-M7 cells are a CD4$^+$, CCR5$^+$, CXCR4$^+$ T/B cell hybrid cell line and contain HIV LTR-driven luciferase and green fluorescent protein (GFP) reporter gene cassettes. The HIV LTR is a weak transcriptional regulator in the absence of its cognate, virally-encoded *trans*-activator, Tat. As a result, luciferase and GFP expression levels in these cells are directly responsive to HIV-1 infection; this property therefore provides a convenient method to determine the extent of viral infection. In this assay, BTA-EG$_6$ effectively inhibited SEVI-mediated enhancement

of HIV infection in a dose-dependent fashion. The extent of infection was brought down to nearly baseline levels at the highest concentration of BTA-$EG_6$ (44 μM, Figure 6.4A). Importantly, BTA-$EG_6$ had no effect on the infectivity of HIV virus alone, even at the highest concentration (Figure 6.4B), suggesting that this effect was not due to direct inhibition of intrinsic virus infectivity.

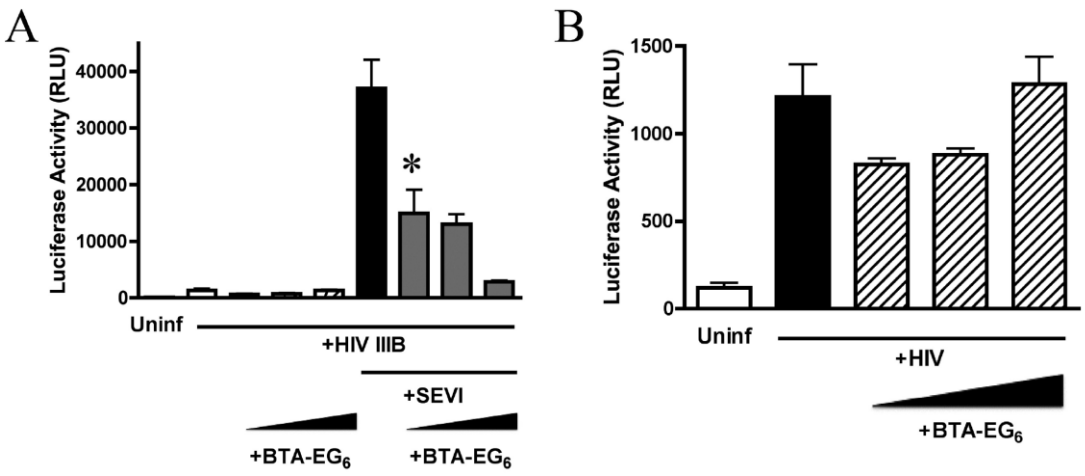


*Figure 6.4. BTA-$EG_6$ inhibits SEVI-mediated enhancement of HIV-1 infection. A) HIV-$1_{IIIB}$ virions were preincubated with increasing concentrations of BTA-$EG_6$ (0, 11, 22, 44 μM) and with or without SEVI. RLU, relative luciferase units. Uninf, uninfected B) A magnification of panel A to show data for cells treated with HIV-$1_{IIIB}$ virions with and without increasing concentrations of BTA-$EG_6$, in the absence of SEVI.*

We next calculated the $IC_{50}$ of BTA-$EG_6$ for inhibition of SEVI-mediated enhancement of HIV-1 infection. To determine the $IC_{50}$, CEM-M7 cells were infected with HIV-$1_{ADA}$ and 15 μg/ml SEVI in the presence of BTA-$EG_6$. Ten different BTA-$EG_6$ concentrations were tested, ranging from 0.4 to 50 μg/ml. The data were fit to an exponential decay curve and the $IC_{50}$ was determined to be 6.6 μg/ml for BTA-$EG_6$ (equivalent to 13 μM, figure 6.5).

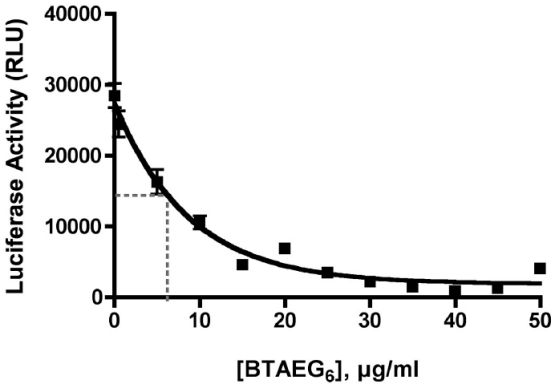


*Figure 6.5. CEM-M7 cells were infected with HIV-$1_{ADA}$+SEVI and various concentrations of BTA-$EG_6$. An exponential decay curve was fit to the data to calculate the $IC_{50}$ of the inhibitory effect of BTA-$EG_6$ on SEVI-mediated enhancement of HIV-1 infection.*

For BTA-$EG_6$ to be a viable microbicide candidate, it must be effective not just against the effects of SEVI, but should be able to effectively inhibit the infection-enhancing activity of human semen. Therefore, we examined the effect of BTA-$EG_6$ on semen-mediated enhancement of HIV-1 infection in Jurkat cells (an immortalized T-cell line). BTA-$EG_6$ was able to efficiently inhibit semen-mediated enhancement of HIV-$1_{IIIB}$ infection, at the same concentrations tested with SEVI alone (Figure 6.6).

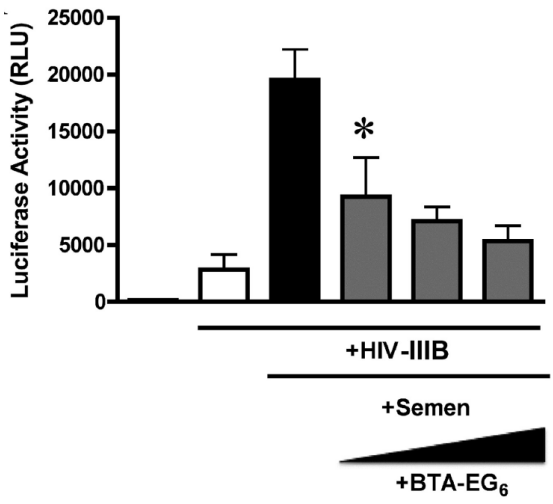


*Figure 6.6. BTA-$EG_6$ inhibits semen-mediated enhancement of HIV-1 infectivity. RLU, relative luciferase units.*

To more closely examine how BTA-$EG_6$ exerts its inhibitory effects on SEVI-mediated HIV-1 infection enhancement, we examined the ability of this compound to interfere with SEVI-enhanced binding of HIV-1 virions to the cell surface. The cationic nature of SEVI has been shown to enhance the binding of HIV-1 virions to the cell surface, which allows it to neutralize the electrostatic repulsion between the negatively charged HIV-1 virion and target cell surface.[204] Jurkat T cells were incubated with HIV-$1_{IIIB}$ virions and 15 μg/mL of SEVI in the presence or absence of increasing concentrations of BTA-$EG_6$. The amount of surface bound virions were then measured by p24 ELISA after rinsing off unbound virus. SEVI strongly promoted the binding of virions to the cell surface, and this effect was efficiently abrogated by BTA-$EG_6$ (Fig. 6.7). Importantly, in the absence of SEVI, BTA-$EG_6$ had no effect on the binding of HIV virions to the cell surface

(Figure 6.7), which suggests that BTA-$EG_6$ does not directly interact with HIV virions.

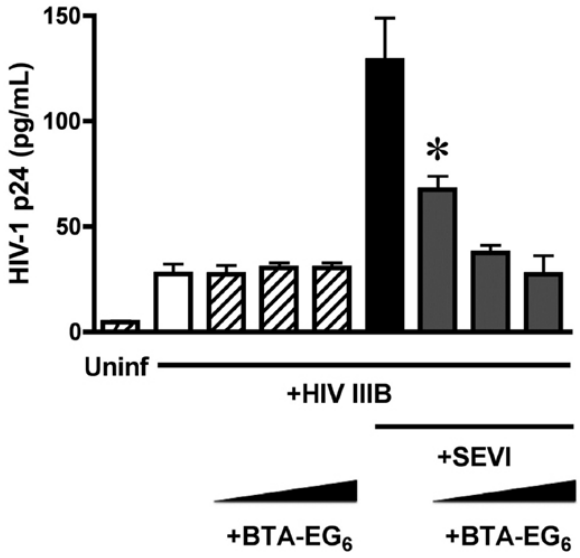


*Figure 6.7. BTA-$EG_6$ prevents SEVI-mediated attachment of HIV-1 to the cell surface*

For a compound to be a legitimate HIV-1 microbicide candidate, it must not have toxic or inflammatory effects on the cervical endothelium. Loss of this protective layer leads to an increased ability for HIV-1 to cross the mucosal barrier, and inflammatory effects drive recruitment of HIV-1 target cells, further decreasing the natural barriers against successful transmission of HIV. Therefore, we examined the effects of BTA-$EG_6$ on A2En cells, a primary-cell derived line from the endocervical endothelium.

To evaluate the effects of BTA-$EG_6$ on cell viability, the compound was added to cells at concentrations up to 10× the $IC_{50}$ (13 μM) for up to 24 hours.

Nonoxynol-9, a spermicide, was used as a positive control for induction of cell death, as it is known to be toxic to cervical epithelial cells.[208] Viability was assessed at 24 hours by using the resazurin cytotoxicity assay. Fig 6.8 shows that BTA-$EG_6$ did not have any detrimental effect on cell viability, even at the highest concentrations tested.

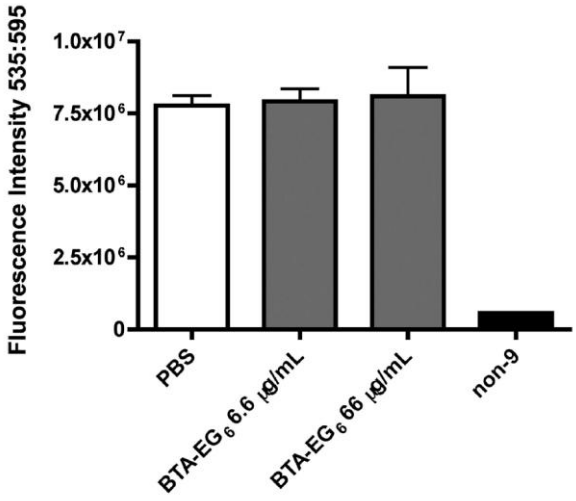


*Figure 6.8. BTA-$EG_6$ is not toxic to cervical cells at concentrations up to 10 times its $IC_{50}$.*

## 6.3 Conclusions

In this study we demonstrate that amyloid-binding small molecules are efficient inhibitors of SEVI- and semen-mediated enhancement of HIV infectivity. We chose to examine the amyloid-binding small molecule BTA-$EG_6$ based on the hypothesis that it would effectively bind and coat SEVI fibrils, as it has been previously shown to do for Aβ.[57] We found that BTA-$EG_6$ bound to the SEVI fibrils and interfered with their ability to enhance HIV infectivity, suggesting that other

amyloid-binding small molecules that target SEVI might also prove to be effective microbicide candidates. Importantly, BTA-$EG_6$ did not have any direct inhibitory effects on the infectivity of HIV-1 alone.

BTA-$EG_6$ inhibited SEVI-mediated enhancement of HIV-1 infection in a dose-dependent fashion and was able to block SEVI-mediated binding of HIV-1 to target cells.

Moreover, our results show that BTA-$EG_6$ effectively prevents semen-mediated enhancement of HIV infectivity, suggesting that this activity of semen can be targeted by specifically inhibiting the SEVI fibrils. These data not only suggest that BTA-$EG_6$ may be an effective microbicide candidate, but also offers proof-of-principle support for the concept that screening amyloid- or SEVI-binding molecules may allow identification of additional anti-SEVI microbicide candidates. In the case of BTA-$EG_6$, it is likely that the BTA moiety intercalates into the SEVI fibrils, while the hexa(ethylene glycol) moiety extends and inhibits the interactions of SEVI with cells and virions.[57] Oligomeric derivatives of BTA-$EG_6$ and related compounds may prove even more effective due to increased avidity and affinity, as may amyloid binders with modified functional groups. Studies toward these hypotheses are discussed in chapter 7 of this thesis.

It is important to compare the properties of the anti-SEVI small molecule described here with those of previously identified inhibitors of SEVI's HIV infection-enhancing activity. Other previously described SEVI inhibitors, such as polyanionic compounds,[204] and the Heparin antagonist Surfen[209] block the actions of SEVI at

least in part due to simple electrostatic interactions with the cationic fibrils. Another example, the anionic polymer PRO-2000 showed robust activity in *in vitro* studies and preclinical models,[210-212] but failed to demonstrate a protective effect against HIV-1 transmission in the phase III Microbicide Development Program (MDP) 301 trial. Reasons for the futility of PRO-2000 remain unclear but may include inhibition of its antiviral activity by seminal plasma;[213] this may contribute to its decreased effectiveness in postcoital cervicovaginal fluid.[214] In our experiments, the presence of semen had no effect on the microbicidal activity of BTA-$EG_6$. Moreover, small cationic peptides are present in both semen and cervicovaginal fluid; anionic SEVI inhibitors may interact nonspecifically with these charged peptides because of their electrostatic properties.[215,216] In contrast, amyloid-binding small molecules typically do not rely on electrostatic properties to bind to SEVI, and are therefore expected to offer a new class of SEVI inhibitors whose effects are more specifically targeted at the fibrils themselves. This is expected to reduce the potential for off-target effects and increase the potential for effectiveness in an *in vivo* setting. Finally, current microbicide candidates target the HIV virus itself,[217] while BTA-$EG_6$ does not. We propose that, since semen is the vector in the vast majority of transmitted HIV-1 infections, it is reasonable to consider that the addition of a SEVI inhibitor to microbicide formulations—such as to the tenofovir (a reverse transcriptase inhibitor) topical ointment that has been recently demonstrated to reduce HIV transmission in 39% of cases[218]—might improve the efficacy of antiviral microbicides.

## 6.4 Materials & Methods

**Cell Culture:** CEM-M7 (a gift from N. Landau, NYU, New York, NY) and Jurkat cells were cultured in RPMI 1640 media supplemented with 10% fetal bovine serum, penicillin (50 U/mL) , and streptomycin (50 µg/mL). A2En cells (a gift from S. Greene, Louisiana State University Health Sciences Center, New Orleans, LA), **SEVI and Semen:** PAP248-286, synthesized by New England Peptide (NEP), was dissolved in PBS at a concentration of 10 mg/mL. Fibrils were formed by agitation in an Eppendorf Thermomixer at 1400 rpm and 37$^{o}$C for 72 hours . Semen samples were obtained from the University of Rochester Fertility Center (Rochester, NY) and Fairfax Cryobank (Fairfax, VA). Samples were pooled, aliquoted and stored at -80$^{o}$C.

**Fluorescence Polarization:** 100 ug/mL of SEVI was mixed with 16 ug/mL FITC-Heparin and concentrations of BTA-$EG_6$ ranging from 0 to 200 µg/mL. Samples were incubated 1 hr at RT and read on a Perkin Elmer Envision 2012 Multilabel reader at an excitation $\lambda$=480 and emission $\lambda$=535. The horizontal (S) and vertical (P) polarized fluorescence intensities were recorded and the calculated polarization was determined in millipolarization units.

**Measurement of the Binding Affinity of BTA monomer and oligomers to amyloid fibrils:** Binding of BTA-$EG_6$ to SEVI fibrils was measured according to the centrifugation assay described by Levine[83] for BTA-1 to Aβ fibrils. Briefly, 200 µl of various concentrations of BTA-$EG_6$ in PBS were incubated in the presence or absence of 10 µg of SEVI fibrils to give a final volume of 220 µl of solution. These

incubations were performed in duplicate runs and allowed to equilibrate overnight at room temperature. After equilibration, each solution was centrifuged at 16,000 × *g* for 30 min. The supernatants were separated from the pelleted fibrils, and 220 µl of fresh PBS was added to resuspend the pellets. 100 µl aliquots of each re-suspended pellet was pipetted into a cuvette (ultramicrocuvette,10-mm light path, Hellma®, Müllheim, Germany), and the fluorescence of the bound molecule was determined at 355 nm excitation and 420 nm emission using a spectrofluorometer (Photon Technology International, Inc., Birmingham, NJ). Each experiment was repeated at least 3 times. Error bars represent standard deviations from the mean. Plots shown in Figure 6.3 of fluorescence intensity versus concentration of BTA-$EG_6$ were plotted and fitted using the following one-site specific binding algorithm to determine $K_d$: $Y = B_{max} \times X/(K_d + X)$, where $X$ is the concentration of BTA-$EG_6$, $Y$ is the specific binding fluorescence intensity, and $B_{max}$ corresponds to the apparent maximal observable fluorescence upon binding of BTA-$EG_6$ to Aβ or SEVI fibrils. The data were processed using Origin 7.0 (MicroCal Software, Inc., Northampton, MA).

**Infectivity Assays:** For infection of CEM-M7 cells, X4 tropic HIV-$1_{IIIB}$ (21 ng/ml p24) was pretreated for 10 min at RT with 15 µg/mL SEVI in the presence or absence of BTA-$EG_6$. Treated virions were then added to $5 \times 10^4$ CEM-M7 cells/ well in 96-well flat-bottomed tissue culture plates. After 2 hours, the media was replaced. Infection was assayed after 48 hours by quantitating luciferase expression using the Promega Luciferase Assay and a Beckman Coulter DTX880 platereader.

For infections using semen, pooled human semen samples were added to virions at a 1:1 dilution and incubated for 10 min at RT in the presence or absence of BTA-$EG_6$. After 10 min, the semen and virus mixture was diluted 1:15 into 5 x $10^4$ CEM-M7 cells/well in a 96 well plate. Cells were washed after 1 hour and infection was assayed at 48 hours as above.

**Virus binding assay:** HIV-$1_{IIIB}$ 15 μg/mL SEVI and added to 5x$10^4$ Jurkat cells in the presence or absence of BTA-$EG_6$. After 90 minutes, cells were washed to remove any unbound virus and bound virions were detected using an HIV-1 p24 antigen capture assay (Advanced Bioscience Laboratory).

**Toxicity studies:** The cervical epithelial cell line was treated for 12 hours with BTA-$EG_6$ at concentrations up to 66 μg/mL, 10 times the $IC_{50}$. At 12 hours cell viability was analyzed by measuring cellular metabolic activity using the resazurin cytotoxicity assay, alamarBlue® (Invitrogen) in accordance with the manufacturer's protocol. Cells were also treated with 0.1% Nonoxynol-9 as a positive control for cytotoxicity.

## Notes about this Chapter

This chapter is based on material that appears in "Amyloid-binding Small Molecules Efficiently Block SEVI (Semen-derived Enhancer of Virus Infection)- and Semen-mediated Enhancement of HIV-1 Infection." Olsen, J. S.; Brown, C.; Capule, C. C.; Rubinshtein, M.; Doran, T. M.; Srivastava, R. K.; Feng, C. Y.; Nilsson, B. L.; Yang, J.; Dewhurst, S. *J. Biol. Chem.* **2010**, *285*, 35488-35496.

Joanna S. Olsen and Caitlin Brown generated a large portion of the work presented here. These studies would not have been possible without the synthetic expertise of Dr. Mark Rubinshtein. My contributions to this chapter focused on quantifying the binding interactions of BTA-$EG_6$ with Aβ and SEVI fibrils.

# Chapter 7

# The Rational Design of Multivalent Oligomers that Bind with High Affinity to Aβ and SEVI Amyloids

## 7.1 Introduction

Multivalent interactions—the simultaneous binding of linked, multiple, identical ligands to multiple receptors—are a ubiquitous phenomenon in nature and are commonly employed to improve the weak affinity of the corresponding monovalent interaction.[219] Multivalent interactions are vital in physiological events such as inflammation, bacterial and viral adhesion to target cells, and in immune recognition and responses. Taking these cues from nature, various research groups

have successfully applied and incorporated the concept of multivalency into the design and synthesis of high affinity ligands for multivalent targets.[220-234]

Amyloid fibrils formed from the self-assembly of peptides putatively display multiple, identical, and periodically spaced binding sites for small molecules along the fibrillar surface,[57,83,85,121,235] and, thus, represent an excellent biological target for multivalent ligand design.

Lockhart *et al.*[85] and Shea *et al.*[235] previously reported that compounds with the benzothiazole aniline (BTA) moiety, derivatives of the well known amyloid-binding agent Thioflavin T (ThT), associate with Aβ fibrils with data suggesting a spacing between adjacent binding sites of ~2 nm.

I, therefore, designed oligovalent compounds based on the BTA moiety with linkers that can span the ~2 nm distance between binding sites on the Aβ fibrillar surface (Figure 7.1). In this chapter, I describe the design, synthesis, and evaluation of oligomeric BTA compounds that bind to Aβ fibrils. Although I demonstrate that these BTA oligomers exhibit improved binding toward Aβ fibrils compared to the monovalent counterpart, the high molecular weights (>500 Da) of these compounds preclude them from readily entering the brain. These compounds, therefore, may not be practical for Alzheimer's-related *in vivo* use. Because we wanted to explore the potential of these compounds for further development in clinical applications, we investigated the interaction of these BTA oligomers with another multivalent target, the HIV-related SEVI ("semen-derived enhancer of virus infection") fibril. SEVI

fibrils are naturally abundant in semen, and, as there are no restrictive barriers in semen, these BTA oligomers should easily reach the SEVI fibril target.

SEVI fibrils are formed from the self-assembly of the peptide PAP248-286—the proteolytic byproduct of prostatic acid phosphatase (PAP) cleavage—abundantly found in semen. A recent study reported that SEVI can potentially increase infection of HIV-1 in cells by up to 400,000-fold.[5] Although the molecular mechanism of SEVI-mediated transmission of HIV-1 remains poorly understood, evidence suggests that SEVI binds to both HIV-1 virions and cell membranes, and facilitates viral infection *in vitro*.[5,55,236,237] Methods to suppress the effects of such natural enhancers of HIV-1 transmission may, therefore, significantly reduce the global spread of HIV through sexual contact among high-risk populations.

We recently reported that targeting SEVI fibrils with the amyloid-binding molecule BTA-$EG_6$, a hexa(ethylene glycol) derivative of benzothiazole aniline (BTA), reduced SEVI- and semen-mediated enhancement of HIV infection in T cells with an $IC_{50}$ of 13 μM.[56] We hypothesized that BTA-$EG_6$ forms a protein-resistive coating on SEVI,[56] effectively blocking the interaction of these fibrils with HIV-1 virions and cells. A key characteristic of this approach to reducing HIV transmission compared to more traditional microbicide candidates is that we target a naturally abundant mediator (i.e., SEVI) in the cellular attachment of HIV, rather than targeting the virions themselves. Although BTA-$EG_6$ was not toxic to cervical cells and did not exhibit any pro-inflammatory activity at a concentration that was 10 times the $IC_{50}$ for efficacy,[56] I explored the multivalent design strategy in order to

create potentially more potent compounds for further development of SEVI-neutralizing agents as supplements to current microbicide candidates.[238-240]

The goals of this project, outlined in this chapter, were 2-fold: 1) Create compounds that would bind with high affinity to Aβ fibrils and SEVI fibrils based on the multivalent design strategy 2) Evaluate whether these oligomers of BTA exhibit improved ability over the BTA monomer to inhibit SEVI-mediated enhancement of HIV infectivity.

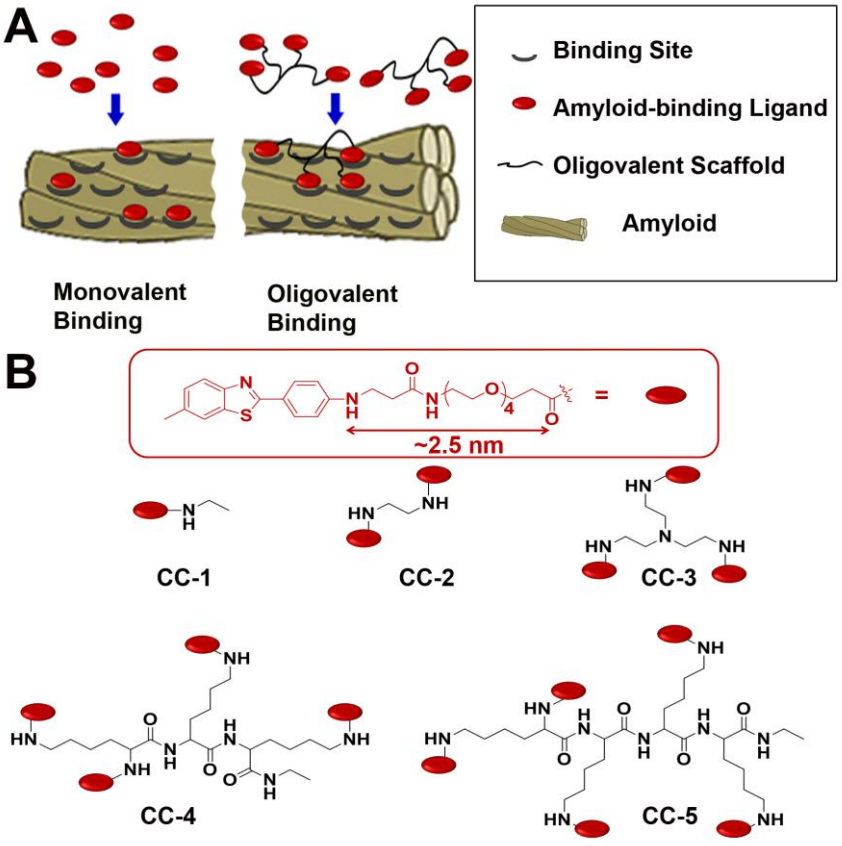


*Figure 7.1. Structures of monovalent and oligovalent amyloid-binding molecules. A) Cartoon depicting the monovalent (left) or oligovalent (right) binding of molecules to amyloid fibrils. B) Chemical structures of monovalent (**CC-1**) and oligovalent (**CC-2** – **CC-5**) derivatives of benzothiazole aniline (BTA). A rudimentary estimate of the length (in fully extended conformation) of the flexible group attached to BTA was calculated using ChemBio3D Ultra 12.0 software.*

## 7.2 Results and Discussion

Despite theoretical predictions that rigid linkers would optimize multivalent binding through the minimization of the loss of conformational entropy upon binding,[219,241-244] flexible linkers have been incorporated into the design of multivalent compounds by several research groups, with demonstrated success.[229,245-248] Moreover, unlike rigid linkers, flexible linkers can adopt several conformations with ease and without strain. The incorporation of flexible linkers in the design of multivalent compounds can thus optimize the binding of the tethered ligands to multiple binding sites.[229] I designed the BTA monomer **CC-1** to carry a tetra(ethylene glycol) group terminated with a carboxyl moiety, which I subsequently used to generate oligovalent BTA derivatives **CC-2 – CC-5** by reaction with commercial oligo-amine spacers using standard amidation chemistry. Although oligo(ethylene glycols) are quite flexible (which theoretically diminishes the potential gain in conformational entropy for oligovalent binding[219,241-244]), I incorporated them into the design of compounds **CC-2 – CC-5** because of their known minimal interaction with proteins[249,250] and for their water solubilizing properties.[251] I estimated that the flexible spacer on each BTA monomer could span a length of ~2.5 nm when modeled in fully extended conformation (modeled in ChemBio3D 12.0, Figure 7.1), suggesting that the BTA units on oligomers **CC-2 – CC-5** could easily span the expected ~2 nm distance between binding sites on Aβ fibrils.[252] Additionally, dimers of Thioflavin T, where the ThT moieties were linked by 2-5 ethylene glycol units, have recently been reported to associate with Aβ fibrils

with increased affinity compared to ThT alone.[253] These studies suggest that BTA oligomers **CC-2 – CC-5** could also bind oligovalently to Aβ amyloid.

Table 7.1 lists the measured $K_d$ values for compounds **CC-1 – CC-5** to fibrils formed from Aβ(1-42) peptides, as determined using a known fluorescence binding assay.[56,83,194,254] As expected, BTA dimer **2** bound more strongly than monomer **CC-1** to Aβ(1-42) fibrils, albeit with only a modest 8-fold lower $K_d$ value. The flexibility of the oligo(ethylene glycol) groups presumably attenuates the degree of cooperative binding of the two BTA units in **CC-2** to the fibrillar surface. Surprisingly, BTA trimer **CC-3** and tetramer **CC-4** bound only with similar $K_d$ values to Aβ(1-42) fibrils compared to dimer **CC-2**. One possible explanation for this result is that the structures of **CC-3** and **CC-4** make it preferable for these molecules to bind divalently to the amyloid surface. Alternatively, it may also be possible that **CC-3** and **CC-4** bind to amyloid fibrils with a valency greater than 2, but incur significant loss in binding energy due to partial docking of the BTA units to their respective binding sites. For BTA pentamer **CC-5**, the measured $K_d$ value was an additional 10-fold lower than tetramer **CC-4** and was 117-fold lower than monomer **CC-1**. Although the effects of multivalent binding to Aβ fibrils are modest for compounds **CC-2 – CC-5**, there appears to be a general trend of improved binding from monomer to pentamer (most notably from monomer to dimer and from tetramer to pentamer) within this series of compounds.

*Table 7.1. Table of $K_d$ values obtained for compounds **CC-1 – CC-5** for binding to fibrils formed from synthetic Aβ(1-42) or SEVI. These values were estimated using a known fluorescence binding assay.*[83]

| Compound # | $K_d$ (nM) to Aβ(1-42) fibrils | $K_d$ (nM) to SEVI fibrils |
|---|---|---|
| **CC-1** | 235 ± 75 | 236 ± 90 |
| **CC-2** | 29 ± 4 | 69 ± 1 |
| **CC-3** | 26 ± 6 | 40 ± 6 |
| **CC-4** | 20 ± 5 | 59 ± 6 |
| **CC-5** | 2.0 ± 0.4 | 0.4 ± 0.2 |

I previously demonstrated that the related compound, BTA-$EG_6$, bound with similar affinity to both Aβ fibrils and to SEVI fibrils ($K_d$ = 111±32 nM and 127±22 nM, respectively). We, therefore, reasoned that although these BTA oligomers were designed based on the known binding interactions of structurally analogous compounds to Aβ fibrils, these compounds should also exhibit a comparable affinity for SEVI fibrils. When I examined the $K_d$ values of compounds **CC-1 – CC-5** to SEVI fibrils, I found a similar trend for improved binding of the oligomeric BTA compounds as I observed for their binding to Aβ(1-42) fibrils (Table 7.1). I, again, observed the greatest improvement in binding as a function of increasing valence number in the oligomer when we compared the monomer to dimer and the tetramer to pentamer. I found that BTA pentamer **CC-5** had a $K_d$ value of 0.4 nM for binding to aggregated SEVI peptides and exhibited a 590-fold lower $K_d$ value than monomer **CC-1**.

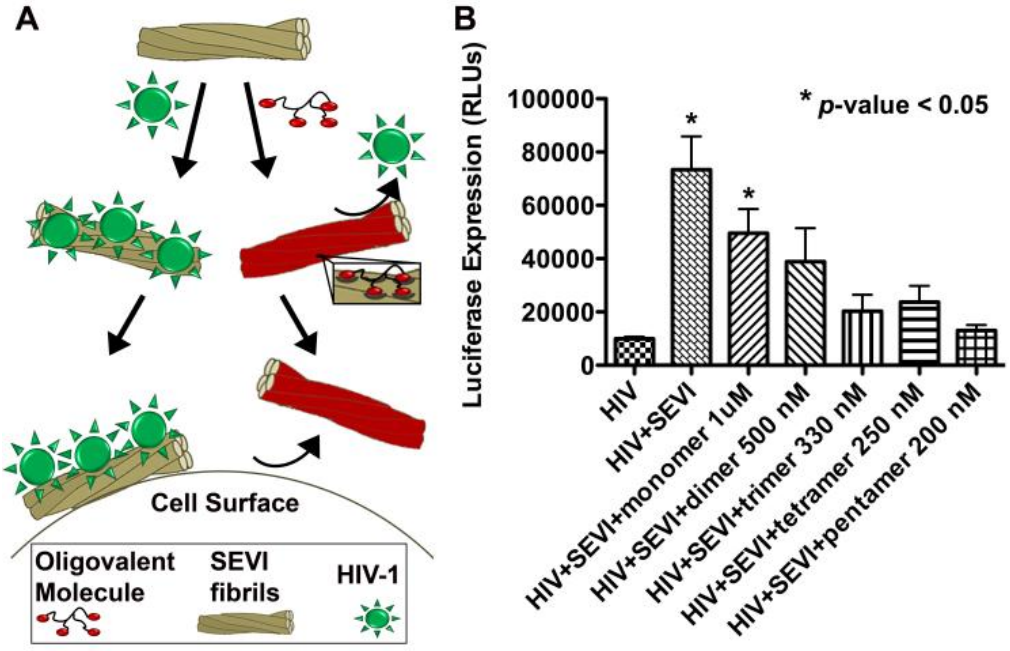


*Figure 7.2. Inhibition of SEVI-mediated enhancement of HIV-1 infection by compounds **CC-1** – **CC-5**. A) Schematic illustration showing the proposed coating of SEVI fibrils with amyloid-binding oligomers. These coatings prevent the direct interaction of HIV-1 with SEVI fibrils and, thus, prevent SEVI-mediated enhancement of viral infection in cells. B) Graph showing the reduction of SEVI-mediated enhancement of HIV-$1_{IIIB}$ infection in TZM-bl cells in the presence of compounds **CC-1** – **CC-5**. RLUs = relative luciferase units. A p-value of < 0.05 was considered statistically significantly different compared to cells treated with HIV-$1_{IIIB}$ alone (i.e., in the absence of SEVI) as determined by 1-way ANOVA with Tukey's post test.*

In order to investigate whether the improved binding of BTA oligomers **CC-2 – CC-5** to SEVI fibrils compared to monomer **CC-1** would translate into improved efficacy for blocking SEVI-mediated HIV-1 infection (Figure 7.2A), we evaluated compounds **CC-1 – CC-5** for their capability to inhibit SEVI-enhanced infection of HIV-$1_{IIIB}$ in TZM-bl cells. TZM-bl cells are a HeLa-derived cell line that express high levels of the CD4 receptor, CCR5 and CXCR4 co-receptors, and contain the HIV-1 LTR-driven luciferase cassette.[255,256] Since HIV-1 LTR is a weak

transcriptional regulator in the absence of its cognate, Tat, the expression levels of luciferase in these cells are directly proportional to the extent of HIV-1 infection. In these HIV-1 infectivity experiments, we chose concentrations of compounds **CC-1 – CC-5** that maintained a 1 μM concentration of the BTA moiety in all samples of monomer and oligomers (e.g., since there are 2 BTA moieties in dimer **CC-2**, we used a 0.5 μM concentration of dimer to afford a 1 μM total concentration of BTA). We expected this experimental design would highlight any multivalent enhancement of efficacy from the oligomers compared to monomer. Figure 7.2B shows that all of the oligomers were more effective at inhibiting SEVI-mediated enhancement of HIV-1 infection compared to monomer **CC-1**. As a control, compounds **CC-1 – CC-5** did not have any significant effect on HIV infection in these cells in the absence of SEVI (Figure 7.3). Satisfyingly, the trend for efficacy of compounds **CC-1 – CC-5** (Figure 7.2B) appeared to parallel the same trend as the binding of these compounds to SEVI (Table 7.1). BTA pentamer **CC-5**, which exhibited the lowest $K_d$ value for binding to SEVI fibrils, reduced SEVI-mediated HIV-1 infectivity almost completely at a concentration of 200 nM (i.e., the level of HIV infection was essentially the same as in the absence of SEVI). This level of activity from BTA pentamer **CC-5** is over 200-fold more effective than the previously reported BTA-$EG_6$ (which required a concentration of 44 μM to completely neutralize the effects of SEVI on HIV-1 infection[56]). We attribute at least part of the increased efficacy of oligomers **CC-2 – CC-5** with respect to the monomer **CC-1** to the capability of the oligomers to bind multivalently to SEVI fibrils.

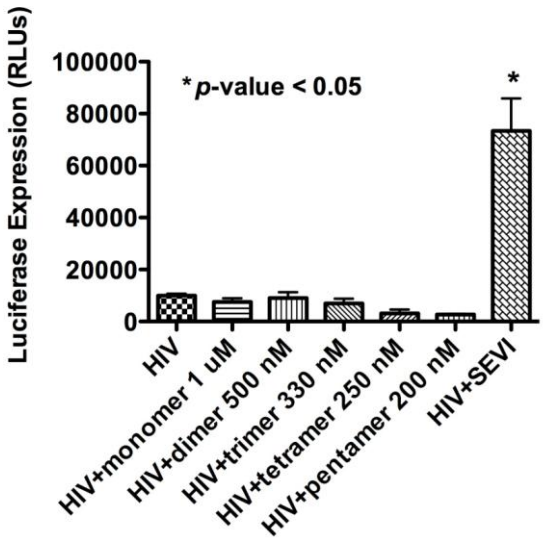


*Figure 7.3. Control studies demonstrating that compounds **CC-1** – **CC-5** do not affect HIV-1 infection in TZM-bl cells in the absence of SEVI fibrils. RLUs, relative luciferase units. Analyses of the data by ANOVA with Tukey's post test revealed that luciferase expression in cells treated with HIV only and cells treated with HIV+compound were not statistically significantly different from one another. * indicates $p < 0.05$ compared to cells treated with only HIV.*

## 7.3 Conclusions

I have, thus, demonstrated proof-of-principle that multivalent display of amyloid-binding groups results in improved binding to both Aβ and SEVI fibrils. We showed that oligomers of BTA were significantly more effective in attenuating SEVI-mediated HIV-1 infectivity than their monomeric counterpart. These studies provide further support that amyloid-targeting agents can form a bio-resistive coating on aggregated amyloids and inhibit deleterious interactions of these naturally occurring biomaterials with other biomolecules.[56-58,121] They also further support that amyloid-targeting agents may have important utility as prophylactic supplements

for microbicides to reduce sexual transmission of HIV. Efforts to use polymeric[219,226,257] and more rigid water-soluble[258] and biocompatible scaffolds[259-261] to generate more potent multivalent amyloid-targeting agents with improved efficacy for reducing SEVI-mediated infection of HIV is an active and ongoing area of research in our lab.

## 7.4 Materials & Methods

### 7.4.1 Materials

Reagents were purchased from Sigma-Aldrich unless otherwise stated. 2-(p-aminophenyl)-6-methyl benzothiazole (BTA) was purchased from City Chemical LLC. Amino-dPEG®-4-acid was purchased from Quanta BioDesign, Ltd. 2,2',2"-triaminotriethylamine (TREN) was purchased from STREM Chemicals. 4-(dimethylamino)pyridine (DMAP) was purchased from Alfa Aesar. Ethylamine-HCl was from Fluka. HEPES (free acid) was purchased from EMD Biosciences, Inc. Sodium Phosphate Monobasic and NaCl were purchased from Fisher Scientific. KCl was purchased from JT Baker Chemicals. All reagents were used without further purification.

Aβ(1-42) peptide was purchased from GL Biochem (Shanghai) Ltd. PAP248–286 peptide was synthesized by New England Peptide.

All solvents used for reactions were obtained from Fisher Scientific. Solvents used for regular silica chromatography were ACS technical grade and used without further purification. Solvents used for amine-functionalized silica chromatography

(Teledyne Isco, Inc.) were HPLC grade and used without further purification. Water (18.2 μΩ/cm) was filtered through a NANOPure Diamond$^{TM}$ (Barnstead) water purification system before use.

NMR spectra were obtained on a Varian 400 MHz spectrometer. Chemical shifts are reported in ppm relative to residual solvent. Low resolution MS analysis was performed on a Micromass Quattro Ultima triple quadrupole mass spectrometer with an electrospray ionization (ESI) source. High resolution MS analysis was performed on an Agilent 6230 Accurate-Mass TOFMS with an ESI source.

Dulbecco's Modified Eagle Medium (DMEM) was purchased from Invitrogen (Catalog # 11965). Fetal bovine serum was purchased from Atlas Biologicals (Catalog # F-0500-A), Pen-strep Glutamine was purchased from Invitrogen (Catalog #10378). Britelite Plus was purchased from Perkin Elmer (Catalog # 6016761). DPBS was purchased from Invitrogen (Catalog #14190).

TZM-bl cells were obtained from the NIH AIDS Research & Reference Reagent Program. HIV-$1_{IIIB}$ was obtained from Zeptometrix.

## 7.4.2 Experimental Methods

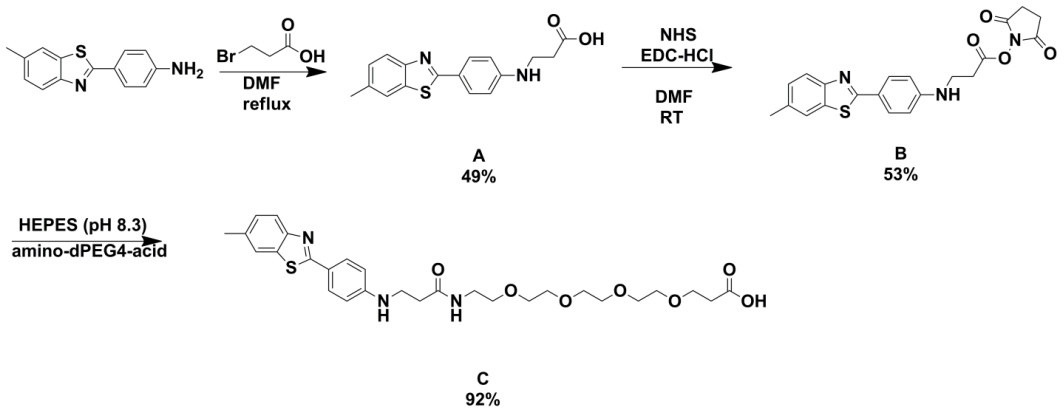


*Figure 7.4. Synthetic Scheme for the synthesis of the precursor of compounds **CC-1 – CC-5***

**Synthesis of BTA Acid (A):** 2-(*p*-aminophenyl)-6-methyl benzothiazole (BTA) (2.00 g, 8.33 mmol) and 3-bromopropionic acid (0.69 g, 4.51 mmol) were added to 25 mL dry dimethylformamide (DMF) and refluxed for 12 h. The reaction was concentrated *in vacuo* and an excess volume of $H_2O$ was added to the mixture to precipitate the product. The product was filtered and purified by re-crystallization in hot dichloromethane (DCM). The solid was filtered and washed with cold DCM to afford a yellow product (0.69 g, 49% yield). $^1$H-NMR (400 MHz, $CD_3OD$): $\delta$ = 2.47 (s, 3H), 2.63 (t, *J*=6.8 Hz, 2H), 3.48 (t, *J*=6.8 Hz, 2H), 6.71 (d, *J*=8.8 Hz, 2H), 7.28 (d, *J*= 8.4 Hz, 1H), 7.72 (s, 1H), 7.75 (d, *J*= 8.4 Hz, 1H), 7.81 (d, *J*=8.8 Hz, 2H). ESI-MS *(m/z)* calculated for $C_{17}H_{17}N_2O_2S$ $[M+H]^+$ 313.10; found 313.35.

**Synthesis of BTA-NHS-Ester (B):** Acid **A** (0.62 g, 1.99 mmol ), N-hydroxy succinamide (NHS) (0.69 g, 6.00 mmol), and 1-Ethyl-3-[3-dimethylaminopropyl]carbodiimide-Hydrochloride (EDC-HCl) (1.14 g, 5.94 mmol) were added to dry DMF and stirred for 12 h at room temperature. The reaction was

concentrated *in vacuo* and an excess volume of $H_2O$ was added to precipitate the product. The precipitate was filtered and washed with $H_2O$ to afford a tan product (0.43 g, 53% isolated yield). $^1$H-NMR (400 MHz, $CDCl_3$): δ = 2.47 (s, 3H), 2.85 (s, 4H), 2.93 (t, *J*= 6.4 Hz, 2H), 3.68 (t, *J*=6.4 Hz, 2H), 6.68 (d, *J*=8.8 Hz, 2H), 7.24 (d, *J*= 9.6 Hz, 1H), 7.63 (s, 1H), 7.86 (d, *J*= 8.4 Hz, 1H), 7.89 (d, *J*=8.4 Hz, 2H). ESI-MS *(m/z)* calculated for $C_{21}H_{20}N_3O_4S$ $[M+H]^+$ 410.11; found 410.21.

**Synthesis of BTA-dPEG4-Acid (C):** Ester **B** (0.17 g, 0.42 mmol) was dissolved in 6 mL 1,4-dioxane and was added in 3 portions to a round bottom flask containing Amino-dPEG®$_4$-acid (0.09 g, 0.35 mmol) in 0.1 M HEPES buffer (pH 8.3, 4 mL). The pH was monitored and maintained between 8.2-8.4 to optimize product yield. After the pH stabilized in the 8.2-8.4 range, the solvent was evaporated. The remaining brown, oily residue was taken up in Methanol (MeOH) and purified by silica chromatography (6:1:1:1 mixture of ethyl acetate (EtOAc):acetonitrile (ACN):$H_2O$:MeOH as eluent) giving the acid **C** as a brown, sticky residue (0.18 g, 92% yield). $^1$H-NMR (400 MHz, acetone-$d_6$): δ = 2.44 (s, 3H), 2.54 (t, *J*= 6.4 Hz, 2H), 2.56 (t, *J*= 6.8 Hz, 2H), 3.36 (q, *J*= 5.6 Hz, 2H), 3.48-3.57 (m, 16H), 3.71 (t, *J*= 6.4 Hz, 2H), 6.75 (d, *J*= 8.4 Hz, 2H), 7.26 (d, *J*= 7.6 Hz, 1H), 7.56 (br. s, 1H), 7.72 (s, 1H), 7.77 (d, *J*= 8 Hz, 1H), 7.84 (d, *J*= 8.8 Hz, 2H). $^{13}$C-NMR (400 MHz, acetone-$d_6$): δ = 20.71, 35.02, 35.27, 39.08, 39.65, 66.89, 69.79, 70.18, 70.32, 70.42, 70.46, 70.48, 112.37, 121.48, 121.86, 127.66, 128.86, 134.44, 134.73, 151.54, 152.91, 167.40, 171.07, 172.68. HR-MS *(m/z)* calculated for $C_{28}H_{38}N_3O_7S$ $[M+H]^+$ 560.2425; found 560.2426.

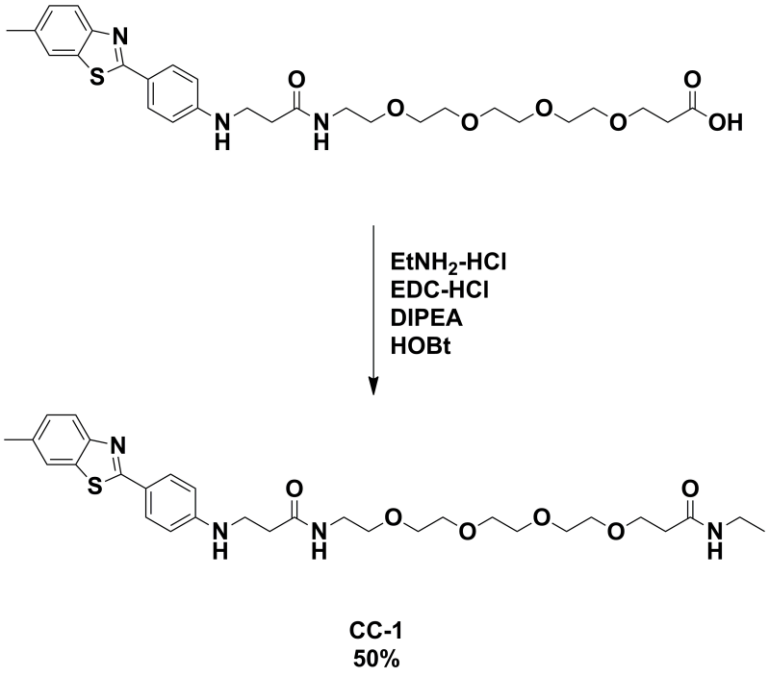


*Figure 7.5. Synthetic Scheme for the synthesis of BTA monomer **CC-1***

**Synthesis of BTA Monomer (CC-1):** Compound **C** (6.3 mg, 11 μmol), N-hydroxybenzotriazole (HOBt) (1 mg, 7.3 μmol), ethylamine-HCl (5.6 mg, 69 μmol), EDC-HCl (7.5 mg, 39 μmol) and diisopropylethylamine (DIPEA) (21 μL) were added to dry DMF and stirred for 12 h at room temperature. The solvent was evaporated *in vacuo* and the reaction mixture was taken up in DCM and then washed with brine, saturated $NaHCO_3$, brine once more, and then dried over $Na_2SO_4$. The residue was further purified by silica chromatography using a gradient of 8:1:0.25:0.25 to 6:1:1:1 mixture of EtOAc:ACN:$H_2O$:MeOH as eluent. Monomer **1** was isolated as a yellow, sticky residue (3.3 mg, 50% yield). $^1$H-NMR (400 MHz, acetone-$d_6$): δ = 1.06 (t, *J*= 7.2 Hz, 3H), 2.38 (t, *J*= 7.2 Hz 2H), 2.45 (s, 3H), 2.54 (t,

*J*= 6.4 Hz, 2H), 3.19 (m, *J*= 5.6 Hz, 2H), 3.36 (q, *J*= 5.6 Hz, 2H), 3.48-3.57 (m, 16H), 3.68 (t, *J*= 6 Hz, 2H), 6.76 (d, *J*= 8.4 Hz, 2H), 7.27 (d, *J*= 8.4 Hz, 1H), 7.63 (br. s, 1H), 7.72 (s, 1H), 7.78 (d, *J*= 8 Hz, 1H), 7.85 (d, *J*= 8.8 Hz, 2H). $^{13}$C-NMR (400 MHz, acetone-$d_6$): δ = 14.53, 20.71, 33.87, 35.33, 36.72, 39.20, 39.72, 67.33, 69.90, 70.17, 70.20, 70.31, 70.41, 70.43, 70.45, 112.38, 121.49, 121.86, 127.68, 128.86, 134.47, 134.70, 151.56, 152.89, 167.39, 171.13, 171.20. HR-MS *(m/z)* calculated for $C_{30}H_{42}N_4O_6SNa$ $[M+Na]^+$ 609.2717; found $[M+Na]^+$ 609.2720.

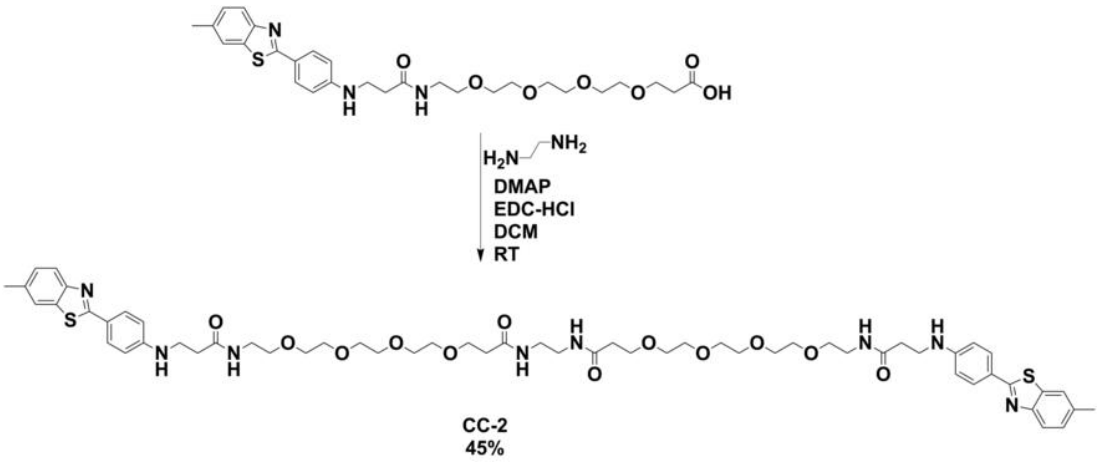


*Figure 7.6. Synthetic scheme for compound **CC-2***

**Synthesis of BTA Dimer (CC-2):** Compound **C** (22 mg, 39 μmol), 4-(dimethylamino)pyridine (DMAP) (12 mg, 98 μmol), ethylene diamine (1.1 μl, 16 μmol), EDC-HCl (29 mg, 151 μmol) were added to dry DCM and stirred for 12 h at room temperature. The reaction mixture was washed with brine, 1M HCl, saturated $NaHCO_3$, brine once more, then dried over anhydrous $Na_2SO_4$. The DCM layer was concentrated *in vacuo*, then purified by an amine-functionalized silica column (Redisep $R_f$ Gold®, Teledyne Isco, Inc.) using a gradient of 0% to 25% MeOH in EtOAc over 50 minutes. The product was isolated as a sticky, yellow residue (8.3 mg, 45% yield). $^1$H-NMR (400 MHz, acetone-$d_6$): δ = 2.39 (t, *J*= 6.4 Hz, 4H), 2.45 (s, 6H), 2.54 (t, *J*= 6.4 Hz, 4H), 3.29 (m, 4H), 3.36 (q, *J*= 5.6 Hz, 4H), 3.48-3.57 (m, 32H), 3.69 (t, *J*= 6 Hz, 4H), 6.75 (d, *J*= 8.8 Hz, 4H), 7.26 (d, *J*= 8.4 Hz, 2H), 7.34 (br. s, 2H), 7.39 (br. s, 2H), 7.74 (s, 2H), 7.76 (d, *J*= 8.4 Hz, 2H), 7.85 (d, *J*= 8.8 Hz, 4H). $^{13}$C-NMR (400 MHz, acetone-$d_6$): δ = 20.73, 35.36, 36.86, 39.23, 39.28, 39.74, 67.28, 69.28, 70.24, 70.28, 70.39, 70.52, 112.40, 121.49, 121.87, 127.67, 128.89,

134.44, 134.74, 151.57, 152.92, 167.41, 171.10, 171.28. HR-MS *(m/z)* calculated for $C_{58}H_{78}N_8O_{12}S_2Na$ $[M+Na]^+$ 1165.5073; found 1165.5065.

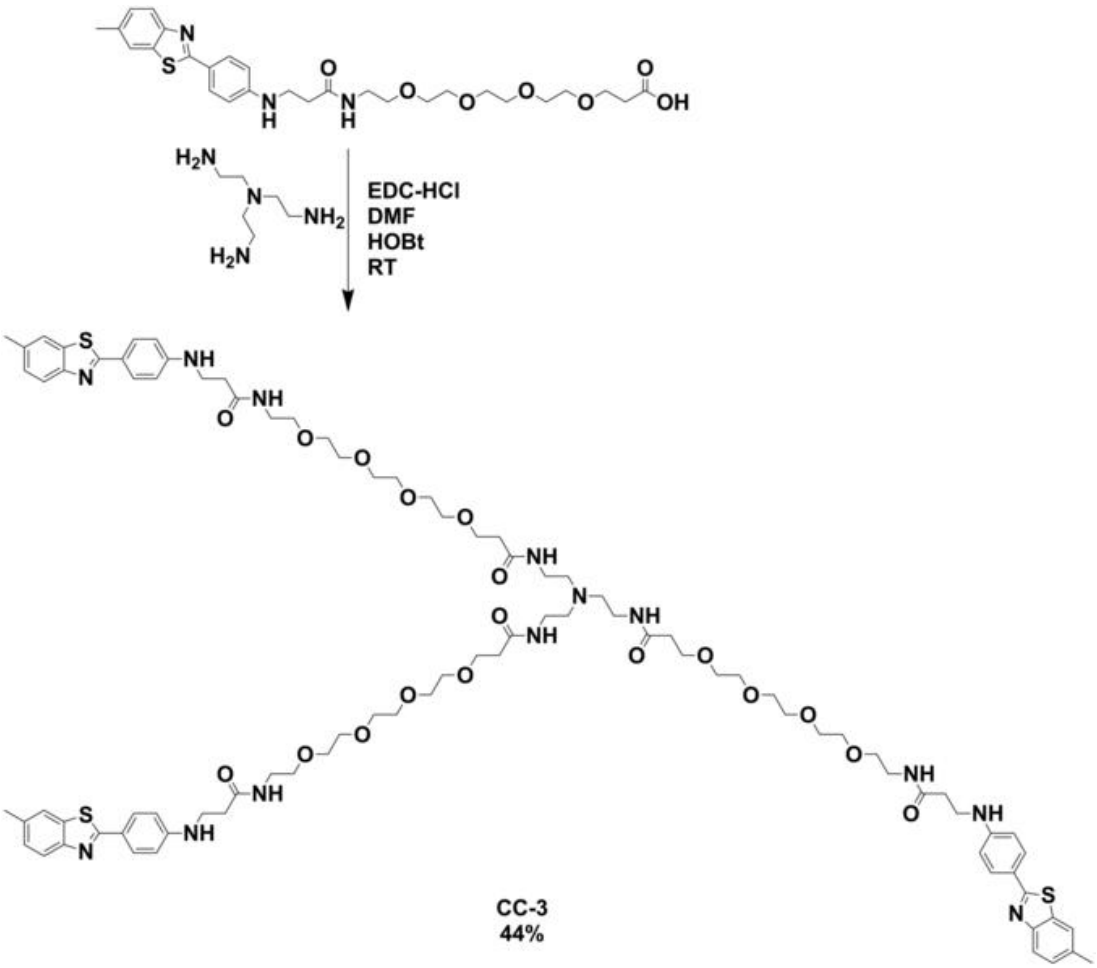


*Figure 7.7. Synthetic scheme for compound **CC-3***

**Synthesis of BTA Trimer (CC-3):** A mixture of HOBt hydrate (24 mg, 178 μmol) and 2,2',2"-triaminotriethylamine (TREN) (2.1 μl, 14 μmol) in 1 ml dry DMF was added to a vial containing **C** (26 mg, 47 μmol) in 2 mL of dry DMF. EDC-HCl (19 mg, 99 μmol) was added in 3 portions and the reaction was stirred for 12 h at room temperature. The reaction solvent was evaporated *in vacuo* and the residue was taken up in DCM. The DCM layer was washed with brine, 1M HCl, saturated $NaHCO_3$, brine once more, then dried over anhydrous $Na_2SO_4$. The DCM layer was concentrated *in vacuo*, then purified by an amine-functionalized silica column

(Redisep $R_f$ Gold®, Teledyne Isco, Inc.) using a gradient of 0% to 25% MeOH in EtOAc over 50 minutes. The product was isolated as a sticky, yellow residue (11 mg, 44% yield). $^1$H-NMR (400 MHz, acetone-$d_6$): δ = 2.44 (s, 9H), 2.46-2.56 (m, 18H), 3.21 (q, *J*= 5.6 Hz, 6H), 3.36 (q, *J*= 5.6 Hz, 6H), 3.49-3.56 (m, 48 H), 3.71 (t, *J*= 6.4 Hz, 6H), 6.75 (d, *J*= 8.4 Hz, 6H), 7.26 (d, *J*= 7.2 Hz, 3H), 7.41 (br.s, 6H), 7.73 (s, 3H), 7.76 (d, *J*= 8 Hz, 3H), 7.84 (d, *J*= 8.4 Hz, 6H). $^{13}$C-NMR (400 MHz, acetone-$d_6$): δ = 20.74, 35.37, 36.78, 37.86, 39.30, 39.75, 54.50, 67.44, 69.78, 70.29, 70.40, 70.54, 112.40, 121.50, 121.87, 127.67, 128.90, 134.43, 134.75, 151.57, 152.92, 167.41, 171.10, 171.14. HR-MS *(m/z)* calculated for $C_{90}H_{123}N_{13}O_{18}S_3Na$ $[M+Na]^+$ 1792.8163; found 1792.8157.

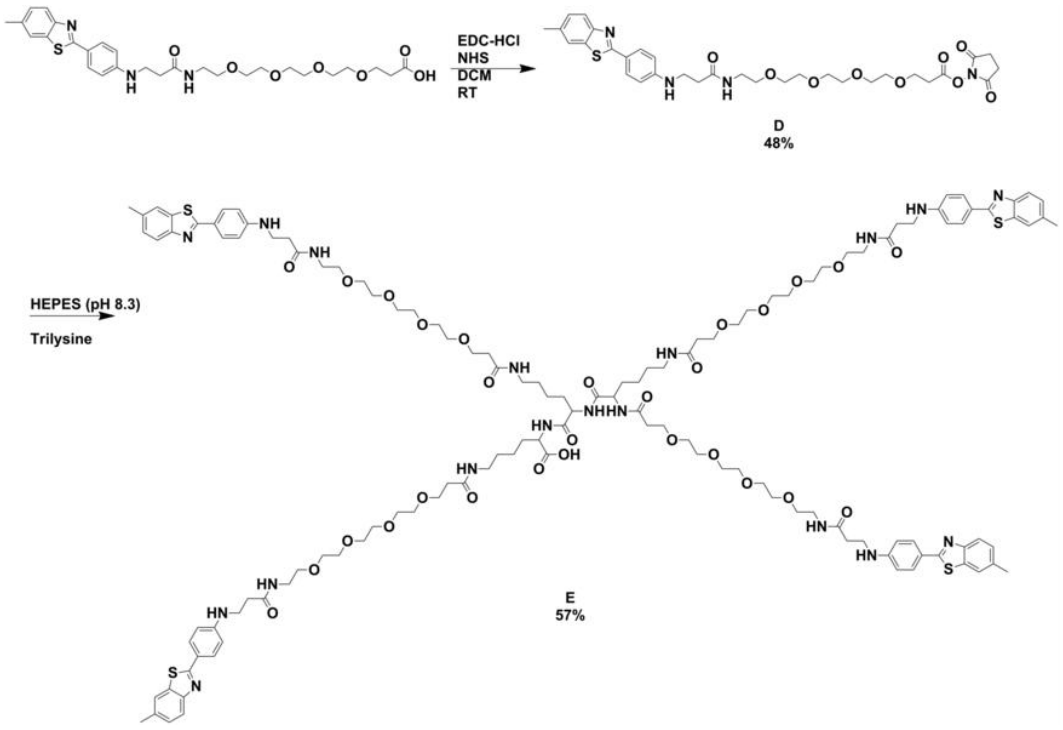


*Figure 7.8. Synthetic scheme for the synthesis of compounds **D** and **E***

**Synthesis of BTA-dPEG4-NHS Ester (D):** Compound **C** (0.26 g, 0.47 mmol), NHS (0.16 g, 1.39 mmol) and EDC-HCl (0.90 g, 4.69 mmol) were added to dry DCM and stirred for 12 h at room temperature. The reaction mixture was washed 3 times with brine and the DCM layer was dried over anhydrous $Na_2SO_4$. The DCM layer was concentrated *in vacuo* and purified by silica chromatography (8:1:0.25:0.25 mixture of ethyl acetate (EtOAc):acetonitrile (ACN):$H_2O$:MeOH as eluent) to afford the product as a sticky, brown residue (0.14 g, 48% yield). $^1$H-NMR (400 MHz, $CDCl_3$): $\delta$ = 2.47 (s, 3H), 2.52 (t, *J*= 6.4 Hz, 2H), 2.78 (s, 4H), 2.87 (t, *J*= 6.4 Hz, 2H), 3.45 (q, *J*= 5.2 Hz, 2H), 3.50-3.63 (m, 16H), 3.81 (t, *J*= 6.4 Hz, 2H), 6.66 (d, *J*= 8.8 Hz, 2H), 6.74 (br. s, 1H), 7.23 (d, *J*= 7.6 Hz, 1H), 7.63 (s, 1H), 7.83 (d, *J*= 8.4 Hz, 1H),

7.86 (d, *J*= 8.4 Hz, 2H). ESI-MS *(m/z)* calculated for $C_{32}H_{40}N_4O_9S$ $[M]^+$ 656.3; found $[M+H]^+$ 657.2 and $[M+Na]^+$ 679.2.

**Synthesis of BTA-Tetramer-Acid (E):** Compound **D** (81 mg, 123 μmol) in 2 mL 1,4-dioxane was added to 0.1 M HEPES buffer (pH 8.3, 2 mL) containing trilysine (9 mg, 22 μmol). The pH was maintained between 8.2-8.4 to favor complete acylation of all amines. The solvent was evaporated and the remaining yellow, oily residue was taken up in DCM and purified by silica chromatography (6:1:1:1 mixture of EtOAc:ACN:$H_2O$:MeOH as eluent) giving **E** as a brown, sticky residue (32 mg, 57% yield). $^1$H-NMR (400 MHz, $CDCl_3$): δ = 1.25-1.50 (2 broad peaks, 12 H), 1.55-1.90 (2 broad peaks, 6H), 2.35-2.55 (broad peaks 28H), 3.05-3.25 (br, 6H), 3.35-3.75 (broad peaks 80 H), 6.66 (d, *J*= 8.8 Hz, 8H), 7.23 (d, *J*= 7.6 Hz, 4H), 7.63 (s, 4H), 7.83 (d, *J*= 8.4 Hz, 4H), 7.86 (d, *J*= 8.4 Hz, 4H). $^{13}$C-NMR (400 MHz, $CDCl_3$): δ = 21.67, 22.76, 22.94, 28.99-29.20 (br), 29.90, 31.54 (br), 35.63, 36.83(br), 39.10, 39.48, 39.98, 67.47, 70.33 (br), 112.65, 121.45, 121.86, 122.47, 127.77, 129.12, 134.54, 134.74, 150.80, 152.49, 168.06, 171.94 (br), 172.19 (br). HR-MS *(m/z)* calculated for $C_{130}H_{180}N_{18}O_{28}S_4$ $[M+2H]^{2+}$ 1284.6043; found 1284.6035.

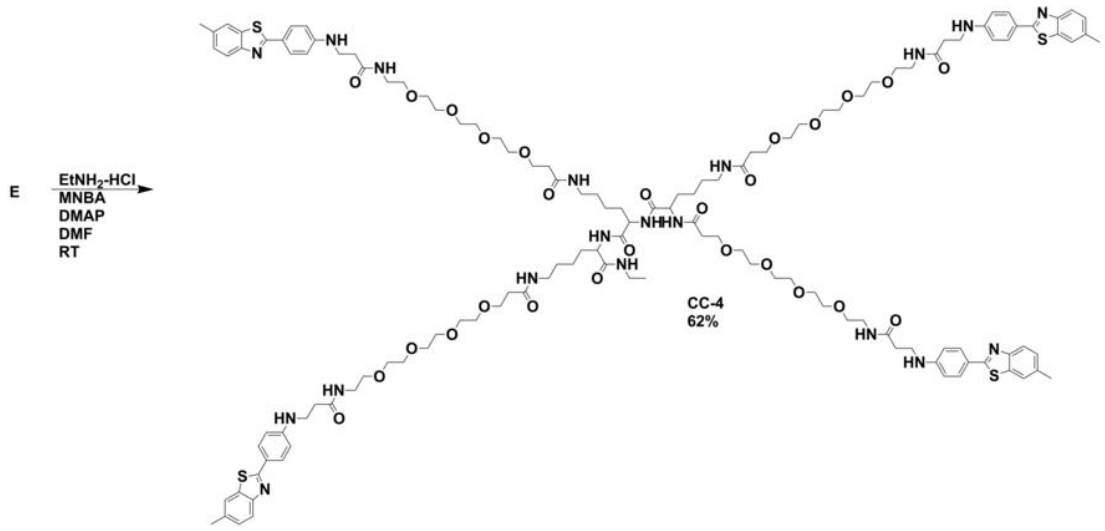


*Figure 7.9. Synthetic scheme for the synthesis of compound **CC-4***

**Synthesis of BTA Tetramer (CC-4):** Compound **E** (48 mg, 19 μmol), 2-Methyl-6-nitrobenzoic anhydride (MNBA) (15 mg, 44 μmol), DMAP (15 mg, 123 μmol), Ethylamine hydrochloride ($EtNH_2$-HCl) (8 mg, 99 μmol) were stirred at room temperature for 12 h in 2 mL dry DMF. The DMF was evaporated *in vacuo* and the residue was taken up in DCM, washed with saturated $NaHCO_3$, washed three times with brine, and dried over anhydrous $Na_2SO_4$. The crude product was purified by silica chromatography (6:1:1:1 mixture of EtOAc:ACN:$H_2O$:MeOH as eluent) to afford **CC-4** as a sticky, yellow residue (30 mg, 62% yield). $^1$H-NMR (400 MHz, $CDCl_3$): δ = 1.08 (t, *J*= 7.2 Hz, 3H), 1.25-1.50 (2 broad peaks, 12 H), 1.55-1.90 (2 broad peaks, 6H), 2.35-2.55 (broad peaks 28H), 3.05-3.25 (br, 8H), 3.35-3.75 (broad peaks 80 H), 6.66 (d, *J*= 8.8 Hz, 8H), 7.23 (d, *J*= 7.6 Hz, 4H), 7.63 (s, 4H), 7.83 (d, *J*= 8.4 Hz, 4H), 7.86 (d, *J*= 8.4 Hz, 4H). $^{13}$C-NMR (400 MHz, $CDCl_3$): δ = 14.76 (br), 23.31 (br), 29.04 (br), 35.62, 36.90, 39.46, 40.02, 67.49, 70.25 (br), 112.65,

121.48, 121.88, 122.48, 127.78, 129.12, 134.57, 134.76, 150.83, 152.51, 168.08, 172.05-172.20 (br). HPLC analysis was performed on a Spheri-5 phenyl column (5 µm, 250x4.6mm, Applied Biosystems, Inc.) using a gradient of 0 to100% MeOH in ACN and a flow rate of 1 mL/min over 50 minutes. The HPLC trace was monitored at 355 nm absorbance and retention time of **CC-4** was at 10.3 minutes. HR-MS *(m/z)* calculated for $C_{132}H_{185}N_{19}O_{27}S_4$ $[M+2H]^{2+}$ 1298.1280; found 1298.1234.

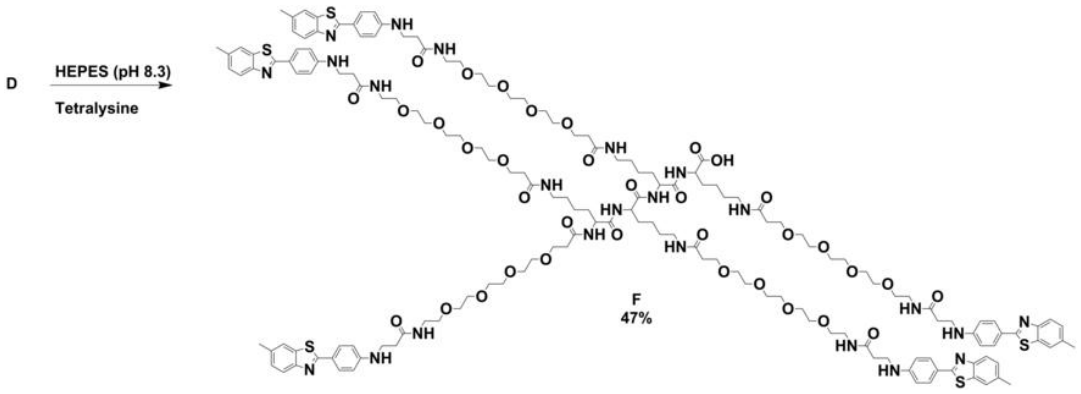


*Figure 7.10. Synthetic scheme for the precursor of the pentamer, compound **F***

**Synthesis of BTA-Pentamer-Acid (F):** Compound **D** (78 mg, 119 μmol) in 2 mL 1,4-dioxane was added to 0.1 M HEPES buffer (pH 8.3, 2 mL) containing tetralysine (10 mg, 19 μmol). The pH was maintained between 8.2-8.4 to favor complete acylation of all amines. The solvent was evaporated and the remaining yellow, oily residue was taken up in DCM and purified by silica chromatography (6:1:1:1 mixture of EtOAc:ACN:$H_2O$:MeOH as eluent) giving the BTA pentamer acid **F** as a brown, sticky residue (29 mg, 47% yield). $^{1}$H-NMR (400 MHz, $CDCl_3$): δ = 1.25-1.50 (2 broad peaks, 16 H), 1.55-1.90 (2 broad peaks, 8H), 2.35-2.55 (broad peaks 35H), 3.05-3.25 (br, 8H), 3.35-3.75 (broad peaks 100 H), 6.66 (d, *J*= 8.8 Hz, 4H), 7.23 (d, *J*= 7.6 Hz, 10H), 7.63 (s, 5H), 7.83 (d, *J*= 8.4 Hz, 5H), 7.86 (d, *J*= 8.4 Hz, 15H). $^{13}$C-NMR (400 MHz, $CDCl_3$): δ = 21.67, 22.90, 23.10, 29.05-29.20 (br), 29.90, 31.53 (br), 35.65, 36.80 (br), 39.00, 39.48, 40.01, 67.49, 70.32 (br), 112.66, 121.45, 121.88, 122.48, 127.76, 129.12, 134.54, 134.77, 150.82, 152.52, 168.04,

172.05 (br), 172.25 (br). HR-MS *(m/z)* calculated for $C_{164}H_{225}N_{23}O_{35}S_5Na_2$ $[M+2Na]^{2+}$ 1641.2461; found 1641.2443.

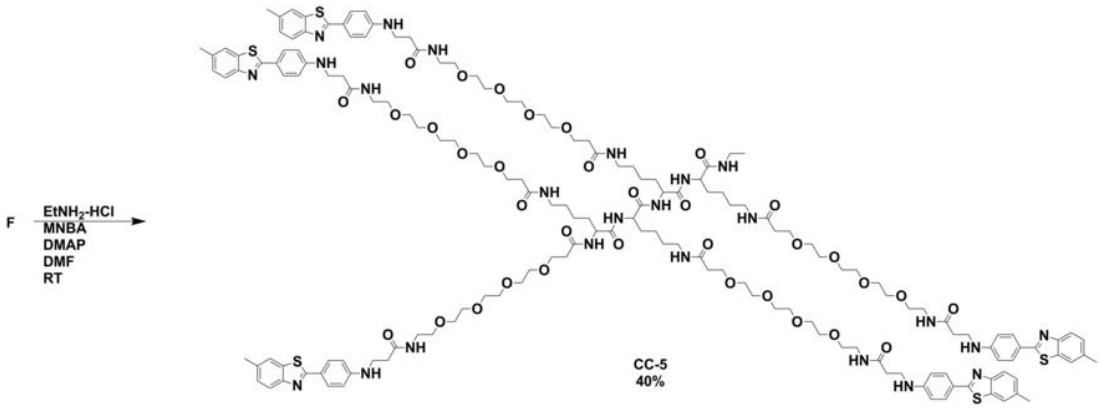


*Figure 7.11. Synthetic scheme for synthesis of pentamer **CC-5***

**Synthesis of BTA Pentamer (CC-5):** Compound **F** (46 mg, 14 μmol), MNBA (12 mg, 35 μmol), DMAP (23 mg, 188 μmol), and $EtNH_2$-HCl (20 mg, 245 μmol) were stirred at room temperature for 12 h in 2 mL dry DMF. DMF was evaporated *in vacuo* and the residue was taken up in DCM, washed with saturated $NaHCO_3$, washed three times with brine, and dried over anhydrous $Na_2SO_4$. The crude product was purified by silica chromatography (6:1:1:1 mixture of EtOAc:ACN:$H_2O$:MeOH as eluent) to afford CC-**5** as a sticky, yellow residue (18 mg, 40% yield). $^1$H-NMR (400 MHz, $CDCl_3$): δ = 1.10 (t, *J*= 7.2 Hz, 3H), 1.25-1.50 (2 broad peaks, 16 H), 1.55-1.90 (2 broad peaks, 8H), 2.35-2.55 (broad peaks 35H), 3.05-3.25 (br, 10H), 3.35-3.75 (broad peaks 100 H), 6.66 (d, *J*= 8.8 Hz, 4H), 7.23 (d, *J*= 7.6 Hz, 10H), 7.63 (s, 5H), 7.83 (d, *J*= 8.4 Hz, 5H), 7.86 (d, *J*= 8.4 Hz, 15H).$^{13}$C-NMR (400 MHz,

$CDCl_3$): δ = 14.42(br), 21.69, 23.20, 29.17 (br), 35.64, 37.00 (br), 39.50 (br), 40.00, 67.48, 70.30 (br), 112.70, 121.46, 121.94, 122.61, 127.77, 129.14, 134.53, 134.82, 150.73, 152.57, 167.95, 172.02-172.20 (br). HPLC analysis was performed on a Spheri-5 phenyl column (5 µm, 250 x 4.6mm, Applied Biosystems, Inc.) using a gradient of 0 to100% MeOH in ACN and a flow rate of 1 mL/min over 50 minutes. The HPLC trace was monitored at 355 nm and the retention time of **5** was at 9.6 minutes. HR-MS *(m/z)* calculated for $C_{166}H_{232}N_{24}O_{34}S_5$ $[M+2H]^{2+}$ 1632.7878; found 1632.7850.

**Growth of Aβ Fibrils:** Aβ fibrils were grown from synthetic Aβ(1-42) peptides by incubating the peptides (111 µM) in PBS at 37 °C for 24 h, with stirring. The presence of fibrils was confirmed by a previously described Congo Red spectroscopic assay.[1]

**Growth of SEVI Fibrils:** PAP248–286 was dissolved in PBS at a concentration of 10 mg/mL. Fibrils were formed by agitation in an Eppendorf Thermomixer at 1400 rpm and 37 °C for 72 h. The presence of fibrils was confirmed by a previously described Congo Red spectroscopic assay.[1]

**Congo Red spectroscopic assay:** Fibril formation was characterized by a Congo Red assay.[1] A fresh solution of 7 mg/ml Congo Red (CR) was prepared in PBS and filtered through a 0.2 µm syringe filter. 5 µl of this solution was pipetted in 1 ml PBS to make a dilute solution of Congo Red. 160 µl of the dilute CR solution was pipetted into wells of a 96-well plate. To each well was added 40 µl of fibrils or 40 µl PBS. The microplate was covered in parafilm and incubated for 30 minutes at

room temperature. The contents of the wells were pipet-mixed then the spectrum of each well (400-700 nm) was recorded on a UV-Vis microplate reader (SpectraMax 190, Molecular Devices, LLC). A maximal absorbance shift (Congo Red has a maximal absorbance at 490 nm) to approximately 540 nm indicates the presence of fibrils.

**Measurement of the Binding Affinity of BTA monomer and oligomers to amyloid fibril:** The binding of BTA monomer and oligomers to amyloid fibrils was measured according to the centrifugation assay described by Levine[83] for BTA-1 to Aβ fibrils. Briefly, 200 µL of various concentrations of BTA derivatives CC-**1** – CC-**5** in 5 % DMSO/PBS were incubated in the presence or absence of 10 µg of fibrils to give a final volume of 220 µL of solution. These incubations were performed in duplicate runs and allowed to equilibrate for 12 h at room temperature. After equilibration, each solution was centrifuged at 16,000 × *g* for 20 min at 4˚C. The supernatants were separated from the pelleted fibrils, and 220 µL of fresh 5% DMSO/PBS was added to re-suspend the pellets. 100 µl aliquots of each re-suspended pellet was pipetted into a cuvette (ultramicrocuvette,10-mm light path, Hellma®, Müllheim, Germany), and the fluorescence of the bound molecule was determined at 355 nm excitation and 420 nm emission using a spectrofluorometer (Photon Technology International, Inc., Birmingham, NJ). Each experiment was repeated at least 3 times. Error bars represent standard deviations from the mean. Graphs shown in Figures 7.12 and 7.13 of fluorescence intensity versus concentration of compounds **CC-1 - CC-5** were plotted and fitted using the

following one-site specific binding algorithm to determine $K_d$: $Y = B_{max} \times X/(K_d + X)$, where $X$ is the concentration of BTA oligomer, $Y$ is the specific binding fluorescence intensity, and $B_{max}$ corresponds to the apparent maximal observable fluorescence upon binding of BTA oligomer to Aβ or SEVI fibrils. The data were processed using Origin 7.0 (MicroCal Software, Inc., Northampton, MA).

**Evaluation of SEVI-mediated enhancement of HIV-1 infectivity of TZM-bl cells in the presence of BTA monomer and oligomers:** TZM-bl cells (in DMEM supplemented with 10% FBS, 50 units/mL penicillin, and 50 μg/mL streptomycin) were seeded on 96-well flat-bottomed tissue culture plates at a density of $4x10^3$ cells/well. Plates were incubated for 12 h (in a humidified atmosphere of 95% air, 5% $CO_2$ at 37˚C) to promote attachment of cells to the wells. HIV-$1_{IIIB}$ was pretreated for 10 min at room temperature with 15 μg/mL SEVI fibrils in the presence or absence of **CC-1 – CC-5** (in 5% DMSO/DPBS). Treated virions were then added to the plated TZM-bl cells and incubated for 2 h at 37˚C. After incubation, the cells were washed with DPBS and the media was replaced. Infection was assayed after 72 hours by quantifying luciferase expression with PerkinElmer Britelite Plus and measuring luminescence with a microplate reader (DTX880, Beckman Coulter). All data are represented as the mean ± S.D. of triplicate measurements. ANOVA with Tukey's post test was employed in all analyses of data. A $p$-value < 0.05 was considered statistically significant compared to control cells.

# 7.5 Additional Figures

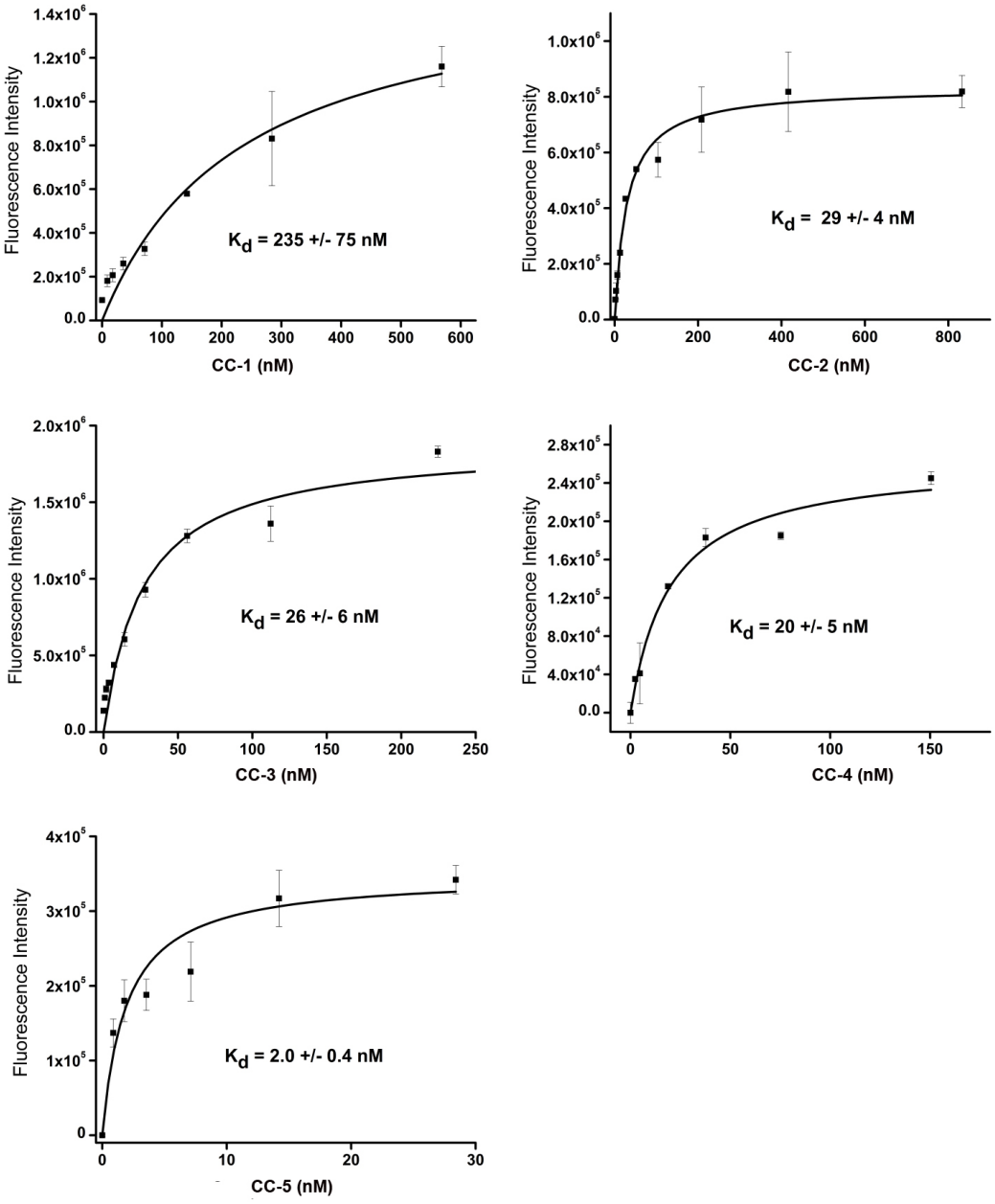


*Figure 7.12. Fluorescence saturation binding curves of compounds* ***CC-1 – CC-5*** *to Aβ fibrils.* $\lambda_{ex}$*: 355 nm;* $\lambda_{em}$*: 420 nm.*

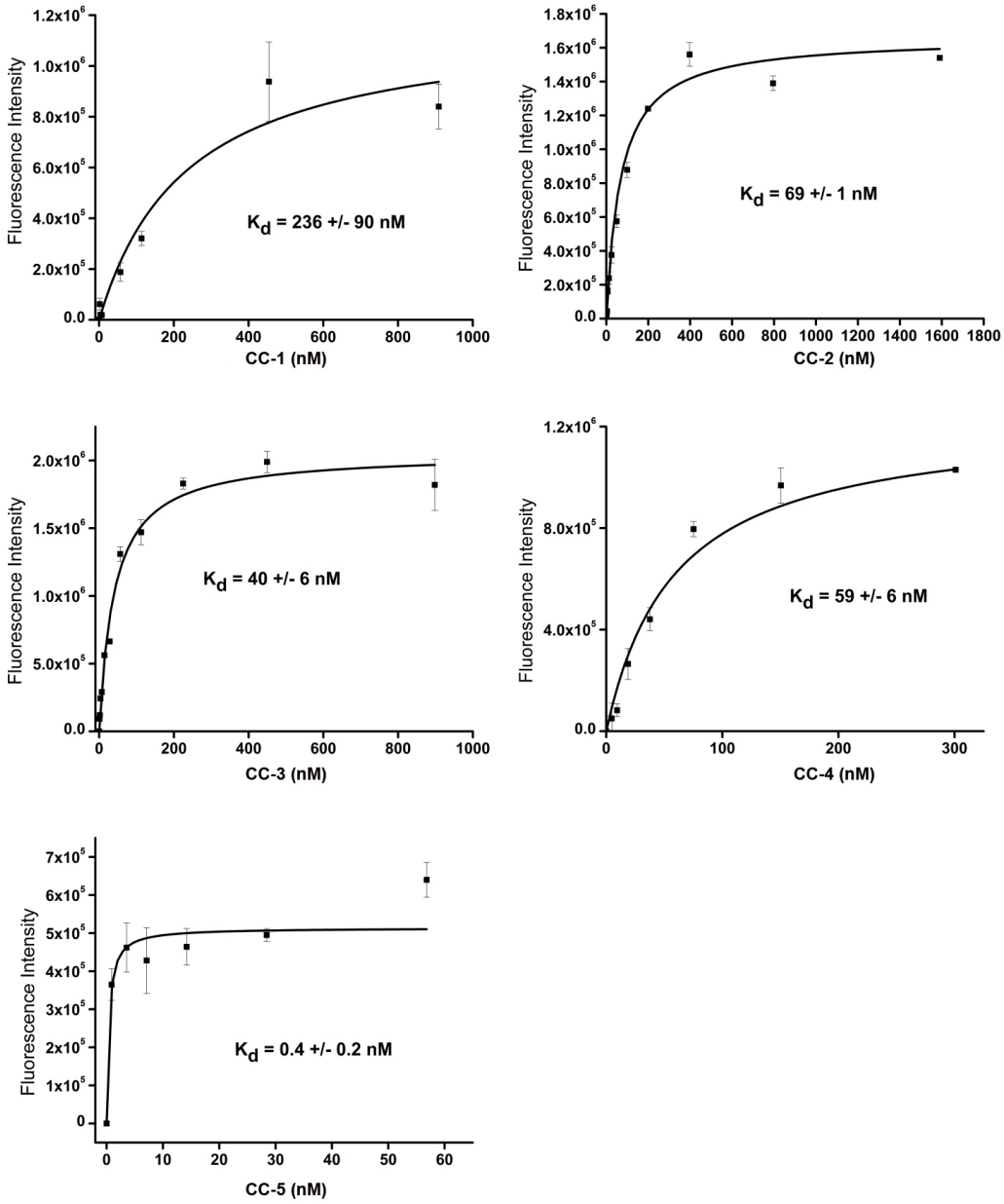


*Figure 7.13. Fluorescence saturation binding curves of BTA monomer and oligomers to SEVI fibrils. $\lambda_{ex}$: 355 nm; $\lambda_{em}$: 420 nm.*

# Notes about this Chapter

A significant portion of the work presented here was generated by me. I would like to thank Caitlin Brown and Joanna S. Olsen for their contributions in the

cellular assays. Material in this chapter is currently being prepared for submission for publication: "Oligovalent Amyloid-Binding Agents Reduce SEVI-Mediated Enhancement of HIV-1 Infection." Capule, C.C.; Brown, C.; Olsen, J.S.; Dewhurst, S.; Yang, J. I am the primary author of this pending manuscript.

REFERENCES

(1) Nilsson, M. R. *Methods* **2004**, *34*, 151-160.

(2) Gertz, M. A.; Rajkumar, S. V.; Humana ;
Springer [distributor]: Totowa, N.J.
London, 2010, p x, 238 p.

(3) Groenning, M. *J Chem Biol* **2009**.

(4) Westermark, P. *Febs Journal* **2005**, *272*, 5942-5949.

(5) Munch, J.; Rucker, E.; Standker, L.; Adermann, K.; Goffinet, C.; Schindler, M.; Wildum, S.; Chinnadurai, R.; Rajan, D.; Specht, A.; Gimenez-Gallego, G.; Sanchez, P. C.; Fowler, D. M.; Koulov, A.; Kelly, J. W.; Mothes, W.; Grivel, J. C.; Margolis, L.; Keppler, O. T.; Forssmann, W. G.; Kirchhoff, F. *Cell* **2007**, *131*, 1059-71.

(6) Graeber, M. B. *Brain Pathol* **1999**, *9*, 237-40.

(7) Graeber, M. B.; Kosel, S.; Egensperger, R.; Banati, R. B.; Muller, U.; Bise, K.; Hoff, P.; Moller, H. J.; Fujisawa, K.; Mehraein, P. *Neurogenetics* **1997**, *1*, 73-80.

(8) Graeber, M. B.; Kosel, S.; Grasbon-Frodl, E.; Moller, H. J.; Mehraein, P. *Neurogenetics* **1998**, *1*, 223-8.

(9) Dawbarn, D.; Allen, S. J. *Neurobiology of Alzheimer's disease*; 3rd ed.; Oxford University Press: Oxford ; New York, 2007.

(10) Thies, W.; Bleiler, L. *Alzheimers Dement*, *7*, 208-44.

(11) Lleo, A. *Curr. Genomics* **2007**, *8*, 550-8.

(12) Orhan, G.; Orhan, I.; Sener, B. *Letters in Drug Design & Discovery* **2006**, *3*, 268-274.

(13) Sweetman, S. C. *Martindale : the complete drug reference*; 36th ed.; Pharmaceutical Press: London, 2009.

(14) Demuro, A.; Parker, I.; Stutzmann, G. E. *J. Biol. Chem.*, *285*, 12463-12468.

(15) Rogawski, M. A.; Wenk, G. L. *CNS Drug Rev.* **2003**, *9*, 275-308.

(16) Robinson, D. M.; Keating, G. M. *Drugs* **2006**, *66*, 1515-34.

(17) Selkoe, D. J.; Podlisny, M. B. *Annu. Rev. Genomics Hum. Genet.* **2002**, *3*, 67-99.

(18) Arai, T.; Ikeda, K.; Akiyama, H.; Shikamoto, Y.; Tsuchiya, K.; Yagishita, S.; Beach, T.; Rogers, J.; Schwab, C.; McGeer, P. L. *Acta Neuropathol* **2001**, *101*, 167-73.

(19) Lee, V. M.; Goedert, M.; Trojanowski, J. Q. *Annu. Rev. Neurosci.* **2001**, *24*, 1121-59.

(20) Haass, C.; Selkoe, D. J. *Cell* **1993**, *75*, 1039-42.

(21) Iwatsubo, T.; Odaka, A.; Suzuki, N.; Mizusawa, H.; Nukina, N.; Ihara, Y. *Neuron* **1994**, *13*, 45-53.

(22) Jarrett, J. T.; Lansbury, P. T., Jr. *Cell* **1993**, *73*, 1055-8.

(23) Knauer, M. F.; Soreghan, B.; Burdick, D.; Kosmoski, J.; Glabe, C. G. *Proc. Natl. Acad. Sci. USA* **1992**, *89*, 7437-41.

(24) Mayeux, R.; Tang, M. X.; Jacobs, D. M.; Manly, J.; Bell, K.; Merchant, C.; Small, S. A.; Stern, Y.; Wisniewski, H. M.; Mehta, P. D. *Ann. Neurol.* **1999**, *46*, 412-6.

(25) Iwata, N.; Tsubuki, S.; Takaki, Y.; Watanabe, K.; Sekiguchi, M.; Hosoki, E.; Kawashima-Morishima, M.; Lee, H. J.; Hama, E.; Sekine-Aizawa, Y.; Saido, T. C. *Nat. Med.* **2000**, *6*, 143-50.

(26) Selkoe, D. J. *Trends Cell Biol.* **1998**, *8*, 447-53.

(27) Hardy, J. A.; Higgins, G. A. *Science* **1992**, *256*, 184-5.

(28) Lambert, M. P.; Barlow, A. K.; Chromy, B. A.; Edwards, C.; Freed, R.; Liosatos, M.; Morgan, T. E.; Rozovsky, I.; Trommer, B.; Viola, K. L.; Wals, P.; Zhang, C.; Finch, C. E.; Krafft, G. A.; Klein, W. L. *Proc. Natl. Acad. Sci. USA* **1998**, *95*, 6448-53.

(29) Lesne, S.; Koh, M. T.; Kotilinek, L.; Kayed, R.; Glabe, C. G.; Yang, A.; Gallagher, M.; Ashe, K. H. *Nature* **2006**, *440*, 352-7.

(30) Shankar, G. M.; Li, S.; Mehta, T. H.; Garcia-Munoz, A.; Shepardson, N. E.; Smith, I.; Brett, F. M.; Farrell, M. A.; Rowan, M. J.; Lemere, C. A.; Regan, C. M.; Walsh, D. M.; Sabatini, B. L.; Selkoe, D. J. *Nat. Med.* **2008**, *14*, 837-42.

(31) Stiller, D.; Katenkamp, D.; Thoss, K. *Acta Histochem.* **1972**, *42*, 234-45.

(32) Vassar, P. S.; Culling, C. F. *Arch. Pathol.* **1959**, *68*, 487-98.

(33) Sajid, J.; Elhaddaoui, A.; Turrell, S. *Journal of Molecular Structure* **1997**, *408*, 181-184.

(34) Klunk, W. E.; Engler, H.; Nordberg, A.; Wang, Y.; Blomqvist, G.; Holt, D. P.; Bergström, M.; Savitcheva, I.; Huang, G.-F.; Estrada, S.; Ausén, B.; Debnath, M. L.; Barletta, J.; Price, J. C.; Sandell, J.; Lopresti, B. J.; Wall, A.; Koivisto, P.; Antoni, G.; Mathis, C. A.; Långström, B. *Ann. Neurol.* **2004**, *55*, 306-319.

(35) Vandenberghe, R.; Van Laere, K.; Ivanoiu, A.; Salmon, E.; Bastin, C.; Triau, E.; Hasselbalch, S.; Law, I.; Andersen, A.; Korner, A.; Minthon, L.; Garraux, G.; Nelissen, N.; Bormans, G.; Buckley, C.; Owenius, R.; Thurfjell, L.; Farrar, G.; Brooks, D. J. *Ann. Neurol.* **2010**, *68*, 319-329.

(36) Barthel, H.; Gertz, H. J.; Dresel, S.; Peters, O.; Bartenstein, P.; Buerger, K.; Hiemeyer, F.; Wittemer-Rump, S. M.; Seibyl, J.; Reininger, C.; Sabri, O. *Lancet Neurol.* **2011**, *10*, 424-35.

(37) Clark, C. M.; Schneider, J. A.; Bedell, B. J.; Beach, T. G.; Bilker, W. B.; Mintun, M. A.; Pontecorvo, M. J.; Hefti, F.; Carpenter, A. P.; Flitter, M. L.; Krautkramer, M. J.; Kung, H. F.; Coleman, R. E.; Doraiswamy, P. M.; Fleisher, A. S.; Sabbagh, M. N.; Sadowsky, C. H.; Reiman, P. E. M.; Zehntner, S. P.; Skovronsky, D. M.; Grp, A.-A. S. *J. Am. Med. Assoc.* **2011**, *305*, 275-283.

(38) Sepkowitz, K. A. *New England Journal of Medicine* **2001**, *344*, 1764-1772.

(39) Weiss, R. A. *Science* **1993**, *260*, 1273-1279.

(40) Siegal, F. P.; Lopez, C.; Hammer, G. S.; Brown, A. E.; Kornfeld, S. J.; Gold, J.; Hassett, J.; Hirschman, S. Z.; Cunningham-Rundles, C.; Adelsberg, B. R.; et al. *N. Engl. J. Med.* **1981**, *305*, 1439-44.

(41) Gottlieb, M. S.; Schroff, R.; Schanker, H. M.; Weisman, J. D.; Fan, P. T.; Wolf, R. A.; Saxon, A. *N. Engl. J. Med.* **1981**, *305*, 1425-31.

(42) Friedman-Kien, A. E. *J. Am. Acad. Dermatol.* **1981**, *5*, 468-71.

(43) *MMWR Morb Mortal Wkly Rep* **1982**, *31*, 507-8, 513-4.

(44) *http://www.cdc.gov/hiv/resources/factsheets/us.htm*.

(45) World Health Organization.; World Health Organization: Geneva, Switzerland, 2011, p v.

(46) Royce, R. A.; Sena, A.; Cates, W., Jr.; Cohen, M. S. *N Engl J Med* **1997**, *336*, 1072-8.

(47) Feldman, C. *Curr. Opin. Infect. Dis.* **2005**, *18*, 165-70.

(48) Services, U. D. o. H. H. *HIV and its Treatments* **2011**.

(49) Clapham, P. R.; McKnight, A. *Br. Med. Bull.* **2001**, *58*, 43-59.

(50) Cunningham, A. L.; Donaghy, H.; Harman, A. N.; Kim, M.; Turville, S. G. *Curr. Opin. Microbiol.* **2010**, *13*, 524-9.

(51) Desport, M. *Lentiviruses and macrophages : molecular and cellular interactions*; Caister Academic Press: Norkfolk, UK.

(52) Coffin, J. M.; Hughes, S. H.; Varmus, H. *Retroviruses*; Cold Spring Harbor Laboratory Press: Plainview, N.Y., 1997.

(53) Clapham, P. R.; McKnight, A. *J. Gen. Virol.* **2002**, *83*, 1809-29.

(54) *http://aidsinfo.nih.gov*.

(55) Roan, N. R.; Munch, J.; Arhel, N.; Mothes, W.; Neidleman, J.; Kobayashi, A.; Smith-McCune, K.; Kirchhoff, F.; Greene, W. C. *J. Virol.* **2009**, *83*, 73-80.

(56) Olsen, J. S.; Brown, C.; Capule, C. C.; Rubinshtein, M.; Doran, T. M.; Srivastava, R. K.; Feng, C. Y.; Nilsson, B. L.; Yang, J.; Dewhurst, S. *J. Biol. Chem.* **2010**, *285*, 35488-35496.

(57) Inbar, P.; Li, C. Q.; Takayama, S. A.; Bautista, M. R.; Yang, J. *Chembiochem* **2006**, *7*, 1563-6.

(58) Habib, L. K.; Lee, M. T. C.; Yang, J. *J. Biol. Chem.* **2010**, *285*, 38933-38943.

(59) Cecchelli, R.; Dehouck, B.; Descamps, L.; Fenart, L.; Buee-Scherrer, V.; Duhem, C.; Lundquist, S.; Rentfel, M.; Torpier, G.; Dehouck, M. P. *Adv. Drug Deliv. Rev.* **1999**, *36*, 165-178.

(60) Kadir, A.; Marutle, A.; Gonzalez, D.; Scholl, M.; Almkvist, O.; Mousavi, M.; Mustafiz, T.; Darreh-Shori, T.; Nennesmo, I.; Nordberg, A. *Brain* **2011**, *134*, 301-317.

(61) Newberg, A. B.; Wintering, N. A.; Plossl, K.; Hochold, J.; Stabin, M. G.; Watson, M.; Skovronsky, D.; Clark, C. M.; Kung, M. P.; Kung, H. F. *J. Nucl. Med.* **2006**, *47*, 748-54.

(62) Kung, M. P.; Hou, C.; Zhuang, Z. P.; Zhang, B.; Skovronsky, D.; Trojanowski, J. Q.; Lee, V. M.; Kung, H. F. *Brain Res.* **2002**, *956*, 202-10.

(63) Khurana, R.; Coleman, C.; Ionescu-Zanetti, C.; Carter, S. A.; Krishna, V.; Grover, R. K.; Roy, R.; Singh, S. *J Struct Biol* **2005**, *151*, 229-38.

(64) Ballabh, P.; Braun, A.; Nedergaard, M. *Neurobiology of Disease* **2004**, *16*, 1-13.

(65) Wolburg, H.; Neuhaus, J.; Kniesel, U.; Krauss, B.; Schmid, E. M.; Ocalan, M.; Farrell, C.; Risau, W. *Journal of Cell Science* **1994**, *107*, 1347-1357.

(66) Raub, T. J. *American Journal of Physiology-Cell Physiology* **1996**, *271*, C495-C503.

(67) Dehouck, B.; Dehouck, M. P.; Fruchart, J. C.; Cecchelli, R. *Journal of Cell Biology* **1994**, *126*, 465-473.

(68) Lipinski, C. A.; Lombardo, F.; Dominy, B. W.; Feeney, P. J. *Adv. Drug Deliv. Rev.* **2001**, *46*, 3-26.

(69) Cecchelli, R.; Dehouck, B.; Descamps, L.; Fenart, L.; Buee-Scherrer, V.; Duhem, C.; Lundquist, S.; Rentfel, M.; Torpier, G.; Dehouck, M. P. *Advanced Drug Delivery Reviews* **1999**, *36*, 165-178.

(70) Cecchelli, R.; Berezowski, V.; Lundquist, S.; Culot, M.; Renftel, M.; Dehouck, M. P.; Fenart, L. *Nature Reviews Drug Discovery* **2007**, *6*, 650-661.

(71) Dehouck, M. P.; Meresse, S.; Delorme, P.; Fruchart, J. C.; Cecchelli, R. *J. Neurochem.* **1990**, *54*, 1798-1801.

(72) Dehouck, B.; Dehouck, M. P.; Fruchart, J. C.; Cecchelli, R. *J. Cell Biol.* **1994**, *126*, 465-473.

(73) Dehouck, B.; Fenart, L.; Dehouck, M. P.; Pierce, A.; Torpier, G.; Cecchelli, R. *J. Cell Biol.* **1997**, *138*, 877-889.

(74) Descamps, L.; Dehouck, M. P.; Torpier, G.; Cecchelli, R. *Am. J. Physiol.* **1996**, *270*, H1149-H1158.

(75) Culot, M.; Lundquist, S.; Vanuxeem, D.; Nion, S.; Landry, C.; Delplace, Y.; Dehouck, M. P.; Berezowski, V.; Fenart, L.; Cecchelli, R. *Toxicol. In Vitro* **2008**, *22*, 799-811.

(76) Lundquist, S.; Renftel, M.; Brillault, J.; Fenart, L.; Cecchelli, R.; Dehouck, M. P. *Pharm. Res.* **2002**, *19*, 976-981.

(77) Young, R. C.; Mitchell, R. C.; Brown, T. H.; Ganellin, C. R.; Griffiths, R.; Jones, M.; Rana, K. K.; Saunders, D.; Smith, I. R.; Sore, N. E.; et al. *J. Med. Chem.* **1988**, *31*, 656-71.

(78) Abraham, M. H.; Takacs-Novak, K.; Mitchell, R. C. *J. Pharm. Sci.* **1997**, *86*, 310-5.

(79) Song, J. M.; Spitzer, M. H.; Megill, A.; Rubinshtein, M.; Habib, L. K.; Capule, C. C.; Xie, Y.; Keenoy, K. E.; Mayer, M.; Turner, S. R.; Yang, J.; Pak, D. T. S.; Lee, H.-K.; Hoe, H.-S. *unpublished results* **2011**.

(80) Siflinger-Birnboim, A.; Del Vecchio, P. J.; Cooper, J. A.; Blumenstock, F. A.; Shepard, J. M.; Malik, A. B. *J. Cell. Physiol.* **1987**, *132*, 111-7.

(81) Klunk, W. E.; Engler, H.; Nordberg, A.; Bacskai, B. J.; Wang, Y.; Price, J. C.; Bergstrom, M.; Hyman, B. T.; Langstrom, B.; Mathis, C. A. *Neuroimaging Clin. N. Am.* **2003**, *13*, 781-9.

(82) Nordberg, A. *Neuropsychologia* **2008**, *46*, 1636-41.

(83) LeVine, H., 3rd *Amyloid* **2005**, *12*, 5-14.

(84) Cai, L. S.; Innis, R. B.; Pike, V. W. *Curr. Med. Chem.* **2007**, *14*, 19-52.

(85) Lockhart, A.; Ye, L.; Judd, D. B.; Merritt, A. T.; Lowe, P. N.; Morgenstern, J. L.; Hong, G. Z.; Gee, A. D.; Brown, J. *J. Biol. Chem.* **2005**, *280*, 7677-7684.

(86) Inbar, P.; Bautista, M. R.; Takayama, S. A.; Yang, J. *Anal. Chem.* **2008**, *80*, 3502-6.

(87) Friguet, B.; Djavadi-Ohaniance, L.; Goldberg, M. E. *Mol. Immunol.* **1984**, *21*, 673-677.

(88) Hollander, Z.; Katchalskikatzir, E. *Mol. Immunol.* **1986**, *23*, 927-933.

(89) Levine, H. *Protein Sci.* **1993**, *2*, 404-410.

(90) Kowalewski, T.; Holtzman, D. M. *Proc. Natl. Acad. of Sci. USA* **1999**, *96*, 3688-3693.

(91) Zhu, M.; Souillac, P. O.; Ionescu-Zanetti, C.; Carter, S. A.; Fink, A. L. *J. Biol. Chem.* **2002**, *277*, 50914-50922.

(92) Rocha, S.; Thuneman, A. F.; Pereira, M. D.; Coelho, M.; Mohwald, H.; Brezesinski, G. *Biophys. Chem.* **2008**, *137*, 35-42.

(93) Giacomelli, C. E.; Norde, W. *Biomacromolecules* **2003**, *4*, 1719-1726.

(94) Giacomelli, C. E.; Norde, W. *Macromol. Biosci.* **2005**, *5*, 401-407.

(95) Krimm, S.; Bandekar, J. *Adv. Protein Chem.* **1986**, *38*, 181-364.

(96) Susi, H.; Byler, D. M. *Methods Enzymol.* **1986**, *130*, 290-311.

(97) Surewicz, W. K.; Mantsch, H. H. *Biochim. Biophys. Acta.* **1988**, *952*, 115-30.

(98) Dong, A.; Huang, P.; Caughey, W. S. *Biochemistry* **1990**, *29*, 3303-8.

(99) Lin, S. Y.; Chu, H. L. *Int. J. Biol. Macromol.* **2003**, *32*, 173-7.

(100) Susi, H.; Byler, D. M. *Biochem. Biophys. Res. Commun.* **1983**, *115*, 391-7.

(101) Ahmed, M.; Davis, J.; Aucoin, D.; Sato, T.; Ahuja, S.; Aimoto, S.; Elliott, J. I.; Van Nostrand, W. E.; Smith, S. O. *Nat. Struct. Mol. Biol.* **2010**, *17*, 561-U56.

(102) Cerf, E.; Sarroukh, R.; Tamamizu-Kato, S.; Breydo, L.; Derclaye, S.; Dufrene, Y. F.; Narayanaswami, V.; Goormaghtigh, E.; Ruysschaert, J. M.; Raussens, V. *Biochem. J.* **2009**, *421*, 415-423.

(103) Garbassi, F.; Morra, M.; Occhiello, E. *Polymer surfaces : from physics to technology*; Rev. and updated ed.; Wiley: Chichester, England ; New York, 1998.

(104) Hollahan, J. R.; Bell, A. T. *Techniques and applications of plasma chemistry*; Wiley: New York, 1974.

(105) Dupont-Gillain, C. C.; Adriaensen, Y.; Derclaye, S.; Rouxhet, P. G. *Langmuir* **2000**, *16*, 8194-8200.

(106) Onyiriuka, E. C. *J. Appl. Polym. Sci.* **1993**, *47*, 2187-2194.

(107) Balanzat, E.; Bouffard, S.; Bouquerel, A.; Devy, J.; Gate, C. *Nuclear Instruments & Methods in Physics Research Section B-Beam Interactions with Materials and Atoms* **1996**, *116*, 159-163.

(108) Yasuda, T.; Gazicki, M.; Yasuda, H. *Applied Polymer Symposia* **1984**, 201-214.

(109) Liston, E. M.; Martinu, L.; Wertheimer, M. R. *Journal of Adhesion Science and Technology* **1993**, *7*, 1091-1127.

(110) Hall, D. B.; Underhill, P.; Torkelson, J. M. *Polym. Eng. Sci.* **1998**, *38*, 2039-2045.

(111) *See supporting information for details on determining the dissociation constant between the IgG and Aβ.*

(112) Cheng, Y.; Prusoff, W. H. *Biochem. Pharmacol.* **1973**, *22*, 3099-3108.

(113) Ye, L.; Morgenstern, J. L.; Gee, A. D.; Hong, G. Z.; Brown, J.; Lockhart, A. *J. Biol. Chem.* **2005**, *280*, 23599-23604.

(114) Zhen, W.; Han, H.; Anguiano, M.; Lemere, C. A.; Cho, C. G.; Lansbury, P. T. *J. Med. Chem.* **1999**, *42*, 2805-2815.

(115) Klunk, W. E.; Bacskai, B. J.; Mathis, C. A.; Kajdasz, S. T.; McLellan, M. E.; Frosch, M. P.; Debnath, M. L.; Holt, D. P.; Wang, Y. M.; Hyman, B. T. *J. Neuropathol. Exp. Neurol.* **2002**, *61*, 797-805.

(116) Agdeppa, E. D.; Kepe, V.; Petric, A.; Satyamurthy, N.; Liu, J.; Huang, S. C.; Small, G. W.; Cole, G. M.; Barrio, J. R. *Neuroscience* **2003**, *117*, 723-730.

(117) Groenning, M.; Olsen, L.; van de Weert, M.; Flink, J. M.; Frokjaer, S.; Jorgensen, F. S. *J. Struct. Biol.* **2007**, *158*, 358-69.

(118) LeVine, H. *Methods Enzymol.* **1999**, *309*, 274-84.

(119) Yang, J.; Mayer, M.; Kriebel, J. K.; Garstecki, P.; Whitesides, G. M. *Angew. Chem. Int. Ed. Engl.* **2004**, *43*, 1555-8.

(120) Zhao, X. B.; Yang, J. *ACS Chem. Neurosci.* **2010**, *1*, 655-660.

(121) Inbar, P.; Yang, J. *Bioorg. Med. Chem. Lett.* **2006**, *16*, 1076-9.

(122) Friguet, B.; Chaffotte, A. F.; Djavadi-Ohaniance, L.; Goldberg, M. E. *J. Immunol. Methods* **1985**, *77*, 305-19.

(123) Janus, C.; Pearson, J.; McLaurin, J.; Mathews, P. M.; Jiang, Y.; Schmidt, S. D.; Chishti, M. A.; Horne, P.; Heslin, D.; French, J.; Mount, H. T. J.; Nixon, R. A.; Mercken, M.; Bergeron, C.; Fraser, P. E.; St George-Hyslop, P.; Westaway, D. *Nature* **2000**, *408*, 979-982.

(124) Minati, L.; Edginton, T.; Bruzzone, M. G.; Giaccone, G. *Am. J. Alzheimers Dis.* **2009**, *24*, 95-121.

(125) Schott, J. M.; Kennedy, J.; Fox, N. C. *Curr. Opin. Neurol.* **2006**, *19*, 552-558.

(126) Mathis, C. A.; Wang, Y.; Klunk, W. E. *Curr. Pharm. Des.* **2004**, *10*, 1469-92.

(127) Kim, Y.; Lee, J. H.; Ryu, J.; Kim, D. J. *Curr. Pharm. Des.* **2009**, *15*, 637-58.

(128) Matthews, B.; Siemers, E. R.; Mozley, P. D. *Am. J. Geriatr. Psychiatry* **2003**, *11*, 146-59.

(129) Nichols, L.; Pike, V. W.; Cai, L.; Innis, R. B. *Biol. Psychiatry* **2006**, *59*, 940-7.

(130) Golde, T. E.; Bacskai, B. J. *Nat. Biotechnol.* **2005**, *23*, 552-4.

(131) Kitts, C. C.; Vanden Bout, D. A. *J. Phys. Chem. B* **2009**, *113*, 12090-5.

(132) Schmidt, M. L.; Schuck, T.; Sheridan, S.; Kung, M. P.; Kung, H.; Zhuang, Z. P.; Bergeron, C.; Lamarche, J. S.; Skovronsky, D.; Giasson, B. I.; Lee, V. M.; Trojanowski, J. Q. *Am. J. Pathol.* **2001**, *159*, 937-43.

(133) Mathis, C. A.; Bacskai, B. J.; Kajdasz, S. T.; McLellan, M. E.; Frosch, M. P.; Hyman, B. T.; Holt, D. P.; Wang, Y.; Huang, G. F.; Debnath, M. L.; Klunk, W. E. *Bioorg. Med. Chem. Lett.* **2002**, *12*, 295-8.

(134) Ryu, E. K.; Chen, X. *Front. Biosci.* **2008**, *13*, 777-89.

(135) Stephenson, K. A.; Chandra, R.; Zhuang, Z. P.; Hou, C.; Oya, S.; Kung, M. P.; Kung, H. F. *Bioconjug. Chem.* **2007**, *18*, 238-46.

(136) Nordberg, A. *Curr. Opin. Neurol.* **2007**, *20*, 398-402.

(137) Garcia-Alloza, M.; Bacskai, B. J. *Neuromol. Med.* **2004**, *6*, 65-78.

(138) Bacskai, B. J.; Klunk, W. E.; Mathis, C. A.; Hyman, B. T. *J. Cereb. Blood Flow Metabol.* **2002**, *22*, 1035-1041.

(139) Burn, D. J.; O'Brien, J. T. *Mov. Disord.* **2003**, *18 Suppl 6*, S88-95.

(140) Nesterov, E. E.; Skoch, J.; Hyman, B. T.; Klunk, W. E.; Bacskai, B. J.; Swager, T. M. *Angew. Chem. Intl. Ed.* **2005**, *44*, 5452-5456.

(141) Zhuang, Z. P.; Kung, M. P.; Kung, H. F. *J. Med. Chem.* **2006**, *49*, 2841-2844.

(142) Li, Q. A.; Lee, J. S.; Ha, C.; Park, C. B.; Yang, G.; Gan, W. B.; Chang, Y. T. *Angew. Chem. Intl. Ed.* **2004**, *43*, 6331-6335.

(143) Kung, H. F.; Lee, C. W.; Zhuang, Z. P.; Kung, M. P.; Hou, C.; Plossl, K. *J. Am. Chem. Soc.* **2001**, *123*, 12740-1.

(144) Grabowski, Z. R.; Rotkiewicz, K.; Rettig, W. *Chem. Rev.* **2003**, *103*, 3899-4032.

(145) Haidekker, M. A.; Theodorakis, E. A. *Org. Biomol. Chem.* **2007**, *5*, 1669-78.

(146) Loutfy, R. O. *Pure Appl. Chem.* **1986**, *58*, 1239-1248.

(147) Viriot, M. L.; Carre, M. C.; Geoffroy-Chapotot, C.; Brembilla, A.; Muller, S.; Stoltz, J. F. *Clin. Hemorheol. Microcirc.* **1998**, *19*, 151-60.

(148) Haidekker, M. A.; Brady, T. P.; Lichlyter, D.; Theodorakis, E. A. *Bioorg. Chem.* **2005**, *33*, 415-25.

(149) Nipper, M. E.; Majd, S.; Mayer, M.; Lee, J. C.; Theodorakis, E. A.; Haidekker, M. A. *Biochim. Biophys. Acta, Biomembr.* **2008**, *1778*, 1148-53.

(150) Haidekker, M. A.; Ling, T.; Anglo, M.; Stevens, H. Y.; Frangos, J. A.; Theodorakis, E. A. *Chem. Biol.* **2001**, *8*, 123-31.

(151) Haidekker, M. A.; Tsai, A. G.; Brady, T.; Stevens, H. Y.; Frangos, J. A.; Theodorakis, E.; Intaglietta, M. *Am. J. Physiol. Heart Circ. Physiol.* **2002**, *282*, H1609-14.

(152) Frochot, C.; Muller, C.; Brembilla, A.; Carre, M. C.; Lochon, P.; Viriot, M. L. *Int. J. Polym. Anal. Charact.* **2000**, *6*, 109-122.

(153) Damas, C.; Adibnejad, M.; Benjelloun, A.; Brembilla, A.; Carre, M. C.; Viriot, M. L.; Lochon, P. *Colloid and Polym. Sci.* **1997**, *275*, 364-371.

(154) Lord, S. J.; Conley, N. R.; Lee, H. L.; Samuel, R.; Liu, N.; Twieg, R. J.; Moerner, W. E. *J. Am. Chem. Soc.* **2008**, *130*, 9204-5.

(155) Lord, S. J.; Conley, N. R.; Lee, H. L.; Nishimura, S. Y.; Pomerantz, A. K.; Willets, K. A.; Lu, Z.; Wang, H.; Liu, N.; Samuel, R.; Weber, R.; Semyonov, A.; He, M.; Twieg, R. J.; Moerner, W. E. *Chemphyschem* **2009**, *10*, 55-65.

(156) LeVine, H., III. *Protein Sci.* **1993**, *2*, 404-10.

(157) Agdeppa, E. D.; Kepe, V.; Liu, J.; Flores-Torres, S.; Satyamurthy, N.; Petric, A.; Cole, G. M.; Small, G. W.; Huang, S. C.; Barrio, J. R. *J. Neurosci.* **2001**, *21*, RC189.

(158) Abad, S.; Vaya, I.; Jimenez, M. C.; Pischel, U.; Miranda, M. A. *Chemphyschem* **2006**, *7*, 2175-83.

(159) Spies, C.; Gehrke, R. *J. Phys. Chem. A* **2002**, *106*, 5348-5352.

(160) Schuddeboom, W.; Jonker, S. A.; Warman, J. M.; Leinhos, U.; Kuhnle, W.; Zachariasse, K. A. *J. Phys. Chem.* **1992**, *96*, 10809-10819.

(161) Il'ichev, Y. V.; Kuhnle, W.; Zachariasse, K. A. *J. Phys. Chem. A* **1998**, *102*, 5670-5680.

(162) Biancalana, M.; Makabe, K.; Koide, A.; Koide, S. *J. Mol. Biol.* **2008**, *383*, 205-13.

(163) Biancalana, M.; Makabe, K.; Koide, A.; Koide, S. *J. Mol. Biol.* **2009**, *385*, 1052-63.

(164) *LogP values were calculated using the Molinspiration Cheminformatics software; http://www.molinspiration.com/ (Last accessed, November 20, 2010).*

(165) Lipinski, C. A.; Lombardo, F.; Dominy, B. W.; Feeney, P. J. *Adv. Drug Deliv. Rev.* **1997**, *23*, 3-25.

(166) Loutfy, R. O.; Arnold, B. A. *J. Phys. Chem.* **1982**, *86*, 4205-4211.

(167) Doolittle, A. K. *J. Appl. Phys.* **1952**, *23*, 236-239.

(168) Iio, T.; Takahashi, S.; Sawada, S. *J. Biochem.* **1993**, *113*, 196-9.

(169) Iwaki, T.; Torigoe, C.; Noji, M.; Nakanishi, M. *Biochemistry* **1993**, *32*, 7589-92.

(170) Sigurdson, C. J.; Nilsson, K. P.; Hornemann, S.; Manco, G.; Polymenidou, M.; Schwarz, P.; Leclerc, M.; Hammarstrom, P.; Wuthrich, K.; Aguzzi, A. *Nat. Methods* **2007**, *4*, 1023-30.

(171) Ran, C.; Xu, X.; Raymond, S. B.; Ferrara, B. J.; Neal, K.; Bacskai, B. J.; Medarova, Z.; Moore, A. *J. Am. Chem. Soc.* **2009**, *131*, 15257-61.

(172) Yang, C. S.; Liu, L.; Mu, T. W.; Guo, Q. X. *Anal. Sci.* **2000**, *16*, 537-539.

(173) Robinson, J. W. *Atomic Spectroscopy* **1996**.

(174) Minati, L.; Edginton, T.; Bruzzone, M. G.; Giaccone, G. *Am J Alzheimers Dis* **2009**, *24*, 95-121.

(175) Selkoe, D. J. *Nature* **1999**, *399*, A23-31.

(176) Dubois, B.; Feldman, H. H.; Jacova, C.; DeKosky, S. T.; Barberger-Gateau, P.; Cummings, J.; Delacourte, A.; Galasko, D.; Gauthier, S.; Jicha, G.; Meguro, K.; O'Brien, J.; Pasquier, F.; Robert, P.; Rossor, M.; Salloway, S.; Stern, Y.; Visser, P. J.; Scheltens, P. *Lancet Neurol.* **2007**, *6*, 734-746.

(177) Mathis, C. A.; Wang, Y.; Klunk, W. E. *Curr. Pharm. Des.* **2004**, *10*, 1469-1492.

(178) Kim, Y. S.; Lee, J. H.; Ryu, J.; Kim, D. J. *Curr. Pharm. Des.* **2009**, *15*, 637-658.

(179) Nichols, L.; Pike, V. W.; Cai, L.; Innis, R. B. *Biol. Phychiatry* **2006**, *59*, 940-947.

(180) Matthews, B.; Siemers, E. R.; Mozley, P. D. *Am. J. Geriatr. Psychiatry* **2003**, *11*, 146-159.

(181) Golde, T. E.; Bacskai, B. J. *Nat. Biotechnol.* **2005**, *23*, 552-554.

(182) Higuchi, M.; Iwata, N.; Matsuba, Y.; Sato, K.; Sasamoto, K.; Saido, T. C. *Nat. Neurosci.* **2005**, *8*, 527-533.

(183) Poduslo, J. F.; Curran, G. L.; Peterson, J. A.; McCormick, D. J.; Fauq, A. H.; Khan, M. A.; Wengenack, T. M. *Biochemistry* **2004**, *43*, 6064-6075.

(184) Stephenson, K. A.; Chandra, R.; Zhuang, Z. P.; Hou, C.; Oya, S.; Kung, M. P.; Kung, H. F. *Bioconjugate Chem.* **2007**, *18*, 238-246.

(185) Johnson, A. E.; Jeppsson, F.; Sandell, J.; Wensbo, D.; Neelissen, J. A. M.; Juréus, A.; Ström, P.; Norman, H.; Farde, L.; Svensson, S. P. S. *J. Neurochem.* **2009**, *108*, 1177-1186.

(186) Newberg, A. B.; Wintering, N. A.; Plossl, K.; Hochold, J.; Stabin, M. G.; Watson, M.; Skovronsky, D.; Clark, C. M.; Kung, M.-P.; Kung, H. F. *J. Nucl. Med.* **2006**, *47*, 748-754.

(187) Kung, M.-P.; Hou, C.; Zhuang, Z.-P.; Zhang, B.; Skovronsky, D.; Trojanowski, J. Q.; Lee, V. M. Y.; Kung, H. F. *Brain Res.* **2002**, *956*, 202-210.

(188) Hintersteiner, M.; Enz, A.; Frey, P.; Jaton, A.-L.; Kinzy, W.; Kneuer, R.; Neumann, U.; Rudin, M.; Staufenbiel, M.; Stoeckli, M.; Wiederhold, K.-H.; Gremlich, H.-U. *Nat. Biotech.* **2005**, *23*, 577-583.

(189) Nesterov, E. E.; Skoch, J.; Hyman, B. T.; Klunk, W. E.; Bacskai, B. J.; Swager, T. M. *Angew. Chem. Int. Ed.* **2005**, *44*, 5452-5456.

(190) Raymond, S. B.; Skoch, J.; Hills, I. D.; Nesterov, E. E.; Swager, T. M.; Bacskai, B. J. *Eur. J. Nucl. Med. Mol. Imaging* **2008**, *35*, S93-S98.

(191) Li, Q.; Lee, J. S.; Ha, C.; Chan, B. P.; Yang, G.; Wen, B. G.; Chang, Y. T. *Angew. Chem. Int. Ed.* **2004**, *43*, 6331-6335.

(192) Ran, C.; Xu, X.; Raymond, S. B.; Ferrara, B. J.; Neal, K.; Bacskai, B. J.; Medarova, Z.; Moore, A. *J. Am. Chem. Soc.* **2009**, *131*, 15257-15261.

(193) Ono, M.; Ishikawa, M.; Kimura, H.; Hayashi, S.; Matsumura, K.; Watanabe, H.; Shimizu, Y.; Cheng, Y.; Cui, M.; Kawashima, H.; Saji, H. *Bioorg. Med Chem.* **2010**, *20*, 3885-3888.

(194) Sutharsan, J.; Dakanali, M.; Capule, C. C.; Haidekker, M. A.; Yang, J.; Theodorakis, E. A. *Chemmedchem* **2010**, *5*, 56-60.

(195) Haidekker, M. A.; Theodorakis, E. A. *Org. Biomol. Chem.* **2007**, *5*, 1669-1678.

(196) Granzhan, A.; Teulade-Fichou, M.-P. *Tetrahedron* **2009**, *65*, 1349-1360.

(197) Guram, A. S.; Rennels, R. A.; Buchwald, S. L. *Angew. Chem. Int. Ed. Engl.* **1995**, *34*, 1348-1350.

(198) Wolfe, J. P.; Buchwald, S. L. *J. Org. Chem.* **2000**, *65*, 1144-1157.

(199) Hartwig, J. F. *Accounts Chem. Res.* **2008**, *41*, 1534-1544.

(200) LeVine III, H. *Protein Sci.* **1993**, *2*, 404-410.

(201) *We previously showed that probes based on the molecular rotor motif do not exhibit a significant change in fluorescence properties in the presence of monomeric Aβ42 peptides, suggesting that these probes do not associate with Aβ monomers.*

(202) Zhao, X.; Yang, J. *ACS Chem. Neurosc.*, *1*, 655-660.

(203) Inbar, P.; Li, C. Q.; Takayama, S. A.; Bautista, M. R.; Yang, J. *ChemBioChem* **2006**, *7*, 1563-1566.

(204) Roan, N. R.; Munch, J.; Arhel, N.; Mothes, W.; Neidleman, J.; Kobayashi, A.; Smith-McCune, K.; Kirchhoff, F.; Greene, W. C. *J Virol* **2009**, *83*, 73-80.

(205) Haase, A. T. *Nat Rev Immunol* **2005**, *5*, 783-92.

(206) Chiti, F.; Dobson, C. M. *Annu Rev Biochem* **2006**, *75*, 333-66.

(207) Lockhart, A.; Ye, L.; Judd, D. B.; Merritt, A. T.; Lowe, P. N.; Morgenstern, J. L.; Hong, G.; Gee, A. D.; Brown, J. *J Biol Chem* **2005**, *280*, 7677-84.

(208) Beer, B. E.; Doncel, G. F.; Krebs, F. C.; Shattock, R. J.; Fletcher, P. S.; Buckheit, R. W., Jr.; Watson, K.; Dezzutti, C. S.; Cummins, J. E.; Bromley, E.; Richardson-Harman, N.; Pallansch, L. A.; Lackman-Smith, C.; Osterling, C.; Mankowski, M.; Miller, S. R.; Catalone, B. J.; Welsh, P. A.; Howett, M. K.; Wigdahl, B.; Turpin, J. A.; Reichelderfer, P. *Antimicrob Agents Chemother* **2006**, *50*, 713-23.

(209) Roan, N. R.; Sowinski, S.; Munch, J.; Kirchhoff, F.; Greene, W. C. *J Biol Chem*, *285*, 1861-9.

(210) Dezzutti, C. S.; James, V. N.; Ramos, A.; Sullivan, S. T.; Siddig, A.; Bush, T. J.; Grohskopf, L. A.; Paxton, L.; Subbarao, S.; Hart, C. E. *Antimicrob. Agents Chemother.* **2004**, *48*, 3834-3844.

(211) Bourne, N.; Bernstein, D. I.; Ireland, J.; Sonderfan, A. J.; Profy, A. T.; Stanberry, L. R. *J. Infect. Dis.* **1999**, *180*, 203-205.

(212) Rusconi, S.; Moonis, M.; Merrill, D. P.; Pallai, P. V.; Neidhardt, E. A.; Singh, S. K.; Willis, K. J.; Osburne, M. S.; Profy, A. T.; Jenson, J. C.; Hirsch, M. S. *Antimicrob. Agents Chemother.* **1996**, *40*, 234-6.

(213) Patel, S.; Hazrati, E.; Cheshenko, N.; Galen, B.; Yang, H.; Guzman, E.; Wang, R.; Herold, B. C.; Keller, M. J. *J. Infect. Dis.* **2007**, *196*, 1394-402.

(214) Keller, M. J.; Mesquita, P. M.; Torres, N. M.; Cho, S.; Shust, G.; Madan, R. P.; Cohen, H. W.; Petrie, J.; Ford, T.; Soto-Torres, L.; Profy, A. T.; Herold, B. C. *PLoS One*, *5*, e8781.

(215) Lai, S. K.; Hida, K.; Shukair, S.; Wang, Y. Y.; Figueiredo, A.; Cone, R.; Hope, T. J.; Hanes, J. *J Virol* **2009**, *83*, 11196-200.

(216) Venkataraman, N.; Cole, A. L.; Svoboda, P.; Pohl, J.; Cole, A. M. *J Immunol* **2005**, *175*, 7560-7.

(217) Cutler, B.; Justman, J. *Lancet Infect Dis* **2008**, *8*, 685-97.

(218) Karim, Q. A.; Karim, S. S. A.; Frohlich, J. A.; Grobler, A. C.; Baxter, C.; Mansoor, L. E.; Kharsany, A. B. M.; Sibeko, S.; Mlisana, K. P.; Omar, Z.; Gengiah, T. N.; Maarschalk, S.; Arulappan, N.; Mlotshwa, M.; Morris, L.; Taylor, D.; Grp, C. T. *Science* **2010**, *329*, 1168-1174.

(219) Mammen, M.; Choi, S. K.; Whitesides, G. M. *Angew. Chem. Intl. Ed.* **1998**, *37*, 2755-2794.

(220) Rao, J. H.; Lahiri, J.; Isaacs, L.; Weis, R. M.; Whitesides, G. M. *Science* **1998**, *280*, 708-711.

(221) Logsdon, L. A.; Schardon, C. L.; Ramalingam, V.; Kwee, S. K.; Urbach, A. R. *J. Am. Chem. Soc., 133*, 17087-92.

(222) Breslow, R.; Zhang, B. L. *J. Am. Chem. Soc.* **1996**, *118*, 8495-8496.

(223) Zhang, B. L.; Breslow, R. *J. Am. Chem. Soc.* **1993**, *115*, 9353-9354.

(224) Kanai, M.; Mortell, K. H.; Kiessling, L. L. *J. Am. Chem. Soc.* **1997**, *119*, 9931-9932.

(225) Mann, D. A.; Kanai, M.; Maly, D. J.; Kiessling, L. L. *J. Am. Chem. Soc.* **1998**, *120*, 10575-10582.

(226) Mortell, K. H.; Weatherman, R. V.; Kiessling, L. L. *J. Am. Chem. Soc.* **1996**, *118*, 2297-2298.

(227) Courtney, A. H.; Puffer, E. B.; Pontrello, J. K.; Yang, Z. Q.; Kiessling, L. L. *Proc. Natl. Acad. Sci. USA* **2009**, *106*, 2500-2505.

(228) Reczek, J. J.; Kennedy, A. A.; Halbert, B. T.; Urbach, A. R. *J. Am. Chem. Soc.* **2009**, *131*, 2408-2415.

(229) Krishnamurthy, V. M. E., L.A.; Whitesides, G.M. *Wiley-VCH Verlag GmbH & Co.: Weinheim, Germany, 2006*, 11-54.

(230) Cheng, Y. Y.; Zhao, L. B.; Li, Y. W.; Xu, T. W. *Chem. Soc. Rev.* **2011**, *40*, 2673-2703.

(231) Wilson, A. J. *Chem. Soc. Rev.* **2009**, *38*, 3289-3300.

(232) Jayaraman, N. *Chem. Soc. Rev.* **2009**, *38*, 3463-3483.

(233) Badjic, J. D.; Nelson, A.; Cantrill, S. J.; Turnbull, W. B.; Stoddart, J. F. *Acc. Chem. Res.* **2005**, *38*, 723-732.

(234) Takahashi, T.; Mihara, H. *Acc. Chem. Res.* **2008**, *41*, 1309-1318.

(235) Wu, C.; Wang, Z. X.; Lei, H. X.; Duan, Y.; Bowers, M. T.; Shea, J. E. *J. Mol. Biol.* **2008**, *384*, 718-729.

(236) Nanga, R. P. R.; Brender, J. R.; Vivekanandan, S.; Popovych, N.; Ramamoorthy, A. *J. Am. Chem. Soc.* **2009**, *131*, 17972-17979.

(237) Brender, J. R.; Hartman, K.; Gottler, L. M.; Cavitt, M. E.; Youngstrom, D. W.; Ramamoorthy, A. *Biophys. J.* **2009**, *97*, 2474-2483.

(238) Kirchhoff, F.; Munch, J. *Future Virol.* **2011**, *6*, 183-186.

(239) Roan, N. R.; Sowinski, S.; Munch, J.; Kirchhoff, F.; Greene, W. C. *J. Biol. Chem.* **2010**, *285*, 1861-1869.

(240) Hauber, I.; Hohenberg, H.; Holstermann, B.; Hunstein, W.; Hauber, J. *Proc. Natl. Acad. Sci. USA* **2009**, *106*, 9033-8.

(241) Lundquist, J. J.; Toone, E. J. *Chem. Rev.* **2002**, *102*, 555-578.

(242) Kitov, P. I.; Sadowska, J. M.; Mulvey, G.; Armstrong, G. D.; Ling, H.; Pannu, N. S.; Read, R. J.; Bundle, D. R. *Nature* **2000**, *403*, 669-672.

(243) Merritt, E. A.; Zhang, Z. S.; Pickens, J. C.; Ahn, M.; Hol, W. G. J.; Fan, E. K. *J. Am. Chem. Soc.* **2002**, *124*, 8818-8824.

(244) Page, M. I.; Jencks, W. P. *Proc. Natl. Acad. Sci. USA* **1971**, *68*, 1678-&.

(245) Kramer, R. H.; Karpen, J. W. *Nature* **1998**, *395*, 710-3.

(246) Krishnamurthy, V. M.; Semetey, V.; Bracher, P. J.; Shen, N.; Whitesides, G. M. *J. Am. Chem. Soc.* **2007**, *129*, 1312-20.

(247) Krishnamurthy, V. M.; Bohall, B. R.; Semetey, V.; Whitesides, G. M. *J. Am. Chem. Soc.* **2006**, *128*, 5802-12.

(248) Kiessling, L. L.; Gestwicki, J. E.; Strong, L. E. *Current Opinion in Chemical Biology* **2000**, *4*, 696-703.

(249) Chapman, R. G.; Ostuni, E.; Liang, M. N.; Meluleni, G.; Kim, E.; Yan, L.; Pier, G.; Warren, H. S.; Whitesides, G. M. *Langmuir* **2001**, *17*, 1225-1233.

(250) Siegers, C.; Biesalski, M.; Haag, R. *Chem. Eur. J.* **2004**, *10*, 2831-2838.

(251) Zalipsky, S. *Bioconj. Chem.* **1995**, *6*, 150-165.

(252) *We also synthesized BTA oligomers comprising shorter spacers (unpublished results), but the poor water solubility of these oligomers made them unsuitable for further analysis in cellular assays.*

(253) Qin, L.; Vastl, J.; Gao, J. *Mol. Biosyst.*, *6*, 1791-5.

(254) Chang, W. M.; Dakanali, M.; Capule, C. C.; Sigurdson, C. J.; Yang, J.; Theodorakis, E. A. *ACS Chem. Neurosci.* **2011**, *2*, 249-255.

(255) Platt, E. J.; Wehrly, K.; Kuhmann, S. E.; Chesebro, B.; Kabat, D. *J. Virol.* **1998**, *72*, 2855-64.

(256) *The CXCR4 coreceptor is endogenously expressed in HeLa cells. See Ref. 38 for additional details.*

(257) Kolonko, E. M.; Kiessling, L. L. *J. Am. Chem. Soc.* **2008**, *130*, 5626-7.

(258) Semetey, V.; Moustakas, D.; Whitesides, G. M. *Angew. Chem. Intl. Ed. Engl.* **2006**, *45*, 588-591.

(259) Yin, Y. H., A.D. *Chemical Biology, Wiley-VCH, 2007* **2007**, 250-269.

(260) Rosenzweig, B. A.; Ross, N. T.; Adler, M. J.; Hamilton, A. D. *J. Am. Chem. Soc.* **2010**, *132*, 6749-6754.

(261) Rosenzweig, B. A.; Ross, N. T.; Tagore, D. M.; Jayawickramarajah, J.; Saraogi, I.; Hamilton, A. D. *J. Am. Chem. Soc.* **2009**, *131*, 5020-5021.